João Pedro Rodrigues Ferreira

Licenciado em Ciências da Engenharia Civil

Influence of temperature on the sorption-desorption curves of earth-based materials and consequences on their hygrothermal behaviour

Dissertação para obtenção do Grau de Mestre em
Engenharia Civil – Perfil de Construção

Orientador: Fionn McGregor, Post doctoral, École Nationale des Travaux Publics de l'État

Co-orientador: Mª Paulina Faria Rodrigues, Professora Associada, Faculdade de Ciências e Tecnologia da Universidade Nova de Lisboa

Júri:

Presidente: Doutora Zuzana Dimitrovová
Arguente: Doutora Ana Armada Brás
Vogais: Doutor Daniel Aelenei
Doutor Fionn McGregor

FACULDADE DE CIÊNCIAS E TECNOLOGIA
UNIVERSIDADE NOVA DE LISBOA

Dezembro 2016

Acknowledgements

Firstly I would like to express all my sincere gratitude to Professor Paulina Faria, this opportunity just happened with your invitation and confidence in me. Also for all the support, advices and motivation despite the distance.

I also would like to thank my supervisors Fionn McGregor and Antonin Fabbri, who agreed in receiving me for the internship and also for the proposal of a new contract, without them this experience would not have been possible. Clearly working under their supervision was a rewarding experience in both human and scientific point of view. They were also responsible for the great work environment that I found at the ENTPE, that I am also thankful to for the financial support and for the sympathy and all the aid received from the staff.

This adventure beside the professional side was equally amazing on the social side, I had the opportunity to meet and work with people from different countries. From who I made good friendships and for sure without them it would have been harder to be far from my country. So I would like to thank my fellows that I have met in ENTPE and in Lyon.

During these months I never felt far from my long term friends, from which I received motivation and even visits. Equally important my friends from FCT, present in all my academic career and for sure for much longer, from the Geological Engineering and Civil Engineering courses. I am very thankful to all of them.

To one of the most important persons, my girlfriend, Rita Ferreira. I'm very grateful for the push to accept this challenge and for all the support, patient, love and kindness during not only this experience but also in all my course.

Finally, the greatest thanks to my family, specially my parents for all the help, affection and motivation, because without them nothing of this would ever be possible. Especially dedicated to my grandfather, Orlindo Ferreira, who passed away on the 12th of November 2016.

Abstract

There has been a rising interest by the building sector in using passive solutions to regulate the indoor relative humidity, since humidity levels can directly affect the health and comfort of the occupants.

Earth based materials are known for their ability to regulate the relative humidity and improve indoor comfort. Another motivation is the potential to reduce the energy consumption of air conditioning systems.

The assessment of the hygrothermal transfers within earthen walls/plasters has been the focus of many researchers, but the proper modelling and coupling of these characteristics for unconventional materials like earthen walls and plasters still is a major scientific and technical challenge.

The main objective of this dissertation consists in first to check the validity of steady state material characteristics obtained through standard procedures. Furthermore, validate different assumptions and the reliability of the different methods to determine the precision of the experimental test results. The second objective is to analyse the influence of temperature on those characteristics and their consequences on the hygrothermal behaviour.

For that purpose, two types of porous hygroscopic materials are studied: compressed earth samples and earth plasters with the addition of organic natural fibres.

Results showed a high variability due to experimental set ups and conditions. However the influence of temperature on the sorption and transfer properties could be determined. An analysis of the results based on thermodynamics gave surface characteristics and the heat involved in the adsorption and condensation process of the materials used.

Keywords: Compressed earth sample; Earth plaster; Hygrothermal behaviour; Temperature; Thermodynamic

Resumo

O sector da construção tem vindo a demonstrar um crescente interesse pelo uso de soluções passivas que contribuam para regular a humidade relativa do interior dos edifícios, uma vez que condições extremas de humidade relativa estão diretamente relacionadas e podem afetar a saúde e o conforto dos ocupantes.

Materiais com base em terra são conhecidos pela sua capacidade em regular a humidade relativa do ar e, consequentemente, melhorar o conforto interior. Esta capacidade apresenta ainda a vantagem de possibilitar a redução de consumo de energia por sistemas de ar condicionado.

As transferências higrotérmicas em paredes e rebocos de terra têm sido amplamente estudadas pela comunidade científica, mas a correta modelação e correspondência destas características para este tipo de materiais não convencionais continua a ser um grande desafio técnico-científico.

Os principais objetivos desta dissertação consistem, primeiramente, em verificar a validade das características do estado estacionário dos materiais, obtidas através dos procedimentos experimentais definidos nas normas existentes. De seguida validar as diferentes hipóteses assumidas e a influência dos diferentes métodos, de forma a aumentar a precisão dos resultados experimentais. O segundo objetivo passa por analisar a influência da temperatura nas propriedades higroscópicas e estudar os efeitos provocados no comportamento higrotérmico dos materiais.

Para o efeito, dois tipos de materiais higroscópicos são estudados: amostras de terra comprimida e de rebocos de terra com adição de fibras orgânicas naturais.

Os resultados demonstraram uma alta variabilidade das características consoante as condições e procedimentos experimentais. No entanto, a influência da temperatura sobre as propriedades de adsorção e de transferência de humidade foram determinadas. Uma análise termodinâmica aos resultados permitiu ainda obter características relativas às superficiais e sobre as transferências de calor envolvidas no processo de adsorção e condensação dos materiais testados.

Palavras-chave: Amostra de terra comprimida; Reboco de terra; Comportamento higrotérmico; Temperatura; Termodinâmica

Notations and symbols

A	Water absorption coefficient ($kg/(m^2.s^{1/2})$)
a	Thermal diffusivity (m^2/s)
c_p	Specific heat (J/(kg.°C))
d	Thickness (m)
d_a	Thickness of the air layer (m)
D_L	Permeability coefficient (kg/(Pa.m.s))
f	Gravity acceleration (m/s^2)
G	Water vapour flow rate (kg/s)
g_L	Liquid flux density vector ($kg/(m^2.s)$)
g_v	Vapour flux density vector ($kg/(m^2.s)$)
L	Avogadro's number (mol^{-1})
n_m	Amount of adsorbed water at monolayer (g/g)
m	Mass of moist sample (g)
m_0	Mass of dried sample (g)
M_a	Molecular area of water (m^2)
M_w	Molecular mass of water (g/mol)
p_{atm}	Atmospheric pressure (Pa)
p_L	Liquid pressure (Pa)
p_v	Water vapour partial pressure (Pa)
$p_{v,sat}$	Saturation water vapour pressure (Pa)
q	Heat flux (W/m^2)
R	Perfect molar gas constant (J/(mol.K))
RH	Relative humidity (%)
s	Exposed surface area (m^2)
S_{BET}	Specific surface area (m^2/g)
S_d	Equivalent air layer thickness (m)
S_r	Saturation ratio (-)

T	Temperature (K)
u	Water content (kg/kg)
w	Water content (%)
W	Water vapour permeance (kg/(m^2.s.Pa))
w_f	Free water saturation (kg/m^3)
Z^s	Surface vapour transfer resistance ((m^2.s.Pa)/kg)
β	Apparent vapour surface transfer coefficient (kg/(m^2.s.Pa))
δ_p	Water vapour permeability (kg/(Pa.m.s))
δ_p^{agc}	Air gap corrected water vapour permeability (kg/(Pa.m.s))
δ_p^{ap}	Apparent water vapour permeability (kg/(Pa.m.s))
δ_p^{β}	Skin factor corrected water vapour permeability (kg/(Pa.m.s))
δ_a	Water vapour permeability of air (kg/(Pa.m.s))
ΔH	Heat of sorption (J/mol)
Δp	Capillary pressure gradient (Pa)
Δp_v	Water vapour pressure gradient (Pa)
θ	Wetting contact angle (º)
λ	Thermal conductivity (W/(m.°C))
μ	Water vapour resistance factor (-)
μ^{agc}	Air gap corrected water vapour resistance factor (-)
μ^{ap}	Apparent water vapour resistance factor (-)
μ^{β}	Skin factor corrected water vapour resistance factor (-)
ξ	Moisture capacity (kg/m^3)
ρ	Apparent density (kg/m^3)
ρ_d	Apparent dry density (kg/m^3)
σ	Surface tension (N/m)
ϕ	Porosity (-)
φ	Relative humidity (-)
Ω	Volume of the material (m^3)

Contents

List of Figures

List of Tables

1. Introduction

1.1. Context

In the building construction sector a lot of studies have targeted the use of local, sustainable and healthy environmental materials in order to replace/minimize the industrial ones. Industrial materials are associated with high environmental impacts (Morel et al., 2001), due to energy consumption and greenhouse gas emissions during the production, transport and implementation process (Labat et al., 2016; Soudani et al., 2016). Alongside with this effort to increase the sustainability of buildings also arises the importance of improving their indoor climate and living comfort, preferentially with passive solutions such as buffering materials, instead of active mechanical solutions.

In this context, earth-based materials seem to be a good alternative. Earth buildings are known for more than nine thousand years (Minke, 2009) and only recently (last century) has the concrete industry made such materials less attractive (Cagnon et al., 2014). Actually this tendency is changing again and nowadays this material is gaining more interest by academics, architects and builders (Hall & Allinson, 2009).

Earth has many advantages when used as a building material. It is a local material available in large quantities that can be obtained directly from the building site with low embodied energy even considering the production process (Bui et al., 2014; Cagnon et al., 2014; Labat et al., 2016; McGregor et al., 2014; Soudani et al., 2016). It also has the particularity of being infinitely reusable when not stabilised (Minke, 2009), which contributes to the reduction of construction wastes.

Building's indoor climate is very important for the health and comfort of the occupants. It depends on many characteristics like the air temperature, air exchange and humidity (Abdul-Wahab et al., 2015; Al Horr et al., 2016; Desogus et al., 2015; Henriques, 2007; McGregor et al, 2014; Minke, 2009). If in one hand a disagreeable temperature can be easily perceived and solved, in the other hand a harmful humidity is more imperceptible (Minke, 2009). There are many risks associated with high relative humidity, such as mould development impacting health through problems like allergies, infections or asthma (Abdul-Wahab et al., 2015; Lima & Faria, 2013; Minke, 2009). Low levels of humidity reduces the mucous membrane available in human's skin, provoking irritations by this drying effect (Abdul-Wahab et al., 2015; Minke, 2009).

The interior conditions levels are influenced by the exterior climate. Portugal and France present similar climates; both countries are characterized by a Mediterranean climate although with some differences. Portugal is located more at the south of Europe with proximity to the Atlantic ocean, which contributes for a milder winter comparing with other southern European countries (Silva & Henriques, 2014), the minimum temperature in some parts of the country can reach almost 0ºC at night. In other hands the summer is "hot and dry with high levels of solar radiation" (Barbosa et al., 2015), with temperatures that can go up until 45°C (although not for many hours of only few days because a big amplitude of temperature generally exist).

In France the climate can vary between different parts of the country, from low altitudes with ocean proximity to an opposite mountain climate at high altitudes. The winter is colder with minimum temperatures that can go below 0 °C and the summer is also hot with maximums temperatures that can go up to 35 °C, both depending on the local.

Those differences leads to two general assumptions. The season that traditionally brings up most concerns is the winter in France and the summer in Portugal. That can be easily observed if we lived in both countries. In France the habitants are more worried and a big effort is done in order to have pleasant indoor temperature in the winter; therefore, almost all the buildings have a heating system. Otherwise in Portugal this effort and preoccupation occurs mostly for the summer. Nevertheless in Portugal there is a high mortality rate during the winter, justified by the fact that the majority of the buildings do not have heating systems and the buildings dating from before the 90s are not thermal insulated.

Generally in buildings, the most common option adopted to cool the indoor climate in summer is the installation of air-conditioning systems, known for their efficiency but also for the high energy consumption

associated. As said by Rupp et al. (2015) “buildings consume about 70% of final energy consumption through air-conditioning systems and artificial lighting”.

Such situation can be prevented through the adoption of particular building elements which can provide some important benefits. According to this, the interest in passive solutions had been rising and several studies continue to be made.

To face these problems it is important to understand and know the hygrothermal properties of the building materials. The performance of the material is mainly dependent on its heat transfer and storage capacity. However, a proper assessment of the contribution of the mass transfer and storage is necessary, which will be the main scope of this dissertation. Such properties play a role in regulating the indoor relative humidity and, thereby, improve the interior climate. This relates to the hygroscopic behaviour of the material and can be analysed by sorption isotherms and the water vapour permeability.

1.2. Objective and methodology

The main objective of this dissertation is to study the influence of the temperature on the hygrothermal behaviour of building envelope eco-efficient elements like walls and plasters, more specifically compressed earth blocks and earth mortar plasters. Hygroscopic characteristics of these materials have been studied by several researchers. However there is still a need to properly assess their coupling with temperature.

Four formulations of each earth-based material were tested: earth blocks STA, STR, CRA, ALX and earth plasters F0, F3, F5 and F6. Firstly, it will be evaluated the steady state characteristics of the materials, by analysing different assumptions and methods used by standard procedures. The aim is to increase the accuracy of the experimental results.

The water vapour transmission properties will be determined for three of the earth plasters (F0, F3 and F5) at two different temperatures. For the determination of the sorption isotherms all the earth blocks and earth plasters will be tested at three different temperatures. Finally a study and analysis of the influence of temperature on the measured properties is done.

1.3. Dissertation structure

A literature review on hygroscopic characteristics and their hygrothermal coupling is given in Chapter 2. Clayed materials are known in the building sector for their capacity to adsorb moisture and so a proper knowledge of all the properties involved is required.

Earth plasters and compressed earth blocks were studied in this dissertation. In Chapter 3 a description of their composition as well as the experimental procedures for determine the sorption isotherms and the vapour diffusion properties are presented.

Thereafter in Chapter 4 a standard characterization of the determined characteristics at 23ºC is given. Also an analysis on the experimental procedures imprecisions and the definition of new protocols and corrections was done.

The influence of temperature is then studied and analysed for the different tests in the Chapter 5 and finally the conclusion of this dissertation and future works suggestions are presented in Chapter 6.

2. Hygrothermal behaviour of clay based construction materials

2.1. Porous media and clays

2.1.1. Different phases

Earth is known to be a porous material with different sizes of particles and voids known by pores. It is possible to classify them, from the standpoint of volume-mass relations, as a three phase system: the solid phase S, the liquid water phase L and the gas phase G assumed to be a mixture of perfect gases composed by dried air and water vapour (Fredlund & Rahardjo, 1993) - see Figure 2.1.

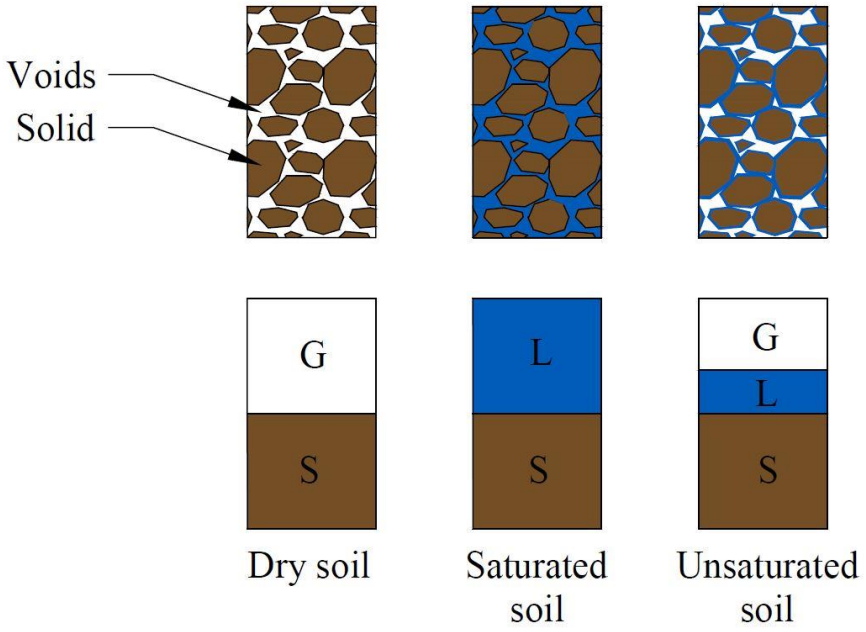

Figure 2.1- Porous material conditions

As well as the three phases, is possible to obtain three different states. If there is no presence of water in the voids it is called the dry state; otherwise if all the voids are filled with water it is named the saturated state; the most common if both water and air are present it is known by the unsaturated state. This morphology can be described by eq. 1 to 3:

$$\Omega_s = (1 - \phi)\Omega \tag{1}$$

$$\Omega_L = \phi_L \Omega = S_r \phi \Omega \tag{2}$$

$$\Omega_G = \phi_G \Omega = (1 - S_r)\phi \Omega \tag{3}$$

where Ω is the volume of the material. Ω_s, Ω_L and Ω_G are respectively the volumes of S, L and G. The material porosity is noted ϕ and ϕ_L the porosity filled by the liquid and gas phase. S_r notes the saturation ratio, corresponding to the ratio between the current liquid volume and the current porous network ratio.

2.1.2. Types of pores

Pores are the spaces formed by the disorderly organization of particles with different shapes and sizes. For this reason their geometry is very varied which in turn makes it difficult for a proper representation of the porous network shape. An approach of the hypothetical types of pores was done by J. Rouquerol et al. (1994) - see Figure 2.2.

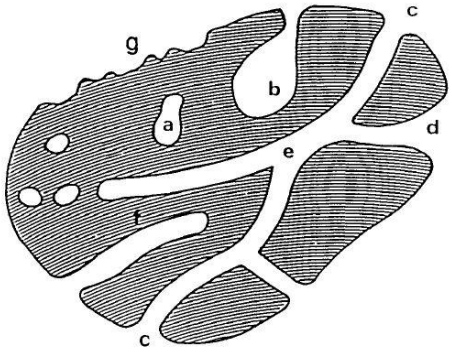

Figure 2.2- Schematic cross-section of a porous solid (J. Rouquerol et al., 1994)

Basically pores are divided in two categories: open and closed. The closed pores (a) are not accessible to water and they are totally isolated. This type of pores do not influence the mass transfer properties; their influence concerns density, mechanical strength and thermal conductivity. In other hand, open pores that can be divided in blind pores, interconnected (e) and through pores (c), open in both sides (J. Rouquerol et al., 1994). These pores provides the available surface area and they are responsible for the mass transfers in a porous material.

2.1.3. Clays as porous media

Clay minerals are powders produced from the weathering of rocks (Douillard & Salles, 2004; McGregor, 2014), with irregular connections that reproduce a varied pore geometry with angular pores connected to slit-shaped spaces (Tuller, Dani, & Dudley, 1999). This characteristics allow the classification as a porous media.

They represent a complex crystallography formed by lamellar aluminosilicates, commonly displayed in stacking of tetrahedral (T) and octahedral (O) layers, that can be organised as T-O structure also known by 1:1 structure (Figure 2.3) or T-O-T structure named 2:1 structure (Figure 2.4), (Douillard & Salles, 2004; McGregor, 2014).

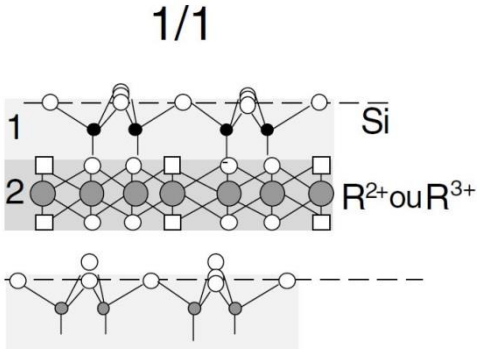

Figure 2.3- 1:1 type clay mineral (Meunier, 2005)

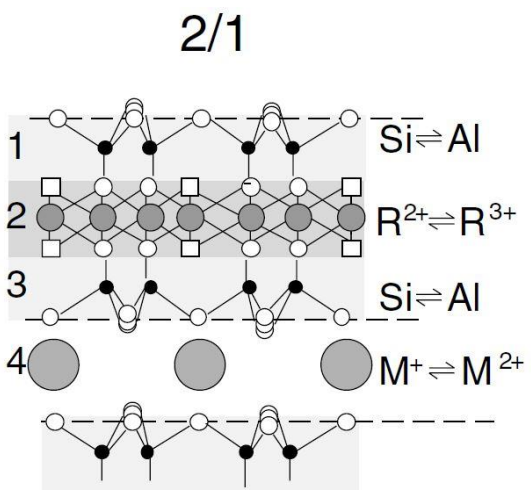

Figure 2.4- 2:1 type clay mineral (Meunier, 2005)

This two types of structures are typically the representation of two types of important clays minerals: a Kaolinite is formed by a 1:1 structure and a Montmorillonite by the 2:1 structure.

2.1.4. Clays characteristics

The size of clay minerals ranges between 10 nm and 10 μm with very different shapes depending on conditions of crystallisation (Meunier, 2005). The combination of these characteristics leads to high porosity with small sized pores, which in turn results in high specific surface area.

The specific surface area represents the total area of all particle surfaces accessible to other molecules; it is normally defined in area by unit mass (Douillard & Salles, 2004). According to Minke (2009), Kaolinite minerals have a specific surface area of 10 m^2/g and Montmorillonite minerals have 1000 m^2/g.

This available surface area is where the active sites of the minerals structures will be present. They result from the isomorphic substitutions in the tetrahedron and octahedron layers, which creates negative surface charges responsible for the adsorption process, when there is a presence of water. As said by Douillard & Salles (2004) "the interface between clay surfaces and water can be viewed as an interface between a charged surface and water".

In the 2:1 structures the negative surface charges are compensated by the interlayer cations, that in turn can hydrate and increase in volume during adsorption, or they can decrease during the desorption. This property is known by the swelling effect present in 2:1 clay minerals as Montmorillonite. On the other hand, 1:1 clay minerals like Kaolinite, have a very low surface charge and no interlayered cations. The main adsorptions sites are on the edges where the Oxygen and Hydrogen groups are present.

At this point is possible to notice that the presence of Montmorillonite in earth materials can bring some benefits concerning the adsorption performance of water vapour. Actually that was proved by Likos & Lu (2002) who analysed the water sorption isotherms with different percentages of Kaolinite and Smectite (Montmorillonite clay type). It was proved that the amount of water adsorbed increases with the increasing of Smectite content. Also McGregor (2014) made a similar study by analysing the influence in the sorption isotherms of clay samples (Kaolinite) with or without percentages of Bentonite, another type of Montmorillonite. Once again the amount of adsorbed water was higher with the higher percentages of Bentonite.

However the use of Montmorillonite type of clay minerals in the building sector should be moderate, and not be excessively used. It has clearly the best capacity to adsorb water vapour but in very high levels it will lead to the appearance of cracks due to the shrinkage during the drying process.

2.2. Moisture storage and sorption isotherms

In general people spend most of their time inside buildings - about 90% (Minke, 2009) - and depending on the activity and the environment the level of moisture will increase with occupancy. High levels of moisture provoke physical discomfort and other problems like described in chapter 1. This problem can be partially solved by the occupants themselves if they have the habit of opening the windows and let the new air flow in, or as well if there is a natural ventilation system.
In many hot countries, including Portugal, natural ventilation may prevail (open windows, weak air tightness of buildings) and moisture levels will fluctuate with external moisture levels, indoor temperature and air renovation.

In buildings with high air tightness the concern is to integrate in the buildings the capacity to somehow dissipate this excess of moisture and this can be obtained "by using specific building materials that present advantages such as thermal mass, moisture buffering (…)" (McGregor, 2014).

Commonly in building physics the amount of water vapour present in the air is referred as the relative humidity (φ) and is defined as the ratio between the partial water vapour pressure (p_v [Pa]) and the saturation water vapour pressure ($p_{v,sat}$ [Pa]) for a certain temperature (eq. 4):

$$\varphi = \frac{p_v}{p_{v,sat}} \tag{4}$$

When inside the buildings a high level of moisture is felt it is due to a high water vapour pressure in the air, which in turn leads to a concentration gradient that will entail the water vapour flow through the buildings elements.

Continuing the analysis of the equation 4, $p_{v,sat}$ corresponds to the maximum of water vapour that can be present in the air at a certain temperature. If the p_v reaches the same value as $p_{v,sat}$, the dew point is reached, corresponding to RH = 100%, and this leads to the condensation of water vapour, to the liquid state. RH can also vary with temperature, since the $p_{v,sat}$ depends on temperature, for example if there is a temperature increase the saturation pressure will also increase and therefore the RH decreases. This relation is represented by the psychrometric chart (Figure 2.5), which is an easy and practical support that relates the temperature with the partial vapour pressure and the relative humidity.

When the material is within the porous network, the maximum vapour pressure which leads to condensation changes. It is due to the interaction between the water molecules and the pores walls, which results in an apparent decrease of liquid water pressure. This point is discussed more in detail in the following of this dissertation. In consequence, condensation processes may occur within the pores of the material even if the RH is lower than 1. The link between this RH of phase change and the in-pore liquid pressure is depicted by the Kelvin's law:

$$p_L - p_{atm} = \frac{\rho_L RT}{M_w} \ln \varphi \tag{5}$$

where p_L is the liquid pressure [Pa], p_{atm} is the atmospheric pressure [Pa], R is the perfect gas constant [J/mol.K], T is the absolute temperature and M_w is the molar mass of water [g/mol].

After the phenomena described until here, becomes important to understand what happens when a moisture gradient step into the material. Hygroscopic materials have the capacity to adsorb water vapour from the air at high moisture environments and release it when the humidity decreases. The enrichment is known by adsorption, which is described by the adhesion of the water vapour to the pores surfaces and the reverse process, the desorption, is the loose of this cohesion and so the water vapour molecules are released.

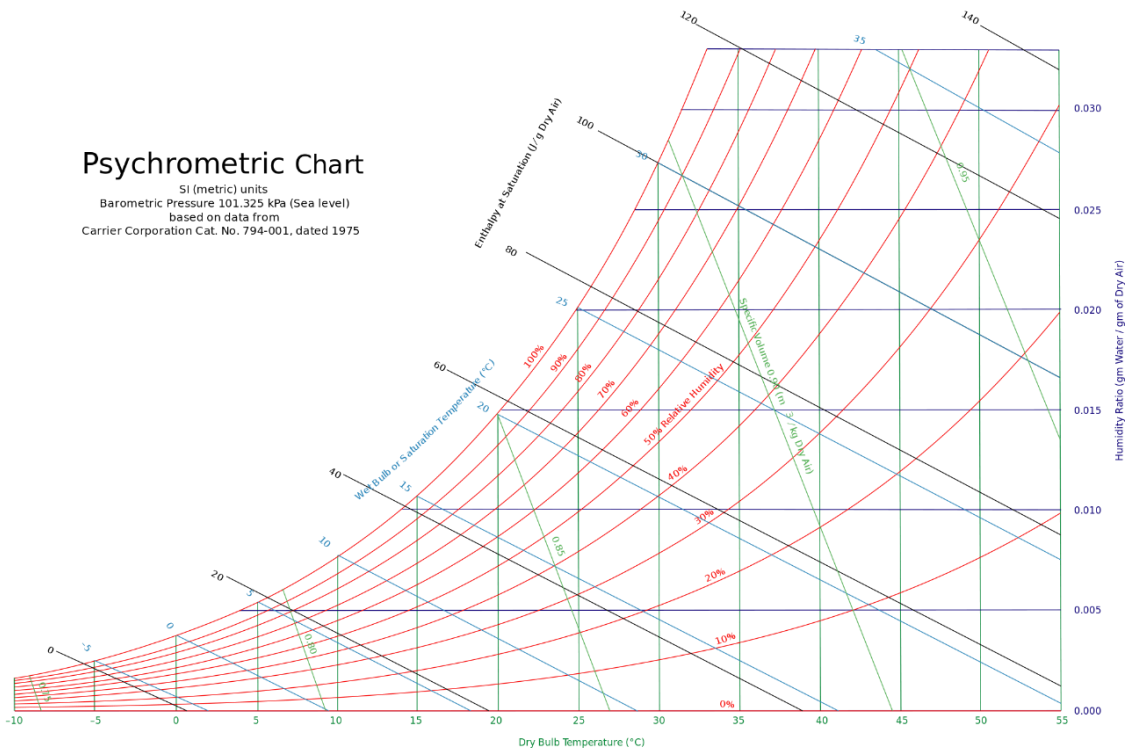

Figure 2.5- Psychrometric chart (open source)

Inside the material, moisture can also be present physically fixed in the pores, or as free water. As RH increases, single layers and multi layers of adsorbed molecules appears and they can nucleate into a liquid water meniscus. So there will be the presence of water vapour and liquid water; all this water content is normally denoted by u, defined by the EN ISO 12571:2000 (CEN 2000) by equation 6:

$$u = \frac{m - m_0}{m_0} \tag{6}$$

where m is the mass of the wet sample and m_0 is the mass of the dried sample. This behaviour determines the moisture buffering capacity of building materials, and it is normally characterised by the sorption isotherms.

The sorption isotherms are curves that relates the adsorbed water content with the relative humidity at a constant temperature. These curves normally are classified in six different types - see Figure 2.6.

Clayey building materials have a type II B isotherm with a hysteresis loop, representing the difference between the adsorption and desorption. It normally occurs at higher relative humidities associated with the capillary condensation (McGregor, 2014).

Earth building materials normally present a “S” shaped isotherm, as can be seen in the Figure 2.7, where at first a single layer of adsorbed molecules occurs, normally until 15% of RH. The observed linear section at humidities between 15% and 50% corresponds to the multiple layers of adsorbed water. After, the sharp increase observed is related to the thickening of the layers and pore filling. When layers start to interconnect forming water meniscus, this represents the end of the hygroscopic regime, normally until 95%. The last phenome also represents the beginning of the capillary regime, between 95% and 98%, where the curves rises very sharply (Hall & Allinson, 2009; McGregor, 2014). Finally, and at least, occurs the super saturation regime, rising to 100%, difficult to reach - only under a vacuum system. The water up-take above the hygroscopic regime is described by the water retention curve which ends with the full saturation of pores by liquid water.

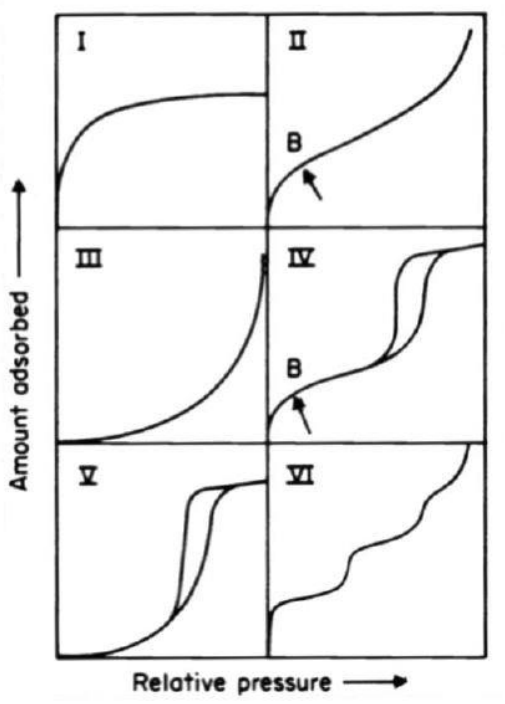

Figure 2.6- Types of isotherms, Sing (1985)

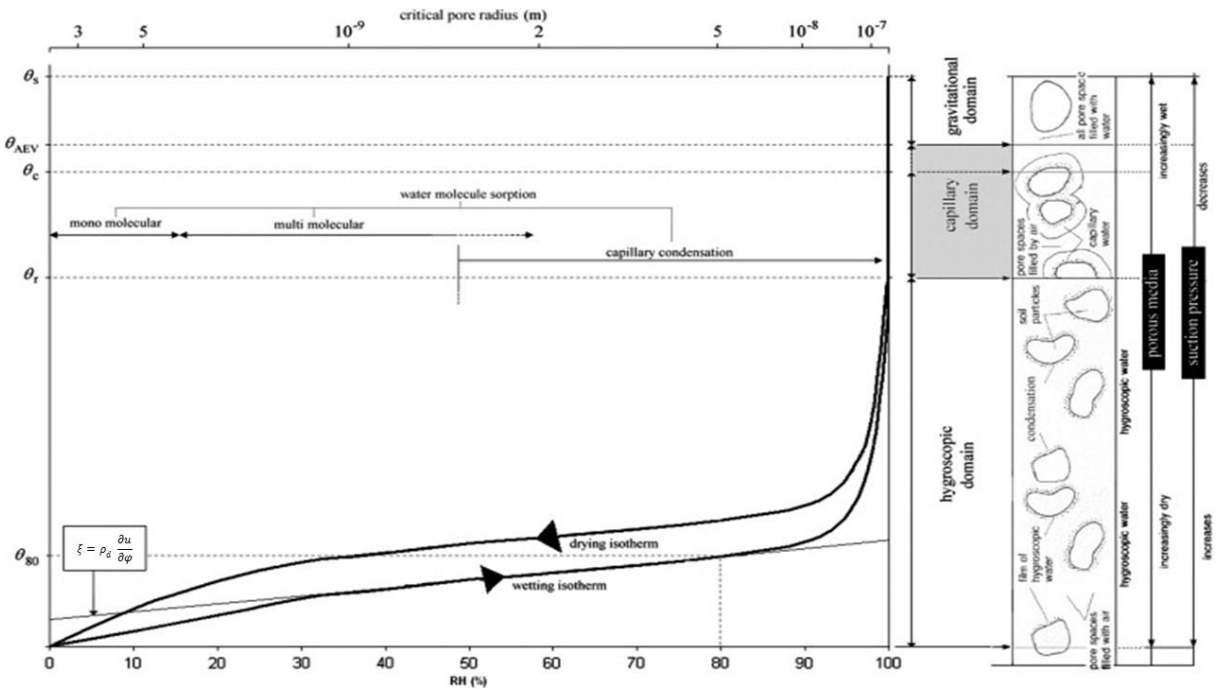

Figure 2.7- Sorption isotherm by Hall & Allinson (2009)

From the isotherms is also possible to obtain the moisture capacity, ξ [kg/m^3], by the following equation 7:

$$\xi = \rho_d \frac{\partial u}{\partial \varphi} \quad (7)$$

where $\frac{\partial u}{\partial \varphi}$ is the average slope of the isotherm and ρ_d the dry density [kg/m^3].

2.3. Moisture transport

According to several studies (Hall & Allinson, 2009; Henriques, 2007; Hens, 2012; Soudani et al., 2016) the mass transfer can be divided in water vapour diffusion and liquid water transport.

2.3.1. Water vapour diffusion

The diffusion process is a response to a gas concentration gradient where a natural redistribution of that concentration will occur until an equilibrium is reached. This generates molecular movements to the direction of lower concentration (Fredlund & Rahardjo, 1993; Henriques, 2007; Hens, 2012). As explained elsewhere (Fredlund & Rahardjo, 1993; Hall & Allinson, 2009; Henriques, 2007; Kunzel, 1995), this phenomenon can be described by the Fick's law. If air pressure is kept equal to the atmospheric pressure and under the assumption of perfect gases, the concentration of vapour in air is directly linked to its partial pressure, and the Fick's law writes in the form of eq. 8:

$$\boldsymbol{g}_v^a = -\delta_a \, \mathbf{grad}(p_v) \tag{8}$$

where $\boldsymbol{g}_v^a$ is the vapour flux density vector [kg/(m^2.s)] due to free diffusion in air, δ_a is a form of the vapour diffusion coefficient within air (s) and $\mathbf{grad}(p_v)$ is the vapour pressure gradient.

Earth materials as porous materials have open and connected voids through which the water vapour can diffuse. Generating under given conditions a flow, its rate is quantified by the water vapour permeability of a material, and it can be obtained according to the standard EN ISO 12572:2001 for building materials and products. The effective water vapour diffusion within the material is denoted by δ_p [Kg/(m.s.Pa)]. Similarly to δ_a, it is defined as the mass of water vapour transferred by time through the specimen thickness, divided by the water vapour pressure between the two faces of a specimen (Henriques, 2007; McGregor, 2014). Most often in the literature it is common to characterize and express the water vapour effective diffusivity using the water vapour resistance factor, μ, which relates the ratio between δ_a and δ_p (eq. 9):

$$\mu = \frac{\delta_a}{\delta_p} \tag{9}$$

It follows that, when vapour diffusion within the porous network is considered, the Fick's law changes in the form of eq. 10:

$$\boldsymbol{g}_v = -\delta_p \, \mathbf{grad}(p_v) = -\frac{\delta_a}{\mu} \, \mathbf{grad}(p_v) \tag{10}$$

where $\boldsymbol{g}_v$ is the vapour flux density vector due to diffusion within the porous network.

2.3.2. Liquid water transport

The flow of water within the material is depicted by the generalized Darcy's law (eq. 11):

$$\boldsymbol{g}_L = -D_L (\, \mathbf{grad}(p_L) - \rho_L \boldsymbol{f}) \tag{11}$$

where $\boldsymbol{g}_L$ is the liquid flux density vector [kg/(m^2.s)], D_L is the permeability coefficient (s), $\mathbf{grad}(p_L)$ is the liquid pressure gradient, ρ_L is the liquid density and $\boldsymbol{f}$ is the gravity [m/s^2]**.** This expression underlines that, depending on the direction of the pressure gradient, water inside a porous material can flow between open pores with movements that can contradict gravity, known as capillarity.

This action is originated by the cohesion between water and air molecules and their adhesion to pore walls and depends on the pores size, surface tension and the contact angle. Liquid molecules cohesion causes the surface tension; all the molecules attract each other, but the ones close to the surface with air have weakest

attraction. In these molecules the attractions forces are not in equilibrium which leads to a rearrangement of these forces. If these surface molecules also touch a pore wall, the rearrangement will occur in two ways depending on the stronger connection between the air and water molecules or water molecules and pore walls. The characteristic that determines the previous phenomenon is the contact angle.

In the first case, stronger attraction between air and water, it means that the contact angle with the pore walls is bigger than 90°; the meniscus is pushed away in a convex shape, designated by hydrophobic behaviour. Otherwise if the water is more attracted to the pore walls, the meniscus in a concave shape adheres to the wall, with a contact angle smaller than 90°; the walls behaviour is hydrophilic.

As explained elsewhere (Fredlund & Rahardjo, 1993; Henriques, 2007; Hens, 2012; Kunzel, 1995), if the Young-Laplace equation that relates the capillary pressure gradient Δp and the surface tension σ is considered (eq. 12):

$$\Delta p = \sigma C \tag{12}$$

where C is a meniscus medium curvature, which depends on the radius in orthogonal directions, if a circular tube with the same radius in both directions is considered and $C = 2/r$. Therefore the last equation can be written as eq. 13:

$$\Delta p = \frac{2\,\sigma\,\cos\theta}{r} \tag{13}$$

In this expression θ is the contact angle and r is the tube radius. In a hydrostatic equilibrium eq. 14 is:

$$h = \frac{2\,\sigma\,\cos\theta}{r\,\rho\,g} \tag{14}$$

and h is the liquid height, ρ the density and g the gravity acceleration. To clarify this relation a scheme is presented in Figure 2.8. It is possible to observe that, as said before, the contact angle and the pore size influences the capillary rise, the smaller those are the higher will be the liquid height.

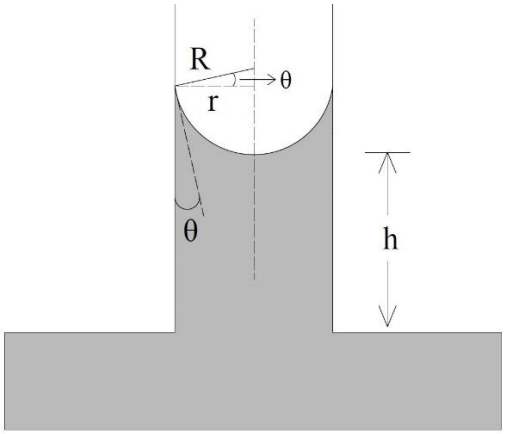

Figure 2.8- Capillary action within a pore

The water permeability coefficient strongly depends on the water content of the material. Several expressions exist to evaluate this variation. For example, Kunzel (1995) proposes the relation (eq. 15):

$$D_L = 3.8 \left(\frac{A}{w_f}\right)^2 \cdot 1000^{\frac{w}{w_f}-1} \frac{dw}{d\varphi} \frac{M_w \varphi}{\rho_L RT} \quad (15)$$

where A is the water absorption coefficient [kg/(m^2.s$^{1/2}$)], w_f the free water saturation [kg/m^3], w the water content [%].

Considering these two forms of transport (water vapour diffusion and liquid water transport) and assuming that the variation of water vapour mass is negligible in comparison with the variation of liquid water mass, the overall conservation of water mass is in the form of eq. 16 (gravity is neglected):

$$\rho_d \frac{\partial u}{\partial t} = -\text{div}(\boldsymbol{g_l} + \boldsymbol{g_v}) = \text{div}[D_L \mathbf{grad}(p_L)] + \text{div}\left[\delta_p \mathbf{grad}(p_v)\right] \quad (16)$$

If equilibrium is assumed between liquid water and its vapour, the liquid pressure and the vapour pressure are linked through the Kelvin's law. It follows that the mass conservation of the overall water (both liquid and vapour) writes in the form of eq. 17:

$$\rho_d \frac{\partial u}{\partial t} = \text{div}\left[\left(3.8 \left(\frac{A}{w_f}\right)^2 \cdot 1000^{\frac{w}{w_f}-1} \frac{dw}{d\varphi} \frac{1}{p_{v,sat}} + \delta_p\right) \mathbf{grad}(p_v)\right] \quad (17)$$

The numerical application with A value of 0.39 kg/(m^2.s$^{1/2}$) and w_f equal to 259 kg/m^3 (Soudani et al., 2016) leads to $3.8 \left(\frac{A}{w_f}\right)^2 \cdot 1000^{\frac{w}{w_f}-1} \frac{dw}{d\varphi} \frac{1}{pv_{sat}} < 1^{-13}$ s, when $\varphi < 0.8$, which is strongly lower than common values of δ_p normally in the range of 2.5^{-11} s. In consequence of that, in this work which is focused on the hygroscopic domain (and thus on low water contents), only the diffusion process of vapour will be considered.

2.4. Heat transfer and hygrothermal coupling

Heat transfer, is divided in three different phenomena:

- conduction;
- convection;
- radiation.

They can be easily explained as heat transfers occurring at the surface of the materials (convection and radiation) and the heat transfer inside the material, conduction (Hall & Allinson, 2009; Henriques, 2007; Hens, 2012).

Earth buildings provide poor performance when dealing with heat conduction in the building elements; therefore, earth is a poor insulation. Fourier formulated the relation between the heat flux q and the temperature gradient, defining the follow equation 18:

$$\boldsymbol{q} = -\lambda \, \mathbf{grad}(T) \quad (18)$$

where λ [W/(m.°C)] is the thermal conductivity, defining the capacity of the material to conduct heat; the lowest this value the best. In fact it is the characteristic to predict the amount of heat that can cross a building material. The presence of water in a porous material will directly influence its thermal conductivity, since water has a higher value of λ than air. This is the first hygrothermal coupling: in hygroscopic building materials the lambda value increase with water content.

2.4.1. Thermal inertia

The thermal inertia is a material characteristic that can be defined as the capacity to impact (damping or slowing) the penetrating heat flow (Heathcote, 2011; Henriques, 2007). It is directly related to the bulk of the material and, for building elements, with their thickness as explained by several authors (Heathcote, 2011; Henriques, 2007; Medjelekh et al., 2016; Orosa & Oliveira, 2012; Serrano et al., 2016; Tonelli & Grimaudo, 2014).

Thermal inertia can be characterized by the thermal diffusivity a (m^2/s) which "defines the capacity of a material to be heated quickly" (Medjelekh et al., 2016), and it is given by equation 19:

$$a = \frac{\lambda}{\rho \cdot c_p} \tag{19}$$

where c_p is the specific heat [J/(kg.°C)] and ρ the bulk density [kg/m^3]. Of course this is a simple explanation of the concept to introduce this performance in earth buildings.

This characteristic is highly recognized in old buildings with heavy construction, large thickness and high mass of the elements (Henriques, 2007; Orosa & Oliveira, 2012; Tonelli & Grimaudo, 2014). Some of them are built with earth; depending on the construction technique the thickness may vary but in general earth buildings have large walls. In old construction they were made with thicknesses between 0.5m to 1m (Serrano et al., 2016), but with modern construction there has been a reduction for values for 0.2m to 0.3m. In the opinion of Heathcote (2011), the earth walls should have at least 0.45m of thickness and it was studied by Taylor et al. (2008) that rammed-earth walls with 0.3m thickness does not give the same indoor comfort.

Earth is a material with a high density; when freshly dug it has a density of 1000 to 1500 kg/m^3, and if it is compressed as in rammed earth or in blocks the values can reach between 1700 to 2200 kg/m^3 (Minke, 2009). Both these properties, as explained before, confirms the good behaviour of earth buildings to attenuate temperature variations through their thermal inertia and providing a greater comfort for the inhabitants.

As explained before one characteristic that influences the thermal inertia is the specific heat, that in turn depends on the temperature (Laurent, 1984). In conclusion, heat transfer properties of earth building materials are dependent on the water content of a material and also the temperature.

2.4.2. Heats involved in sorption/desorption process

2.4.2.1. Integral heat of sorption

The sorption process is associated with heat exchanges. Condensation of water vapour into liquid water at constant temperature will induce heat supply, while evaporation process at constant temperature will consume heat. This phenomenon is quantified by the integral heat of sorption (or integral molar enthalpy of condensation) which is defined as the difference between the molar enthalpies of liquid and water vapour.

For a non-isothermal system, the integral heat of sorption influences the temperature. Indeed, the input of energy required for the evaporation of liquid water causes a reduction in the surrounding temperature, while the energy released by the condensation process increases the temperature. Integral heat of sorption can be interesting in both climates. It may provide passive evaporative cooling in hot climates and some recent work by Holcroft & Shea (2012) suggest that it could provide some passive heating in cold climates, for example if rising humidity levels occurs during occupancy. However, a proper use of this ability requires an appropriate design of the building.

2.4.2.2. Isosteric heat

Another way to quantify the exchange of heat due to the phase change is the isosteric heat (or absolute value of the differential molar enthalpy of sorption), which is equal, at constant pressure, to the partial derivation of the enthalpy difference with respect to material quantity (mole).

The use of this quantity is common because it can be quite easily measured. In particular, it is equal, at first approximation, to the heat flow caused by the adsorption process divided by the rate of adsorption. It can also be derived through the Clapeyron's relation from the analysis of sorption curves at several temperatures.

The study of this source of heat concerning unconventional building materials is quite novel. All the process and calculations are described in F. Rouquerol et al. (1999), where it is applied to clays but with argon and nitrogen as adsorbents.

The quantification of the isosteric heat from water vapour sorption isotherms at several temperatures allows the determination of the energies involved during the process which help to a better knowledge of this phenomenon. It had been already made for cement-materials (Poyet, 2009; Poyet & Charles, 2009), hemp concrete (Aït Oumeziane et al., 2016) and also for clays (Mihoubi & Bellagi, 2006). The general tendencies which is observed is an increase of the isosteric heat (in absolute values) when the water content decrease.

Theoretically, the isosteric heat and the integral heat of sorption are not equal. However, even in the hygroscopic domain, if the water content remains sufficiently high (more than 0.5% to 1%, in function of the specific surface of the material), these two enthalpies of phase change can be assumed to be, at first order, equal.
In the following of this manuscript, even if it is not strictly correct, the term "**heat of sorption**" is used to refer to either "integral heat of sorption" or to opposite of the "isosteric heat".

2.5. Synthesis on hygrothermal coupling

A coupling between thermal and hygric properties is possible to be made. As explained before, the presence of water is a common factor that have directly an impact on different characteristics concerning the heat transfer and sources. In turn the presence of water and its transport can be influenced by the temperature. At this point is possible to question the existence of the correlation in Figure 2.9 (kindly provided by Antonin Fabbri):

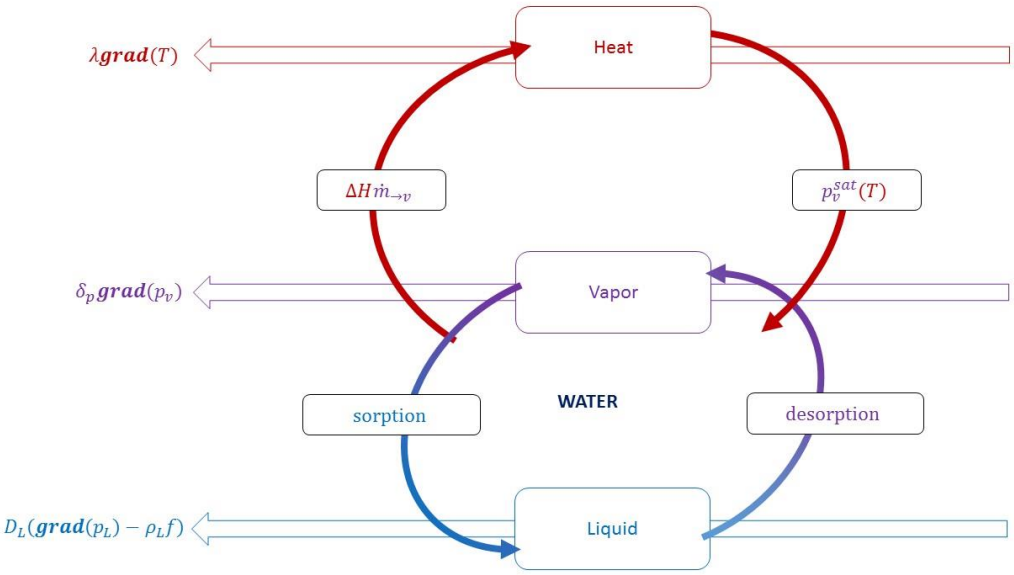

Figure 2.9- Hygrothermal coupling

This coupling is essential to define the global hygrothermal behaviour of a material, which can bring many advantages concerning the well-being of the inhabitants but also for material durability (McGregor et al., 2014). The study of this behaviour concerning earth based materials still is a major scientific and technical challenge. Several studies had been made. Cagnon et al. (2014) measured the hygrothermal properties for extruded earth bricks. Hall & Allinson (2009;2010) analysed the hygrothermal behaviour of stabilised rammed earth, firstly in samples made on the laboratory and after in full scale building. Similar studies had been made but for clay composites as Liuzzi et al. (2013) with unstabilised and lime stabilised clays, McGregor with several articles for unfired clay masonry and more recent Labat et al. (2016) in straw-clay mixtures.

In conclusion, many studies have been made in order to quantify and analyse these characteristics concerning different earth techniques and different sample compositions, but for earth there is a lack of information about the influence of reproducing the experimental tests at different temperatures and analysing the consequences that the energies involved have on the hygrothermal behaviour.

3. Materials and methods

The experimental campaign of this dissertation starts in this chapter. Therefor this chapter describes the tested materials and also the methods used to determine the influence of temperature on the hygroscopic behaviour. At first, the purpose of the experimental protocol is to well understand the tests and their differences, comparisons and variations that can occur regarding different assumptions.

Secondly, and only after the influence of the experimental set ups and protocols is well defined, can be studied the influence of reproducing these tests at different temperatures and their influence on the hygroscopic behaviour of the samples.

3.1. Materials

The materials used in this study are all earth materials with clay as a binder. They can be divided in two categories: earth plasters and compressed earth block samples.

3.1.1. Earth Plasters

For earth plasters four different mortars were tested. They are represented by the main type of clay or commercial name:

- Kaolinite (F0);
- Ascal 10 (F3) is a fine calcareous-clay material from “Carrières du Boulonnais”;
- Enduit C (F5) is a commercial mortar proposed by “Carrière du Boulonnais”; no additional information is known;
- Kaolinite + Montmorrilonite (F6) same formulation as F0 but with the addition of Montmorrilonite.

The following formulations presented in Table 3.1, Table 3.2, Table 3.3 and Table 3.4, were used to prepare the samples, already done by ENTPE with the procedure described by Simões (2015).

Table 3.1- Formulation of F0 plaster

F0	Sand (0/2)	Kaolinite	Water	Sraw (3-5cm)
Volume (l)	15.54	7.77	9.71	15.54
Mass (kg)	23.59	8.00	9.71	0.81

Table 3.2- Formulation of F3 plaster

F3	Sand (0/2)	Ascal 10	Water	Sraw (1-3cm)
Volume (l)	16	-	8.51	-
Mass (kg)	24	11.06	8.51	0.78

Table 3.3- Formulation of F5 plaster

F5	Enduit C	Water
Volume (l)	-	5.70
Mass (kg)	34.4 (32)	5.70

Table 3.4: Formulation of F6 plaster

F6	Sand (0/2)	Kaolinite	Montmorillonite	Water	Sraw (3-5cm)
Volume (l)	15.54	7.67	0.09	9.71	15.54
Mass (kg)	23.59	7.9	0.1	9.71	0.81

With the described formulations it is possible to characterize the samples according to their clay, fibre and water content, see Table 3.5.

Table 3.5- Mass percentage of clay, fibre and water content of earth plasters

	F0	F3	F5	F6
Clay content % (< 2µm)	19.00	3.49	-	19.00
Fibre content %	1.92	1.76	-	1.92
Water content %	23.06	19.19	14.20	23.06

3.1.2. Compressed earth block

For the compressed earth blocks (CEB) also four different formulations were tested, denoted by:

- CRA;
- ALX;
- STR;
- STA.

Their composition are presented in Table 3.6:

Table 3.6: Properties of the compressed earth blocks

	CRA	ALX	STR	STA
Main clay minerals	Illite + Kaolinite	Illite + Vermiculite	Illite + Chlorite	-
Clay content% (< 2µm)	16	6	15	16
Bulk density (g/cm^3)	1.97	1.98	1.95	1.75
Porosity (%)	26	26	25	35

These samples came from existing rammed earth constructions in the South-East of France, “Rhône-Alpes” region. After the extraction they were prepared in ENTPE, being the procedure and properties described in (Chabriac et al., 2014; Champiré et al., 2016).

3.2. Tests procedure

3.2.1. Water vapour permeability

The water vapour permeability quantifies the water vapour flow rate through a porous material. It was performed according to the standard EN ISO12572 (CEN 2001) for vapour permeability of building materials, where the experimental procedure is described, as well as the associated calculations.

The experimental tests are divided in “wet cup” or “dry cup” with respectively the use of aqueous saturated solution or a desiccant. In the chosen protocol, both tests were performed. For the dry cup the aim is to obtain a dry constant value of RH inside the container, preferentially near 0%. To obtain this condition, first it was tested using silica gel and after with a salt solution of Potassium Acetate. The first one corresponding to an uncertain expected values of RH between 0% to 10% (Figure 3.1), and the second one to maintain a RH level of 23%. In the wet cup a salt solution of Potassium Chloride was used to obtain a saturated constant RH value of 85% - see Figure 3.2.

Figure 3.1- Dry cup samples with silica gel

Figure 3.2- Dry cup sample with salt solution

The samples are sealed to the top of the plastic container with a thin layer of silicon, complemented with an aluminium tape. Then they were stored in the Ineltec climatic chamber maintained at 23ºC and 40ºC with a RH level of 50% and 30%, respectively. These conditions and also the ones inside the container were continuously monitored by placing a sensor inside the container (Figure 3.3) and another in the chamber. Only the F0, F3 and F5 plasters were tested, in a total of nine specimens of each with 12cm of diameter and with thicknesses of 1, 2 and 4cm.

During the test, measurements were done daily approximately at the same hour. The total mass, composed by the sample, plastic cup and desiccant or salt solution, were weight in a scale outside the chamber until a constant variation of mass with time is reached. The mass variation rate corresponds to water vapour flux diffusing through the sample.

The mass variation with time can exhibit three different shapes; the first one corresponds to the equilibrium stage where the water vapour flow is dissipated through evaporation but a part is adsorbed by the sample; the second regards the permanent state where the water vapour flow reaches a constant rate; the last one occurs when the desiccant or the salt solutions are saturated or insufficient, respectively.

Figure 3.3- Example of a sample with a placed sensor

The calculations were performed according to the standard EN ISO 12572 (CEN 2001). The vapour flux, G, is given by the experimental results from the slope of the mass variation with time $= \Delta m/\Delta t$, which is then used to calculate the water vapour permeance, W (kg/(m^2.s.Pa)), with the following relation (eq. 20):

$$W = \frac{G}{A \cdot \Delta p_v} \tag{20}$$

where A (m^2) is the specimen surface area and Δp_v is the water vapour pressure difference across the sample. The vapour permeability, δ_p (Kg/(m.s.Pa)), can be obtained with eq. 21:

$$\delta_p = W \cdot d \tag{21}$$

where d is the sample thickness (m). Finally, for convenience the water vapour resistance factor is used, already explained before and given by the equation 8, in chapter 2.

The value of the water vapour permeability of air, δ_a, can be estimated from the relation given by Kunzel (1995) (eq. 22):

$$\delta_a = 2 \times 10^{-7} \frac{T^{0.81}}{p_0} \text{ [kg/(m s Pa)]} \tag{22}$$

where T is the ambient air temperature (K) and p_0 is the atmospheric pressure (Pa). This test was performed at 23ºC and 40ºC, at atmospheric pressure of 101325 Pa, leading to these two values of δ_a, 1.98x10^{-10} kg/(m s Pa) and 2.07x10^{-10} kg/(m s Pa), respectively.

The EN ISO 12572 (2001) standard proposes a correction for the resistance of the air layer between the sample and the salt solution. This correction is normally recommended when the water vapour diffusion-equivalent air layer thickness ($s_d = \mu \cdot d_p$) is lower than 0.2 m. It assumes that the transport of vapour within the cup is only made by diffusion (no convection) and it leads to the equation 23, where d_a is the thickness of the air layer between the salt solution and the sample:

$$\delta_p^{agc} = \frac{G \cdot d}{A \cdot \Delta P_V - G \frac{d_a}{\delta_a}} \;\; ; \;\; \mu^{agc} = \frac{\delta_a}{\delta_p^{agc}} \tag{23}$$

3.2.2. Sorption isotherms

The determination of the sorption isotherms were performed according to two tests: one consisted in the salts solutions method and the other using the Dynamic Vapour sorption (DVS) equipment. The first method presented the advantage that more and larger samples could be tested, but on the other hand it is a lengthy process with some lack of precision. As an example the fact that the samples are weighed outside the chamber; the process of opening the box and remove the samples clearly lead to a variation in the pretended conditions that can vary the weight. The DVS method is more precise as it works at microscale and all the process is made inside the equipment in a controlled environment, but only one sample at the time can be tested, with a limited weight of more and less 1 g. Therefore the representativeness of composite materials like clay-sand-fibre plasters and blocks may be compromised. However this will be verified in the further chapter.

3.2.2.1. Salt solutions

This method was followed by the standard EN ISO 12571 (CEN 2000). All the four CEB and the four plasters were tested, three representative samples of each, with more than 10 g, were placed in aluminium containers to avoid the loose of material - see Figure 3.4.

Figure 3.4- Example of samples used for the sorption isotherms test

At first the samples were dried to obtain the dry mass m_0, the compressed earth samples at 105ºC and the plasters at 50ºC to prevent degradation of the organic fibres. Then they were placed in levels of 23, 43, 53, 75 and 85 % of RH, each one maintained in a plastic box. This test was performed at 40ºC, controlled by a climatic chamber. The conditions inside the plastic boxes were constantly monitored by a sensor - see Figure 3.5.

The salts solutions were prepared according to the Annex B in the EN ISO 12571 (CEN 2000), each one made with different salts corresponding to the required RH - see Table 3.7.

Table 3.7- Salt solutions substances and respective RH at 23ºC

Substance	RH %
Potassium acetate ($KC_2H_3O_2$)	23
Potassium carbonate (K_2CO_3)	43
Magnesium nitrate [$Mg(NO_3)_2$]	53
Sodium chloride (NaCl)	75
Potassium chloride (KCl)	85

Figure 3.5- Samples placed in the plastic box for the sorption isotherms test

The samples were weighed daily with scales of an accuracy of 0.01g. If between three consecutive measurements the mass variation was less than 0.1%, it was considered that the equilibrium moisture content for the respective RH was achieved, and then those samples were able to be placed in the next level of RH. Each RH level took about a week and the equilibrium water content was calculated by the eq. 5, presented in the chapter 2. Plotting the water content over RH gives the adsorption curve (ascending order of RH) and the desorption curve (descending order).

3.2.2.2. Dynamic Vapour Sorption

The other method to determine the sorption isotherms consisted in using the "Intrinsic" model of the Dynamic Vapour Sorption (DVS). As explained before, only one sample at a time could be tested, yet allowing to obtain the adsorption and desorption curves in more or less a week. Also as explained before, this is a microscale process with small samples with a limited weight of 1g, the samples are carefully placed in a small cup - see Figure 3.6.

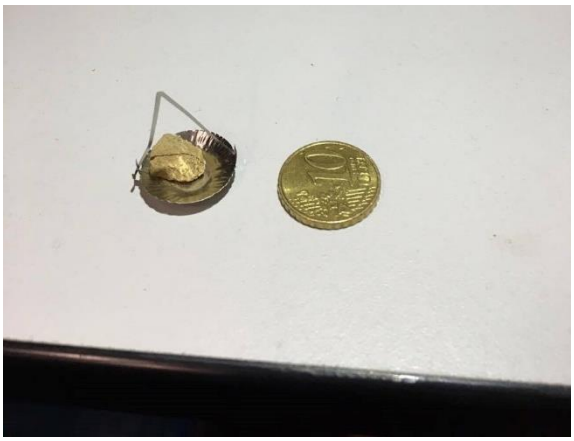

Figure 3.6- Example of a sample used for the DVS test

This method was performed according to McGregor et al. (2014), where several required assumptions were described:

1. Each step in RH during the DVS measurement is incremented either when a stable mass is achieved with less than 0.0001% mass change per minute or a maximum time interval of 600 min is reached for each RH step.

2. The adsorption at very high RH may be undervalued because total equilibrium could not be reached in the specified maximum time allocated, but this is not considered a problem as these high humidity levels are unlikely to be achieved for an extended period in a real building. However during the following tests more steps and longer time is given for higher RH therefore reducing the impact the underevaluation of the equilibrium moisture content.

All samples were tested under the same conditions at 23ºC and 30ºC. The DVS instrument was placed in a closed and air conditioned room (Fig. 3.7).

Figure 3.7- DVS equipment (Intrinsic 2, SMS®)

4. Standard characterization

4.1. Water vapour permeability

4.1.1. Dry cup

The first procedure used to determine water vapour permeability, consisted in performing the dry cup test using silica gel as desiccator (approximately 40 g) with a sensor placed inside the 1cm sample container. The collected experimental data from the water vapour permeability, representing the rate of mass variation over time were plotted in Figure 4.1, Figure 4.2 and Figure 4.3. The F0 and F3 samples showed a similar behaviour, different than the F5 samples, but clearly for all a constant mass variation over time was not reached.

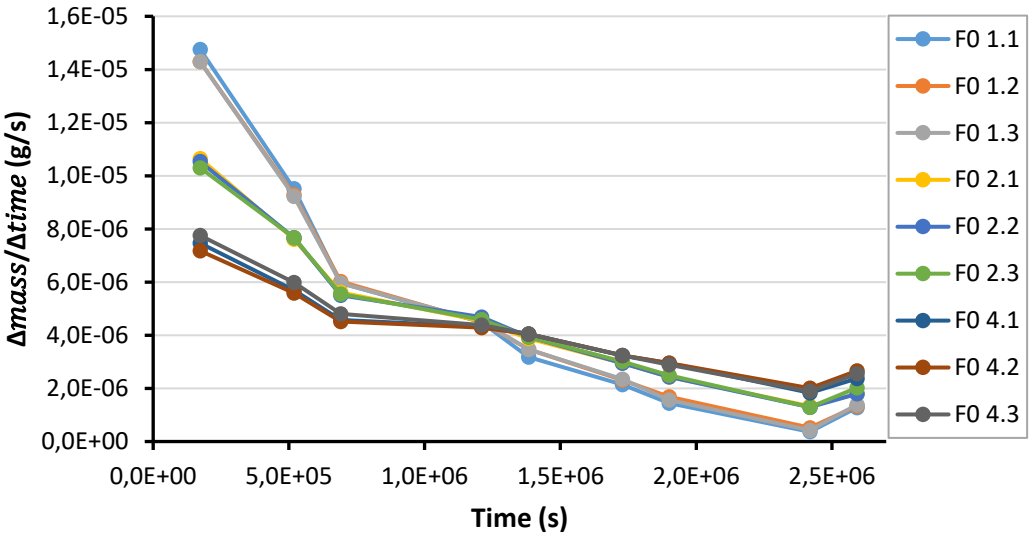

Figure 4.1- Rate of mass variation during the dry cup test (silica gel) of F0 earth plaster

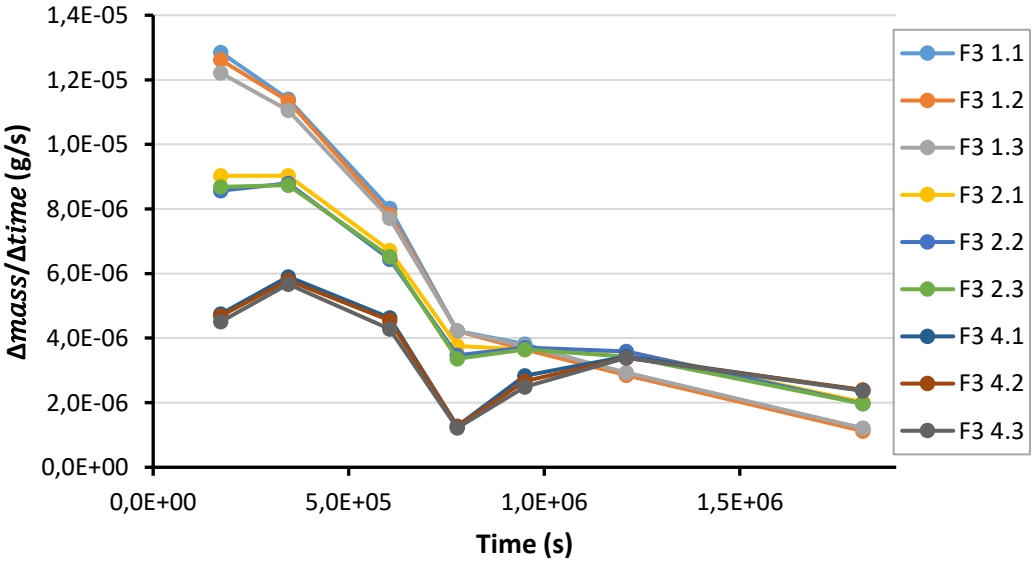

Figure 4.2- Rate of mass variation during the dry cup test (silica gel) of F3 earth plaster

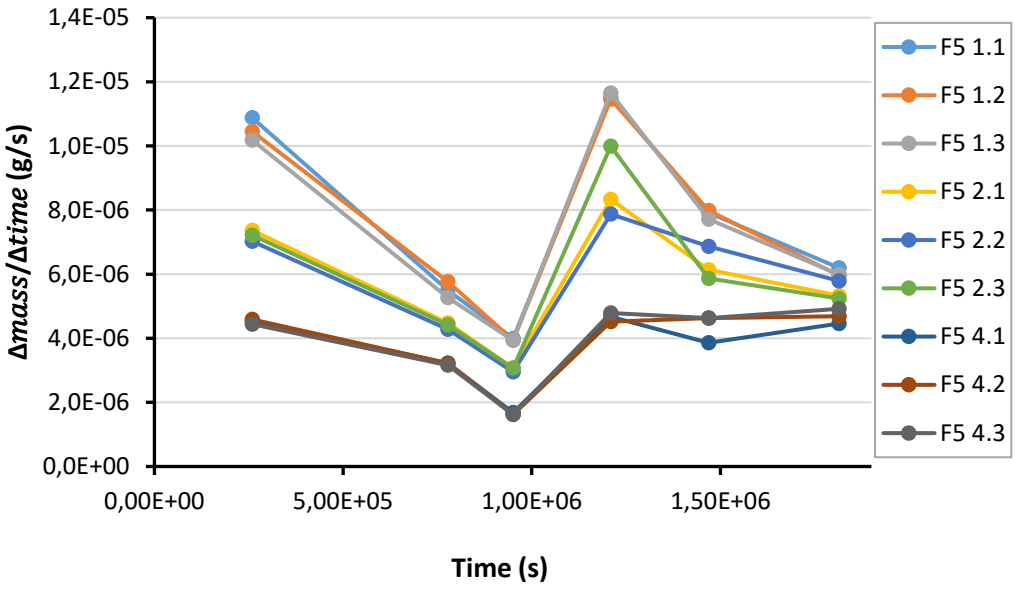

Figure 4.3- Rate of mass variation during the dry cup test (silica gel) of F5 earth plaster

During the tests it could be observed the fast saturation of the silica gel and by analysing the RH data collected from the sensor it was possible to see the constantly growing RH through time. The lowest value at the beginning was about 10% and at the end of the test RH had reached more than 30% - see Figure A.1 in appendix A. This explain the behaviour of the rate of mass variation and leads to refute silica gel as a desiccant.

Therefore, a new methodology was defined to the dry cup and a saline solution of Potassium acetate was used in substitution to the silica gel, which aim is to obtain a more stable RH level of 23%. The preparation of the samples were all the same and the air layer thickness within the cup was maintained to less than 2 cm according to recent recommendations in the literature (Vololonirina & Perrin, 2016). In one of each type of sample, the RH inside the container was monitored during all the test and the RH evolution are presented in appendix A. The experimental data was collected (rate of mass variation presented in appendix A.1) and the same calculations were done; results are presented in Table 4.1 with the respective inside RH levels.

Table 4.1- Average values of water vapour permeability and water vapour resistance factor for each earth plaster (Potassium acetate as desiccant)

Plaster	RH (%)	δ_p^{ap} (kg/s.m.Pa)	μ^{ap} (-)	
		Average	Average	Standard deviation
F0 1	27.8	1.75E-11	11.40	1.67
F0 2		1.85E-11	10.75	
F0 4		2.41E-11	8.24	
F3 1	28.5	1.29E-11	15.38	2.87
F3 2		1.55E-11	12.82	
F3 4		2.06E-11	9.65	
F5 1	27.6	1.01E-11	19.72	4.91
F5 2		1.37E-11	14.50	
F5 4		2.02E-11	9.90	

It can be observed that those results vary with the thickness of the material. The same tendency is observed in all specimens: the 1cm thickness resulted in higher values, 2cm and 4cm the middle and lower values, respectively. When the water vapour resistance is low, it can be due to the difference between vapour pressures at the surface of the material and the ones in the cup or chamber. It can be concluded that thinner samples are more affected by the external skin effect. These values came from the original calculation

without taking into account corrections that can be made for surface transfer resistance inside the cup and outside the cup; therefore two types of corrections were done.

The first correction consists in calculating the equivalent air layer thickness to the results. As follows in the standard EN ISO 12572 (CEN 2001), it is recommended to apply a correction which considers the resistance to diffusion of the air layer in the cup for materials with equivalent air layer thickness below 0.2 m. Yet to understand the variation observed due to the thickness of the material this correction was applied and the results are presented in Table 4.2.

Table 4.2- Average values of water vapour permeability and water vapour resistance factor for each earth plaster after the ISO correction (Potassium acetate as desiccant)

Plaster	**δ_p^{agc} (kg/s.m.Pa)**	**μ^{agc} (-)**	
	Average	Average	Standard deviation
F0 1	2.14E-11	9.40	1.08
F0 2	2.04E-11	9.75	
F0 4	2.57E-11	7.74	
F3 1	1.48E-11	13.38	2.14
F3 2	1.68E-11	11.82	
F3 4	2.17E-11	9.15	
F5 1	1.12E-11	17.72	4.16
F5 2	1.47E-11	13.50	
F5 4	2.13E-11	9.40	

At this point the variation between thicknesses lead to wonder if the ISO correction is enough. With the water vapour diffusion through the sample some convection happens at the boundaries especially on the outer surface, not taken into account by the ISO correction. This leads to propose further correction, which consists in calculating the real partial vapour pressure at the exposed surface of the sample (p_{v1}^*) based on partial pressure measured in the chamber (p_{v1}) and a surface transfer coefficient (β) - see Annex A.2. With this correction the water vapour permeability expression is given by eq. 24:

$$\delta_p^{\beta} = \frac{d}{\frac{s \cdot \Delta P_v}{G} - \left(\frac{d_a}{\delta_a} + \frac{1}{\beta}\right)} \tag{24}$$

where β is the surface transfer coefficient. This value was obtained according to the one used by Vololonirina et al. (2014). This method consists in plotting the ratio of material thickness over water vapour permeability obtained from the ISO correction as a function of the material thickness - see Figure 4.4. When the thickness tends to zero, the vapour flow resistance is only due to the external skin effect and this surface film resistance values, Z^s, are obtained from a linear regression. The inverse of Z^s gives the related transfer coefficient β - see Table 4.3.

For the β correction the values are much more similar, with less influence of the thickness. Figure 4.5 clearly evidence this statement. For the first calculations F0 had the lowest values, followed by the F3 and F5, respectively. However this trend is not persistent for the β coefficient correction, where the values are very close to each other and even F5 reached the lowest values. For a better evaluation of the final results the relative error was calculated (R error) to analyse the thickness effect and also the error that a ± 2% difference in the chamber RH would provoke (RH error). The results are presented in Table 4.4. For both F5 exhibited the biggest error with 16.6% for the repeatability and 23.8% for the RH variation, F0 and F3 presented lower and similar values, with the difference of a bigger percentage of F0 concerning the repeatability.

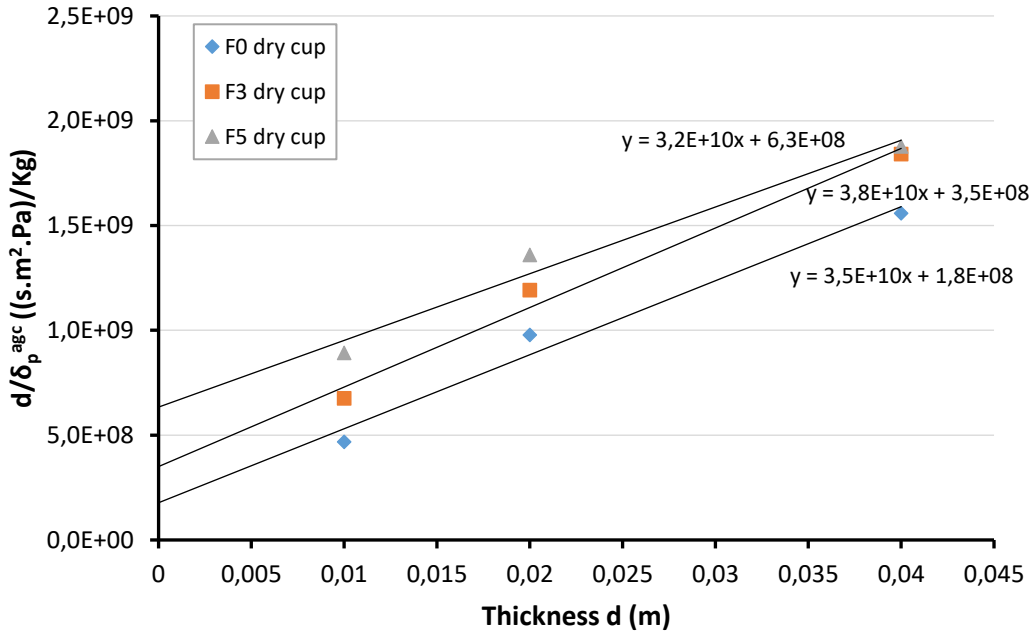

Figure 4.4 – Evolution of d/δ_p^{agc} as a function of the earth plasters thicknesses

Table 4.3- Average values of water vapour resistance factor for each earth plasters after the β correction proposed by Vololonirina et al. (2014) (Potassium acetate as desiccant)

Plaster	δ_p^{agc}	d/δ_p^{agc}	Intersection point (Z^s)	β	μ^β	Standard deviation
F0 1	2.14E-11	4.68E+08	1.78E+08	5.63E-09	5.88	1.06
F0 2	2.04E-11	9.78E+08			7.99	
F0 4	2.57E-11	1.56E+08			6.85	
F3 1	1.48E-11	6.71E+08	3.50E+08	2.85E-09	6.44	0.96
F3 2	1.68E-11	1.19E+09			8.35	
F3 4	2.17E-11	1.84E+09			7.41	
F5 1	1.12E-11	1.13E-11	6.34E+08	1.58E-09	4.94	0.99
F5 2	1.47E-11	1.48E-11			6.91	
F5 4	2.13E-11	1.98E-11			6.00	

Table 4.4- Relative error and the error of ± 2 % RH in the chamber on the Dry cup test for the earth plasters

Plaster	R error (%)	± 2% RH error (%)
F0	15.3	17.6
F3	12.9	17.9
F5	16.6	23.8

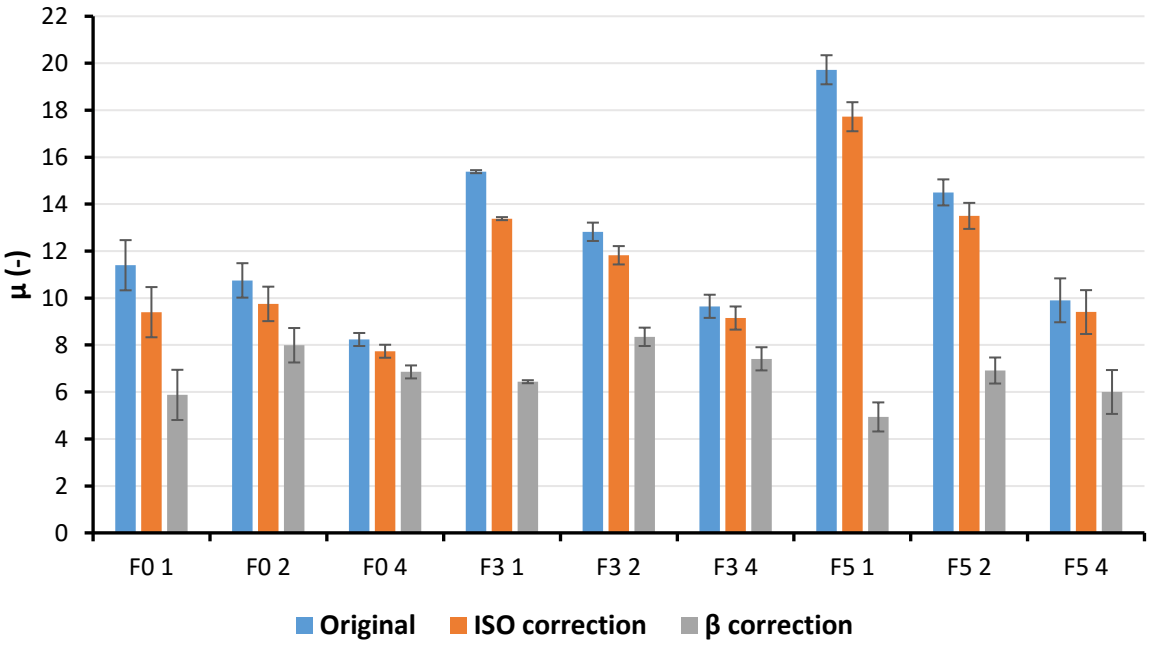

Figure 4.5- Comparison between the water vapour resistance factor results for the earth plasters (Potassium acetate as desiccant)

4.1.2. Wet cup

Once finished the dry cup test, this new methodology was applied to the results of the wet cup test at the same temperature of 23ºC, in order to study their comparability and reliability. The conditions of the RH levels are different and consist in an inside RH level of 85% and the Ineltec chamber was maintained at a RH level of 60%. The results of the original calculation, ISO correction and the β correction according to the new method are presented in Table 4.5, Table 4.6 and Table 4.7, respectively.

Table 4.5- Average apparent values of water vapour permeability and water vapour resistance factor for each earth plaster (Potassium chloride as saturated solution)

Plaster	**δ_p^{ap} (kg/s.m.Pa)**	**μ^{ap} (-)**	
	Average	Average	Standard deviation
F0 1	1.06E-11	18.56	4.01
F0 2	1.42E-11	13.90	
F0 4	1.86E-11	10.57	
F3 1	1.06E-11	18.65	4.02
F3 2	1.39E-11	14.20	
F3 4	1.86E-11	10.62	
F5 1	8.16E-12	24.15	4.92
F5 2	1.09E-11	18.11	
F5 4	1.37E-11	14.41	

Table 4.6- Average values of water vapour permeability and water vapour resistance factor for each earth plaster after the ISO correction (Potassium chloride as saturated solution)

Plaster	δ_p^{agc} (kg/s.m.Pa)	μ^{agc} (-)	
	Average	Average	Standard deviation
F0 1	1.31E-11	15.06	2.68
F0 2	1.62E-11	12.15	
F0 4	2.03E-11	9.70	
F3 1	1.30E-11	15.15	2.70
F3 2	1.58E-11	12.45	
F3 4	2.02E-11	9.74	
F5 1	9.54E-12	20.65	3.58
F5 2	1.20E-11	16.36	
F5 4	1.46E-11	13.53	

Table 4.7- Average values of water vapour resistance factor for each earth plaster after the β correction proposed by Vololonirina et al. (2014) (Potassium chloride as saturated solution)

Plaster	δ_p^{agc}	d/ δ_p^{agc}	Intersection point (Z^s)	β	μ^{β}	Standard deviation
F0 1	1.31E-11	7.64E+08	3.97E+08	2.52E-09	7.18	0.52
F0 2	1.62E-11	1.23E+09			8.21	
F0 4	2.03E-11	1.97E+09			7.73	
F3 1	1.30E-11	7.69E+08	4.12E+08	1.98E-09	7.27	0.63
F3 2	1.58E-11	1.26E+09			8.51	
F3 4	2.02E-11	1.98E+09			7.77	
F5 1	9.54E-12	1.05E+09	5.05E+08	2.42E-09	10.80	0.32
F5 2	1.20E-11	1.66E+09			11.43	
F5 4	1.46E-11	2.75E+09			11.07	

4.1.3. Comparison between wet and dry cup test

By analysing the results obtained by both the dry cup and wet cup, see Table 4.8, it is clearly visible that the dry cup test gives lower values of water vapour resistance, but comparing in order of magnitude they are very consistent: the lowest value of the dry cup also corresponds to the lowest in the wet cup and so on. Moreover, if the values are plot in a graph with a line indicating equality, see Figure 4.6, the F0 and F3 are almost over the line, which leads to state the comparability between the tests. However, if the F5 sample is analysed the same does not happen; the values present the biggest difference between them and it is difficult to justify this phenomenon since not all the information about its composition is known.

From now on it was decided to exclude the F5; this sample was not developed in the laboratory and so there is too much lack of information about its composition and formulation, which was not provided. Therefore, it becomes difficult to draw a proper analysis and conclude with the obtained results.

Table 4.8- Comparison between the results of water vapour resistance of plasters obtain by the dry cup and wet cup

	μ^{β} Dry cup	Variation	μ^{β} Wet cup	Variation
F0 1	5.88	0.15	7,18	0.07
F0 2	7.99		8.21	
F0 4	6.85		7.73	
F3 1	6.44	0.13	7.27	0.08
F3 2	8.35		8.51	
F3 4	7.41		7.77	
F5 1	4.94	0.17	10.80	0.03
F5 2	6.91		11.43	
F5 4	6.00		11.07	

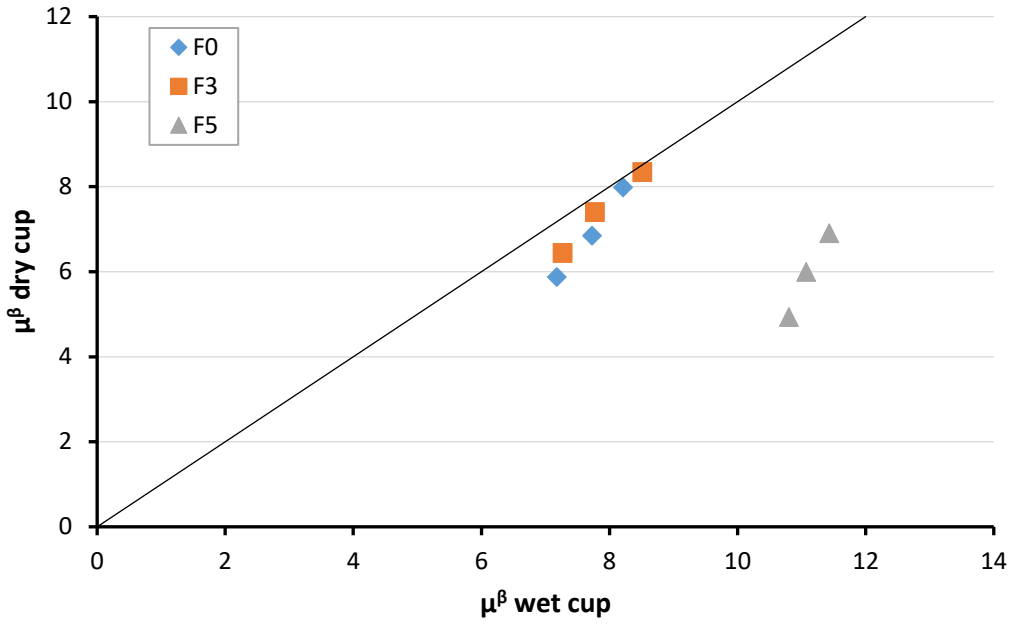

Figure 4.6- Comparison between the water vapour resistance of the dry cup and wet cup

By the results presented from literature in Table 4.9, the obtained values for F0 and F3 are slightly lower than the normal range for this type of materials with **μ** between 8-10. The oldest results of Lustig-Rossler (1992) reached values between 8 and 9 for adobe, silt and clay; the newest ones between 8 to 13 (Dubois et al. 2014a; Faria, dos Santos, & Aubert, 2015; Liuzzi et al., 2012; McGregor, 2014).

Cagnon et al. (2014) also did a comparison between the dry cup and wet cup for earth bricks performed at 20ºC; their trend was much different from the one obtained in this dissertation. They reached higher water vapour resistance values for the dry cup than the ones for the wet cup, whereas similarity was obtained in this dissertation between the dry cup and the wet cup.

More recently Labat et al. (2016) tested straw-clay samples by both dry and wet cup and reached the values of 4.8 and 2.9, respectively. Those are much lower values than the ones obtained in this dissertation. However in the article no reference to the formulation and composition of the samples is made, which makes difficult a proper comparison.

Indeed is very difficult to obtain very accurate results from this test. As demonstrated any small variation on the test conditions may lead to different results, moreover to make an exact comparison with literature results. This was prove by Roels et al. (2004) in a comparison of the water vapour resistance results for the same material in different laboratories, with a final conclusion that the range of variation in the measured results was very large.

Table 4.9- Values for water vapour resistance from literature

Reference	Type of sample	Number of samples	Method	Temperature (ºC)	μ
F0		3	Dry cup	23	5.9- 8.0
		3	Wet cup	23	7.2- 8.2
F0		3	Wet cup	40	7.4
F3		3	Dry cup	23	6.4- 8.4
		3	Wet cup	23	7.3- 8.5
F3		3	Wet cup	40	8.6
Lustig-Rössler (1992)	Adobe, silt, clay	5	-	-	8- 9
Hansen & Hansen (2002)	Unfired clay	3	-	-	12.5- 13.1
Ramos et al. (2010)	Gypsum	-	Wet cup	23	7.1
Allinson & Hall (2010)	Rammed earth	4	Wet cup	-	14.3
Liuzzi et al. (2013)	Clays	6	Wet cup	23	8.8- 11.1
Cagnon et al. (2014)	Earth bricks	5	Dry cup	20	7- 19
			Wet cup	20	3- 7
Dubois et al. (2014)	CEB	6	Wet cup	23	8.3- 8.8
McGregor, (2014)	Clay plasters	24	Wet cup	23	9- 13
	CEB	90			6- 13
Faria, dos Santos, & Aubert (2015)	Earth plasters	-	Wet cup	23	8
Labat et al. (2016)	Straw-clay	3	Dry/Wet cup	23	4.8 / 2.9

4.2. Sorption isotherms

As explained in chapter 3, the sorption isotherms were determined using the salt solution and DVS method, the first one calculated using the eq. 6 and the second by the software itself. It calculates the isotherms based on the ratio of $\frac{\delta m}{\delta t}$, but firstly the dry mass must be obtained during the 0% RH stage and then only after the cycle starts. For the salt solution method the dry mass is obtained, as explained in chapter 3., by placing the plasters and the compressed earth samples in the oven at 50ºC and 105ºC, respectively. For the dry mass it is considered that it correponds to a water content of 0% as well as a RH level of 0%, although this assumption for the earth plasters may not be valid as it is very difficult to obtain this conditions at a 50ºC in the oven.

4.2.1. Earth plasters

The sorption curves of the plasters obtained at 23ºC by the method of the salt solutions and the DVS, are presented in Figures 4.7 and 4.8, respectively. The three formulations follow the same trend in both methods: a linear increase of the water content from 0% RH to 60% RH is then followed by a sharp increase until 97% RH.

F6 (only in DVS) and F0 reached higher values of moisture content, about 2.6% and 2.5% at 97% RH, respectively; moreover by the salt solutions F0 reached 2.7%. Followed by the F3 with a maximum water content of 2% in both methods and, finally, the F5 sample with 1.2% in the salt solutions and 1% in the DVS. These results might be explained by the water contents used for the mixture process; as described in

the Table 3.4, 23% for F0 and F6, 19% and 15% for F3 and F5, respectively. Higher water contents in the mixture leads to higher porosity (swelling process), which in turn may increase the w value. Futhermore, F0 clay mineral is a pure Kaolinite similar to F6 but in this last mortar with the addition of montmorillonite, that increase the charged surface and may explain the higher level of water content. For F3 and F5 the exact compostion of clay mineral proportions is unknwon.

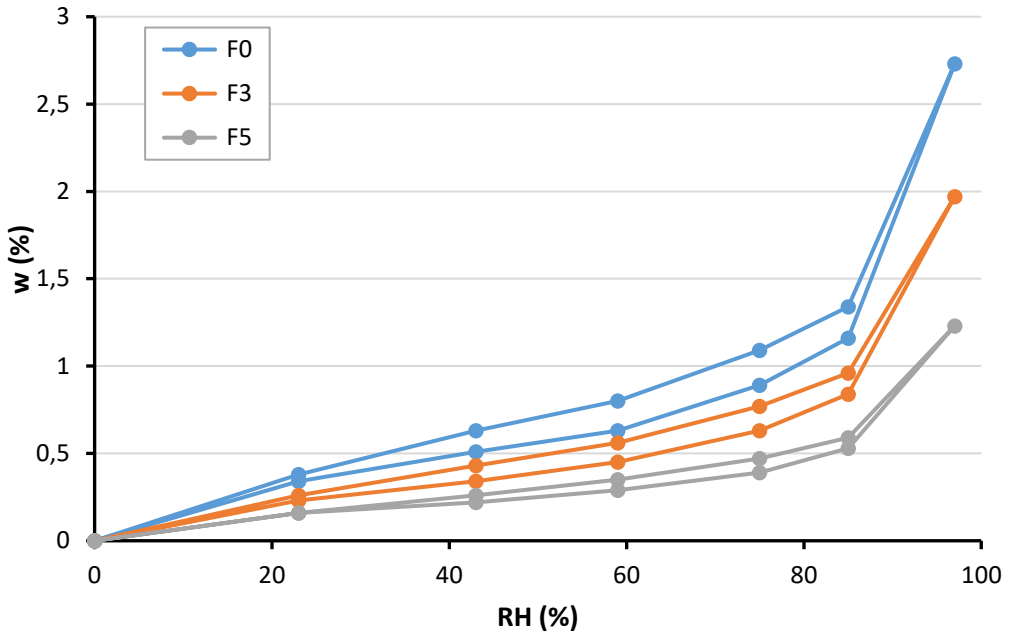

Figure 4.7- Sorption isotherms for the earth plasters (F0, F3 and F5), by the salt solutions test at 23ºC

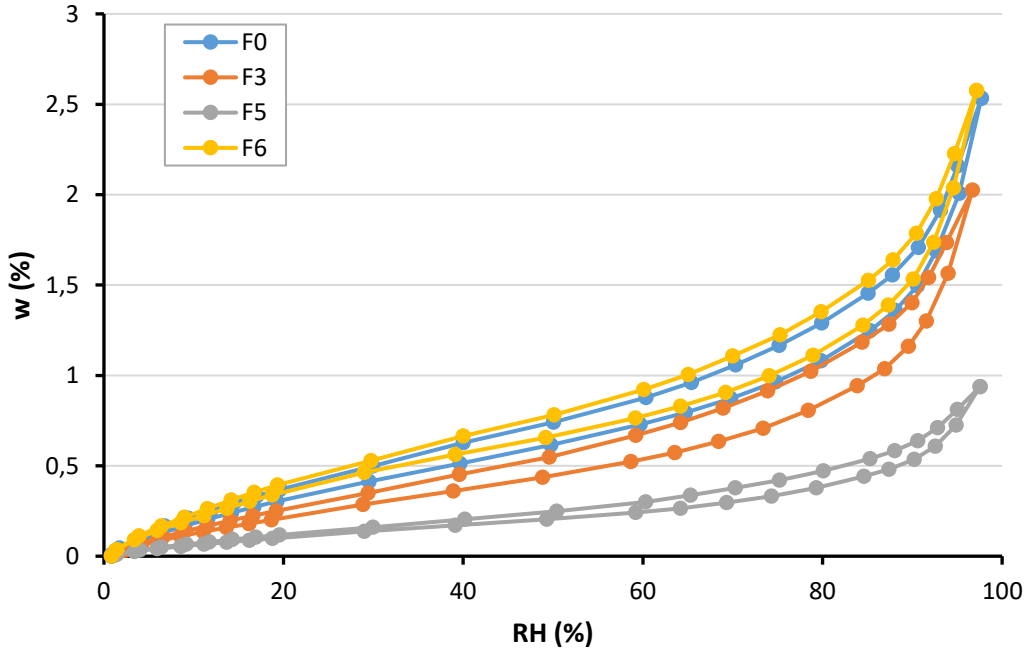

Figure 4.8- Sorption isotherms for the earth plasters (F0, F3, F5 and F6), by the DVS method at 23ºC

By analysing the results with the ones presented in literature, there is no much information concerning the sorption isotherms of earth plasters. Ashour, Georg, & Wu (2011) determinate the sorption isotherms of earth plasters with varying percentages of fibres and sand, with values of maximum water content between 1.6% and 2.1% for more and less the same percentage of straw as the one present in the samples tested in this dissertation. Better performances were reached apart the F5 sample.

4.2.2. Compressed earth block

As well as for the earth plasters, the CEB sorption curves also present the same behaviour between the salt solution and the DVS method - see Figure 4.9 and 4.10. STA is the sample which has the higher water content of about 6% (only performed in the DVS), followed by CRA with a maximum water content of 4.5% in the salt solution method and 4% in the DVS, ahead of the STR with 3.2% and 2.6% in the salt solution and DVS method, respectively. Finally, ALX with a maximum of 2.4% in the salt solution and 2% in the DVS. As presented in table 3.6 in the Chapter 3.1.2. just the clay content of STA composition is known and indeed is one of the highest; in other hand for STR, ALX and CRA a few more characteristics are presented in Champiré et al. (2016), that justify their performance. As in table 3.6, CRA has the higher clay content, followed by STR and finally ALX. Also the blue value and the plastic index results are in agreement with the obtained behaviour.

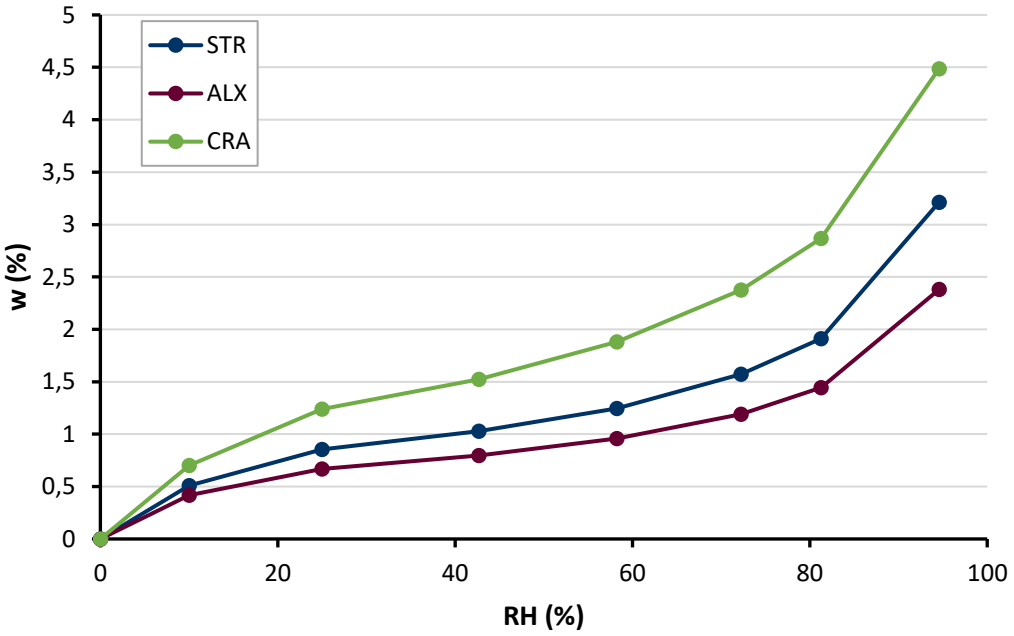

Figure 4.9- Sorption isotherms for the compressed earth samples (STR, ALX and CRA) by the salt solutions test at 23ºC

For CEB more results of this test are presented in literature. Hall & Allinson (2009) obtained for stabilised rammed earth maximum water contents between 1.3% and 1.6%. Liuzzi et al.(2012) for different clay mixes reached values between 3.5% and 5%. More recently Cagnon et al. (2014) for earth bricks determined the sorption isotherms with the DVS and salt solutions method, with slightly higher values for the DVS in the range between 4.5% and 6%. Also McGregor (2014) with several types of compressed earth blocks used the DVS to determine the sorption isotherms and obtained results between 3% and 7% of maximum water content. The measured results are in general within the range exhibited by literature, mainly for STR, CRA and STA; ALX, in other hand, presents a lower performance.

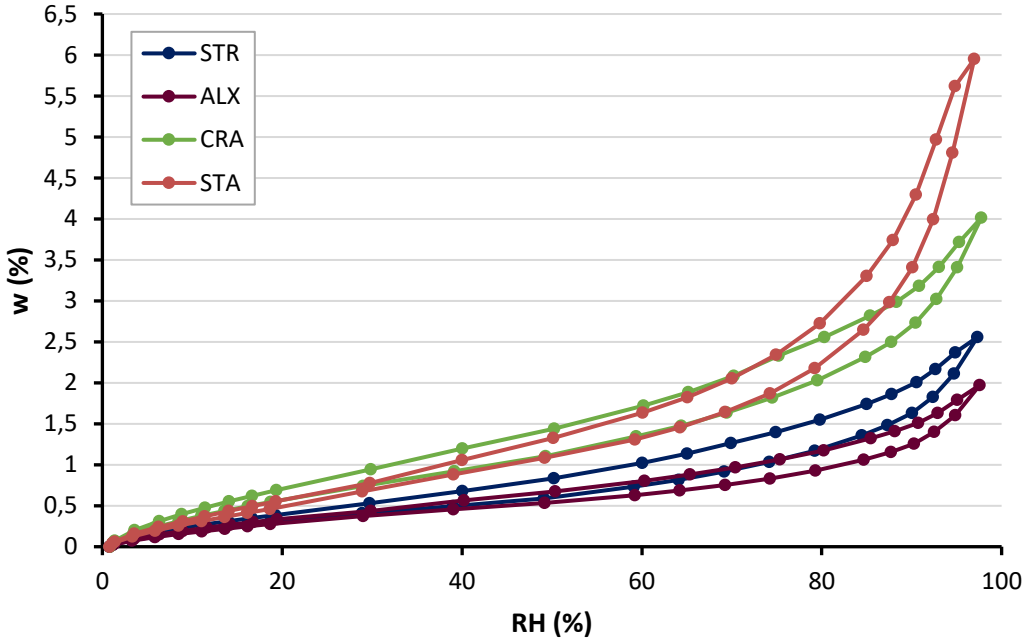

Figure 4.10- Sorption isotherms for the compressed earth samples (STR, ALX, CRA and STA) by the DVS method at 23ºC

4.2.3. Dry mass effect

In order to analyse the comparability and reliability between the salt solutions and the DVS method, the adsorption curves at 23ºC of each method are plotted together. Firstly, the earth plasters - see Figure 4.11. For the F0, F3 and F5, a good approach of the curves are visible. However there is no single trend: the F0 and F3 in DVS results in higher levels of water content while the opposite occurs for the F5. This can be due to a lack of representativeness of the macropores in the small samples. In the Compressed earth blocks the behaviour is much different: there is clearly a difference between the water content obtained for the DVS and the salt solutions - see Figure 4.12. Much higher values are given by the salt solutions method.

Before the starting of each test, there is one common action that consists in obtaining the dry mass. The aim is to reach the lowest mass also corresponding to the lowest percentage of water content, achieved with the combination of high temperatures and low humidities. Analysing the process to obtain the respective dry mass, three different ones can be identified. As explained in the beginning of this chapter, for salt solutions the plasters are dried in the oven at 50ºC and the CEB at 105ºC. For the DVS the sample is first submitted, by a dry air system, to the 0% RH level stage in the temperature programed for the sorption process. As the DVS works with small scale samples, even for a small difference it will induce considerable differences in the results of the curves - see Figure 4.13 where three adsorption curves at 23ºC of the F0 are compared. There are two parameters varying between them, the (2) and (3) were done with the same sample but with a different dry air system and the (1) and (3) with the same dry air system but with different samples.

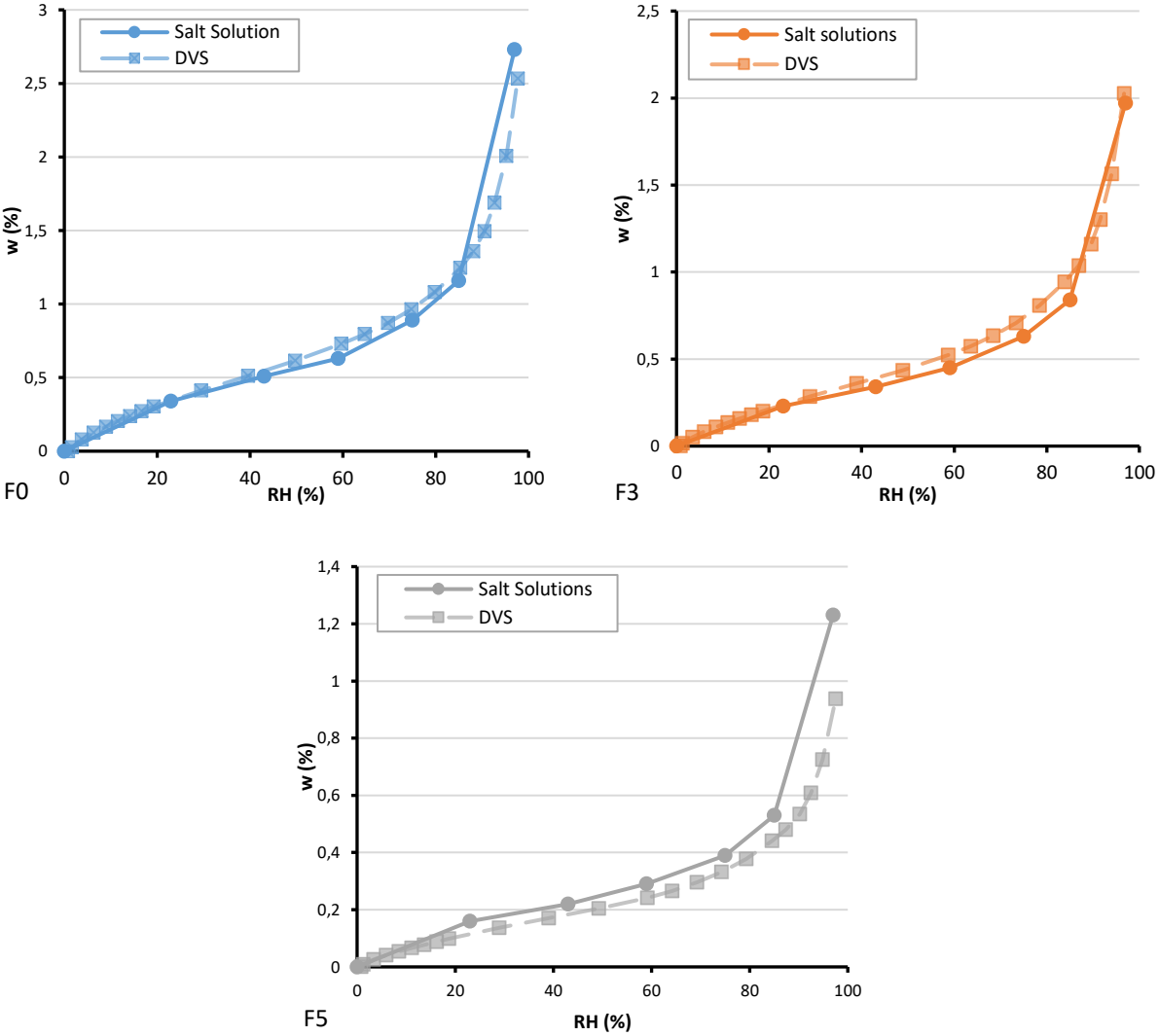

Figure 4.11- Comparison of the adsorption between the salt solutions and the DVS method of F0, F3 and F5

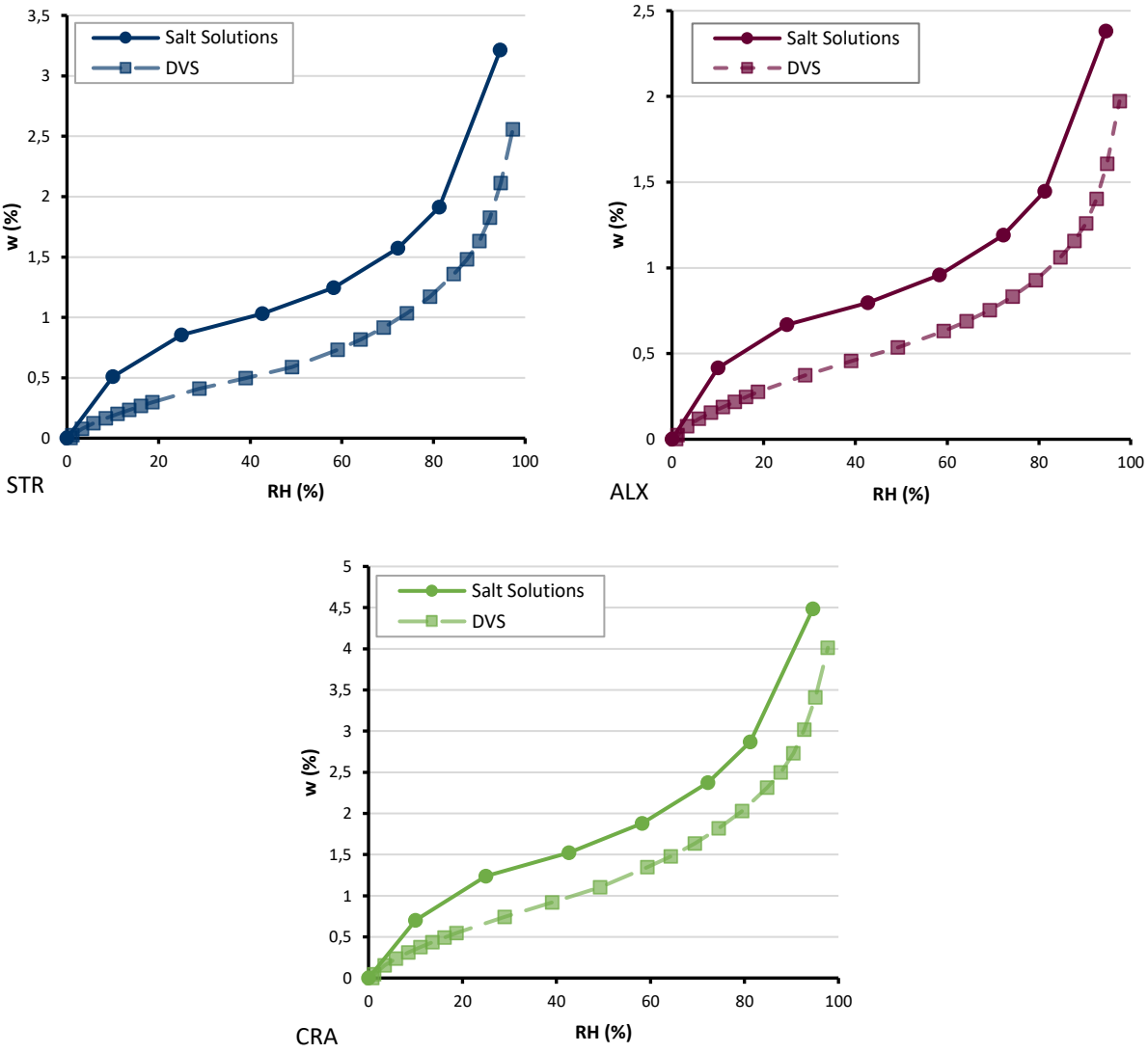

Figure 4.12- Comparison of the adsorption between the salt solutions and the DVS method of STR, ALX and CRA

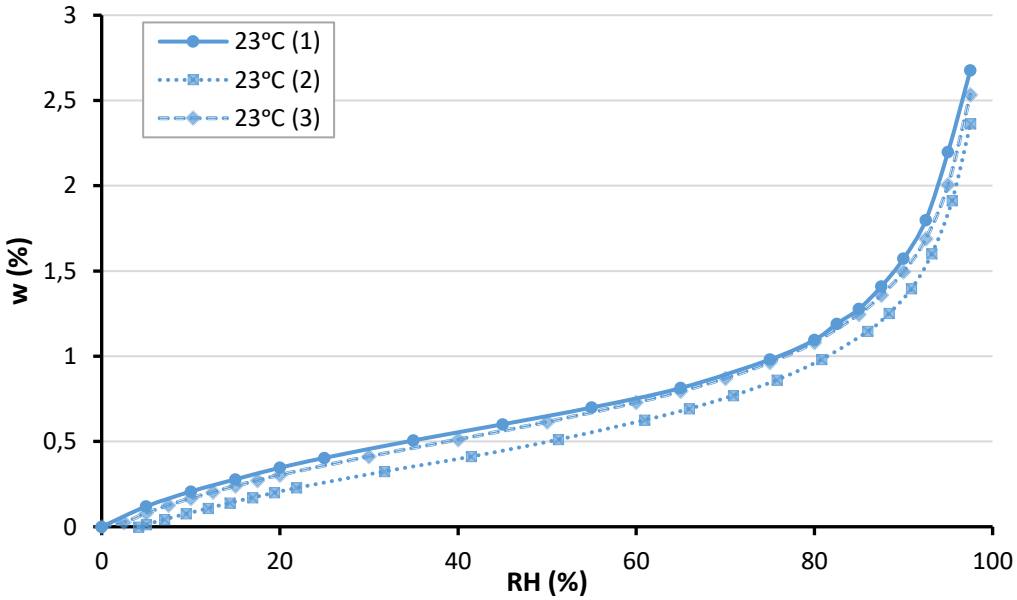

Figure 4.13- Comparison of the F0 adsorption curves between different dry air system (2) and (3); and between the same cycle with different samples (1) and (3)

The DVS results are very sensitive; to obtain accurate and comparable results it is imperative to assure a good and constant dry air system and also to utilize the same sample if comparability between temperatures is desired. Nevertheless in the case of Figure 4.13 the influence of different sample was minimum in comparison with the dry air system. All these procedures show the importance to obtain, as precise as possible, the dry mass of the tested sample.

The lowest the dry mass will be, the higher will be the water content during the sorption, and by the comparison made in Figure 4.11, 4.12 and 4.13, clearly different ways to obtain the dry mass leads to different results. If in one hand for the earth plasters this difference seams negligible, which might lead to the similarity of conditions between both processes. In the other hand for the CEB the processes are much different. Indeed a dry mass obtained in an oven at 105ºC will be much lower than the one obtained in the 0% stage of the DVS (in reality 1% RH) at 23ºC.

Therefore is concluded that in order to be able to compare this two methods and also to achieve accurate results the dry mass process should be the same, to entail the equality of the sorption isotherm. Which leads to a new proceeding: after the DVS cycles the plaster samples are dried at the oven at 50ºC and the CEB at the oven at 105ºC. Therefore is estimated a correction of the dry mass and consequently achieve the comparability between the two tests, and it consists in the following terms. Considering u_{DVS} the water content values from the DVS, m_{dry}^{0} the dry mass obtained from the oven and m_{dry}^{DVS} the dry mass from the DVS, equations 25, 26 and 27 can be constructed:

$$u_{DVS} = \frac{m - m_{dry}^{DVS}}{m_{dry}^{DVS}} \tag{25}$$

$$u = \frac{m - m_{dry}^{0}}{m_{dry}^{0}} \tag{26}$$

$$\delta_m = m_{dry}^{DVS} - m_{dry}^{0} \tag{27}$$

Combining the equations, the corrected value of water content u^* is reached:

$$u_{DVS} = \frac{m - m_{dry}^{0} - \delta_m}{m_{dry}^{0} + \delta_m} = \frac{u - \frac{\delta_m}{m_{dry}^{0}}}{1 + \frac{\delta_m}{m_{dry}^{0}}} \Leftrightarrow u_{DVS} \cdot \left(1 + \frac{\delta_m}{m_{dry}^{0}}\right) = u - \frac{\delta_m}{m_{dry}^{0}} \Leftrightarrow$$

$$u^* = u_{DVS} \cdot \left(1 + \frac{\delta_m}{m_{dry}^{0}}\right) + \frac{\delta_m}{m_{dry}^{0}} = \frac{u_{DVS} \cdot m_{dry}^{DVS}}{m_{dry}^{0}} + \frac{m_{dry}^{DVS} - m_{dry}^{0}}{m_{dry}^{0}}$$

This correction were done for all the samples, after the DVS cycles, where the m_{dry}^{DVS} was obtained. The samples were put inside the oven to reach the m_{dry}^{0} ; the results are presented for the earth plasters in Table 4.10 and the CEB in Table 4.11. By analysing the differences, it is clear that the DVS does not reach the dried mass as possible.

Table 4.10- Dry mass values obtained in the DVS at 23ºC, and in the oven at 50ºC

Plaster	m_{dry}^{DVS} 23ºC (mg)	m_{dry}^{0} 50ºC (mg)	$\Delta_{23ºC-50ºC}$ (mg)
F0	421.76	420,60	1.16
F3	363.35	358.70	4.65
F5	528.53	525.60	2.93
F6	434.08	425.90	8.18

Table 4.11- Dry mass values obtained in the DVS at 23ºC, and in the oven at 105ºC

CEB	m_{dry}^{DVS} 23ºC (mg)	m_{dry}^{0} 105ºC (mg)	$\Delta_{23ºC-105ºC}$ (mg)
STR	535.95	531.90	4.05
ALX	512.82	511.10	1.72
CRA	465.11	462.40	2.71
STA	564.69	560.30	4.39

In Figures 4.14 and 4.15, the sorption isotherms with the dry mass correction for the F0 and STR are presented, respectively. If in one hand for the F0 the correction resulted in a bad approximation between the DVS curve and the salt solution curve, for the STR it reached a better similarity between the curves, mainly if a comparison with the curve in Figure 4.12 is made. This correction clearly raised the global w; indeed the DVS deals with micro samples with weights inferior to one gram, so any small difference will reproduce a big variance. By analysing the weight differences described in Tables 4.10 and 4.11, the bigger the weight difference the higher will be the raised water content. Two reasons can justify why this correction fits better for the compressed earth blocks than for the earth plasters. First the fact of working with so small samples and moreover the plasters with fibres that are very delicate and any grain is easily lost. Secondly the uncertainty of reaching the dry mass at 50ºC and, most important, to achieve repeatable conditions for the samples used in DVS and in the salt solutions.

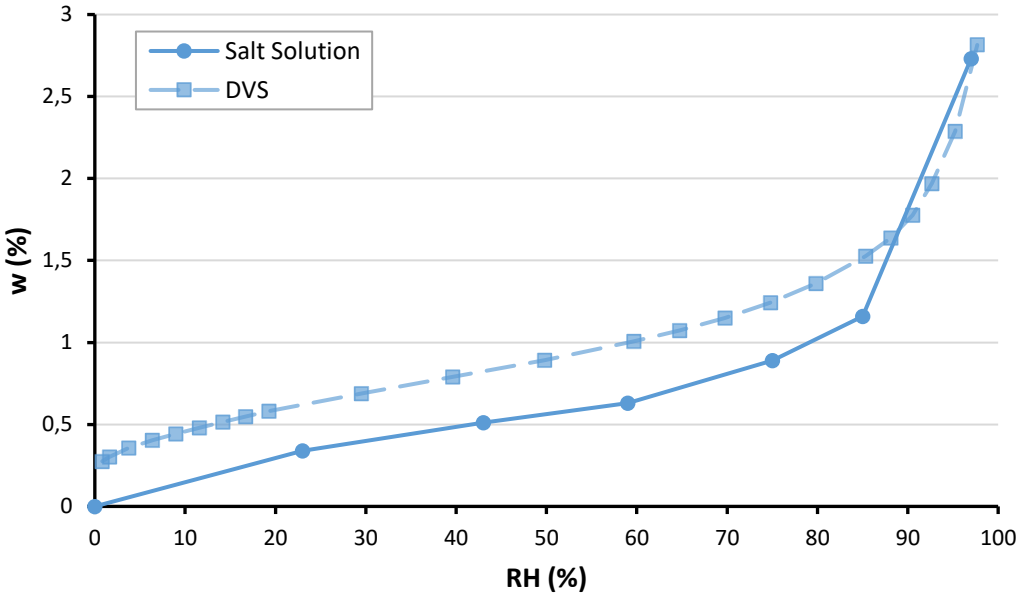

Figure 4.14- F0 sorption isotherms at 23ºC after the dry mass correction

At this point is possible to conclude that this correction is essential to the compressed earth blocks because, as predicted, the DVS dry mass is not comparable to the one obtain at 105ºC and since the curves fits better with this correction, this procedure will be done for all the samples. On the other hand earth plasters clearly

fitted better without the correction than with the correction; it confirms the similarity of conditions between the DVS dry stage and the oven at 50ºC. By the results in Table 4.14 it can induce to a mistake because of the difference obtained between the two masses, but these values are not precise. As referred before these earth plasters samples with fibres are very breakable and all the process to remove them from the DVS equipment, place in another cup, save it in the oven and after weight it, can lead to a loss of material. So for these samples it will be taken into account only the DVS dry mass.

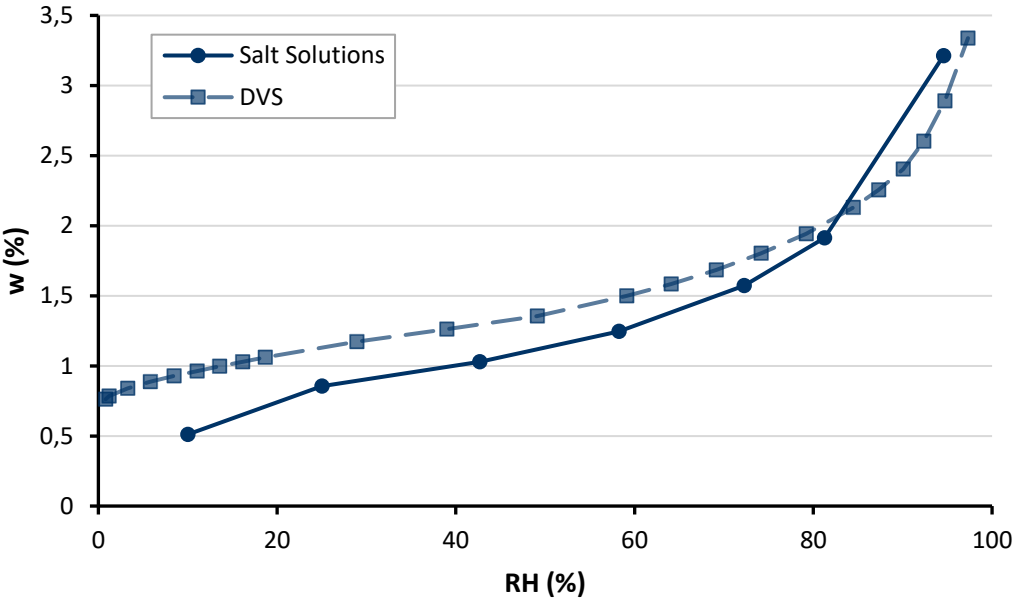

Figure 4.15- STR sorption isotherms at 23ºC after the dry mass correction

4.2.4. Estimation of the specific surface area

As explained in Chapter 2.1.4., the specific surface area represents the total available area where the negative charges responsible for the adsorption process are present. Indeed, it is an important characteristic with direct influence on the capacity of a material to adsorb moisture. There are many ways to define and calculate the specific surface area, the most convenient and utilized in this dissertation is the area by unit mass, and is calculated by the method commonly known as BET. The calculations follows the description by F. Rouquerol et al. (1999).

The BET method consider the existence of multilayer adsorption, where the adsorbed molecules in one layer can act as adsorption sites for the next molecules layer. This leads to variable layer thickness and not constant - see figure 4.16.

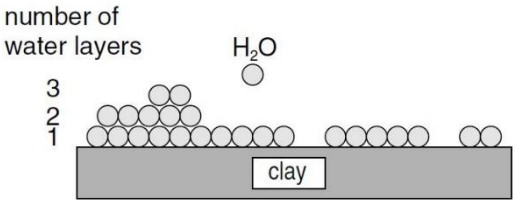

Figure 4.16- Multilayer adsorption by Meunier (2005)

The known BET equation is derived by the sum of each layer adsorbed amount - see equation 28:

$$\frac{1}{n}\cdot\frac{\frac{p}{p_0}}{\left(1-\frac{p}{p_0}\right)}=\frac{1}{n_m C}+\frac{C-1}{n_m C}\cdot\frac{p}{p_0} \tag{28}$$

where n is the specific amount of gas adsorbed at the equilibrium pressure p and temperature, p_0 is the saturation vapour pressure, n_m is the amount adsorbed at monolayer coverage and C is a constant. In order to calculate the surface area by this method is necessary to first construct the BET plot and after derive the n_m value. This is made by plotting $\frac{1}{n}\cdot\frac{\frac{p}{p_0}}{\left(1-\frac{p}{p_0}\right)}$ vs $\frac{p}{p_0}$, which gives a straight line - see figure 4.17. Notice that the RH range should be between 0.5-30 %.

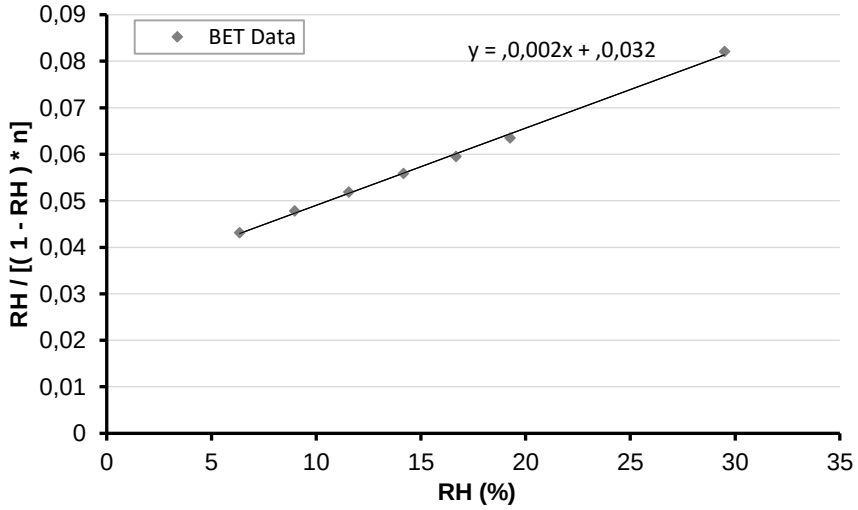

Figure 4.17- BET plot to determine the specific surface area

A typical linear equation can be obtained. Considering s as the slope and i as the interception point, is obtained by equation 29 and 30:

$$s=\frac{C-1}{n_m C} \tag{29}$$

$$i=\frac{1}{n_m C} \tag{30}$$

Solving both equations:

$$n_m=\frac{1}{(s+i)}$$

$$c=\frac{s}{i}+1$$

Once the value of n_m is known, it is possible to determine the specific surface area, S_{BET} (m^2/g), by the application of the simple relation (eq. 31):

$$S_{BET}=\frac{n_m}{M_w}\cdot L\cdot M_a \tag{31}$$

where M_w (g/mol) is the molecular mass of water, L (mol^{-1}) is the Avogadro's number and M_a ($Å^2$) is the effective molecular area.
The DVS himself can be programed to calculate the specific surface area by this method, in order to understand and validate calculations. The same were done separately for the F0 sample. All the calculations are present in Appendix III, and the results are displayed in Table 4.12.

Table 4.12- Comparison of F0 specific surface area between DVS results and manually calculated results

F0	S_{BET} (m^2/g)
DVS	14.23
Calculated	14.32

The calculated results are very similar to the ones given by DVS, with an error of 0.09 that can be neglected. Now on specific surface area values are given by the DVS and they are presented in Table 4.13 for the earth plasters, and in Table 4.14 for the CEB.

Table 4.13- Specific surface area for the earth plasters F0, F3, F5 and F6

Plaster	S_{BET} (m^2/g)
F0	14.3
F3	10.1
F5	4.8
F6	15.9

Table 4.14- Specific surface area for the compressed earth samples STR, ALX, CRA and STA

CEB	S_{BET} (m^2/g)
STR	16.4
ALX	12.4
CRA	24.5
STA	23.4

4.2.5. Discussion

At this a point a conclusion on the analysed characteristics can be made, starting by the importance of measuring, as accurate as possible, the dry mass of the tested sample. Earth plasters are less sensitive to this possible imprecision than the compressed earth samples, due to the fact that there is no dried mass as the one given by the oven at 105ºC. For these samples it becomes essential to proceed according to the dry mass correction deduced in chapter 4.2.3.

The estimation of the specific surface area clearly gave a great extra contribution to understand the different amounts of adsorbed water during the adsorption process. As this characteristic highly influences the adsorption capacity, it was not a surprise that the samples with higher specific surface area are also the ones with higher amount of adsorbed water, for the earth plasters F6 with 15.9 m^2/g and F0 with 14.23 m^2/g, followed by F3 with 10.06 m^2/g and F5 with 4.78 m^2/g. Analogy is made for the CEB, with CRA and STA becoming evidenced with also the biggest specific surface area of 24.5 m^2/g and 23.4 m^2/g, respectively, followed by STR with 16.4 m^2/g and by the end ALX with 12.4 m^2/g.

This last characteristic also justifies why the compressed earth blocks adsorb more moisture than the plasters, but that was something expected by the matter of fact that the earth plasters mixtures have lowest clay content than the compressed earth samples. The fibres indeed increase the porosity but the minor clay content leads to less surface area which plays a main role.

5. Influence of temperature on the hygroscopic characteristics

In this chapter, the same tests were performed at different temperatures in order to analyse the influence of the latest in the earth plasters and in the compressed earth samples. Higher temperatures were chosen for practical reasons, for a better stabilisation of the climatic chambers, as well as the performance of the DVS.

5.1. Water vapour permeability

The earth plasters samples were performed again in the wet cup test at the Ineltec climatic chamber at 40ºC and 30% of RH, and as explained on chapter 3.2.1., with a salt solution of Potassium Chloride inside the container to reach the wet state of about 85% of RH. The last methodology used for the dry cup test is repeated, with a constantly monitoring of the RH level. The first results with the original calculation are presented in table 5.1: the variation with thickness is once again present as well as high values of standard deviation.

Table 5.1- Average values of water vapour permeability and water vapour resistance factor for the earth plasters (wet cup 40ºC)

Plaster	RH %	δ_p^{ap} (kg/s.m.Pa)	μ^{ap} (-)	
		Average	Average	Standard deviation
F0 1	82.9	1.23E-11	16.87	5.02
F0 4		2.12E-11	9.77	
F3 1	82.9	1.17E-11	17.74	4.87
F3 4		1.91E-11	10.85	

As explained in the chapter 4.1, the original calculation does not take in account the impact of the air layer. Therefore, the ISO correction is used to obtain more realistic values. The results are present in the table 5.2. They exhibit the lowest influence of the thickness; however with a difference that cannot be negligible. So the surface transfer coefficient β was estimated in order to obtain the intrinsic vapour permeability of the material whatever the thickness. The results are present in table 5.3.

Table 5.2- Average values of water vapour permeability and water vapour resistance factor for the earth plasters after the ISO correction (wet cup 40ºC)

Plaster	δ_p^{agc} (kg/s.m.Pa)	μ^{agc} (-)	
	Average	Average	Standard deviation
F0 1	1.50E-11	13.87	3.43
F0 4	2.30E-11	9.02	
F3 1	1.41E-11	14.74	3.28
F3 4	2.05E-11	10.10	

Table 5.3- Average values of water vapour resistance for the earth plasters after the β correction proposed by Vololonirina et al. (2014) (Wet cup 40ºC)

Plaster	δ_p^{agc}	d/ δ_p^{agc}	Intersection point (Z^s)	β	μ^{β}	Standard deviation
F0 1	1.50E-11	6.68E+08	3.12E+08	3.21E-09	7.39	0.00
F0 4	2.30E-11	1.74E+09			7.40	
F3 1	1.41E-11	7.09E+08	2.96E+08	3.38E-09	8.60	0.03
F3 4	2.05E-11	1.95E+09			8.56	

The comparison between all calculation procedures is presented in Figure 5.1. In a general visualisation of the values, both formulations present similar values; however with a slightly difference that evidence a higher permeability by the F0. Once again is also possible to visualize that the difference obtained between

thicknesses was higher in the original calculations, as well as in the ISO correction. Only in the β correction the values are more comparable. Also the same method to predict the errors in Chapter 4.1. was done and the results are presented in Table 5.4. The influence of ± 2% RH lead to higher errors percentage comparing to the relative errors but also very small. Here stands up the F0 sample with lower values and even 0.7% ensuring the repeatability.

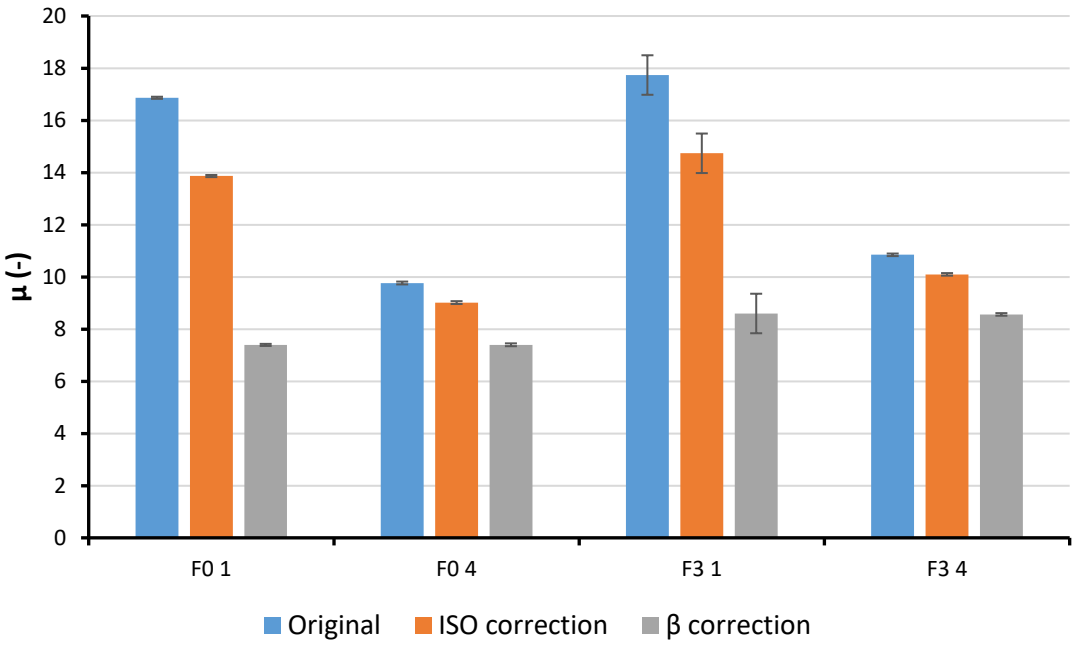

Figure 5.1- Comparison between the water vapour resistance factor results for the earth plasters (Potassium Chloride as saturated solution)

Table 5.4- Relative error and the error of ± 2% RH in the chamber on the Wet cup results

Plaster	R error (%)	± 2% RH error (%)
F0	0.7	6.5
F3	7.2	8.4

In order to understand the influence of temperature on the water vapour resistance, both results at 23ºC and 40ºC need to be compared. In the Table 5.5 and Figure 5.2, where the results for the water vapour resistance after the β correction are presented, a tendency is possible to observe: the 40ºC results are in generally higher than the ones obtained at 23ºC. Although small, this happened in all samples except for the F0 4, what can be explained by the fact that the tests may not have been done in the exactly same samples. However it is possible to state that a higher temperature will slightly reduce the permeability of the earth plaster, being this tendency more evident for the F3 sample.

Table 5.5- Average values of water vapour resistance at 23ºC and 40ºC

Plaster	μ^{β} 23ºC	μ^{β} 40ºC
F0 1	7.18	7.39
F0 4	7.73	7.40
F3 1	7.27	8.60
F3 4	7.77	8.56

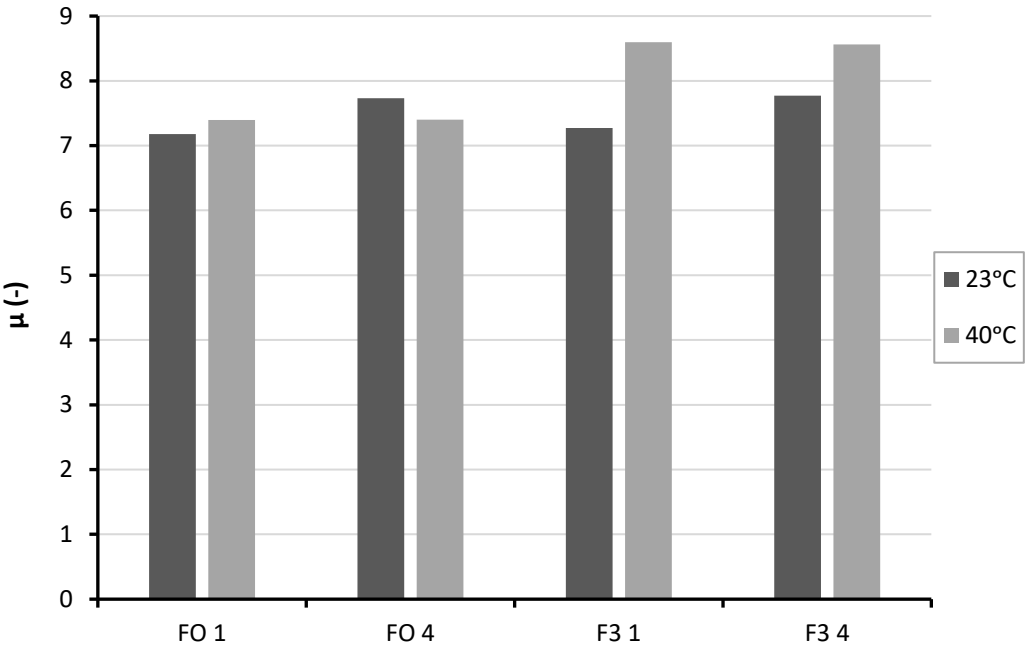

Figure 5.2- Comparison between the water vapour resistance values corrected by β at 23ºC and 40ºC

Feng & Janssen (2016) performed the dry and wet cup test at 14.1ºC, 25.5ºC and 39.2ºC for aerated concrete, calcium silicate board and ceramic brick. They performed the tests at three different RH levels and for the closest as performed in this dissertation the water vapour resistance was slightly bigger at 39.2ºC than for 25.5ºC, but similar to the results at 14.1ºC. So they also neglected the influence of temperature because no consistent tendency was reached and the differences were insufficiently significant. However for the wet cup with RH levels of 84.3% and 97.3% they observed a tendency on the influence of temperature on aerated concrete and calcium silicate board. Indeed the liquid water role is different in the hygroscopic and capillary ranges; therefore they believed that the lower values at higher temperature are related to the liquid water presence, which entails moisture transfer.

5.2. Sorption isotherms

In this chapter, the sorption isotherms are presented for the same samples at 23ºC, 30ºC and 40ºC. The procedure concluded in the Chapter 4.2.3. will be applied in order to reproduce the most reliable results.

5.2.1. Earth plasters

The sorption isotherms at 23ºC and 30ºC by DVS for F0, F3, F5 and F6 plasters are presented in the Figures 5.3, 5.4, 5.5 and 5.6, respectively. The F6 plaster was the one with higher moisture content in all the RH levels for both temperatures: 2.6% at 23ºC and 2.4 at 30ºC. However, presenting a similar curve to the F0 plaster with an w of 2.5% at 23ºC and 2.3% at 30ºC. Their composition is very similar and the differences can be explained by the presence of the montmorillonite in the F6 plaster, which leads to higher amounts of adsorbed water.

Those results are also highlighted by the influence of the temperature on the amount of adsorbed water during the cycle. As it is possible to confirm by the Figures, the w decreases when the temperature increase. However, the temperature does not influence all the samples in the same range: for the F0 and F6 this influence is more pronounced than for the F3 and F5. In a matter of fact, the most influenced by temperature are also the ones with higher amounts of adsorbed water. Indeed the amount of water decrease with the increasing of temperature; the bigger this amount be, the bigger will be the influence of temperature.

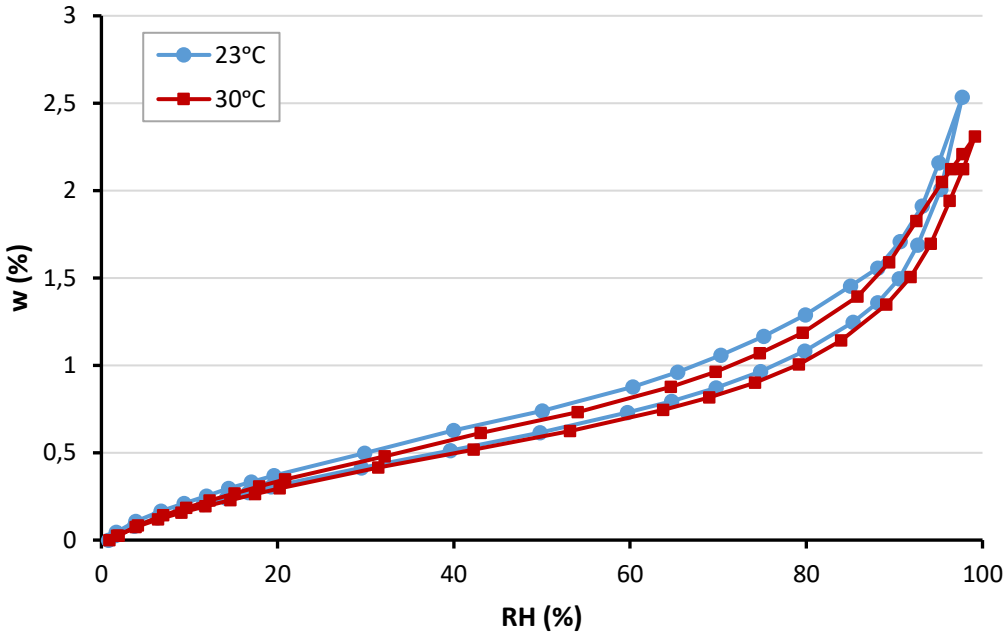

Figure 5.3- Temperature influence in the sorption isotherms of F0

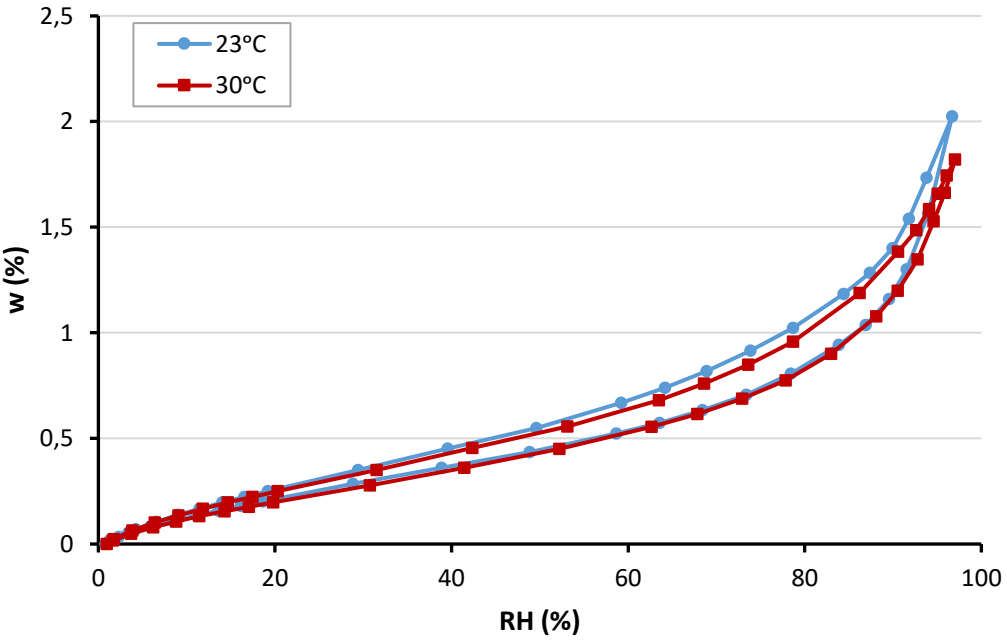

Figure 5.4- Temperature influence in the sorption isotherms of F3

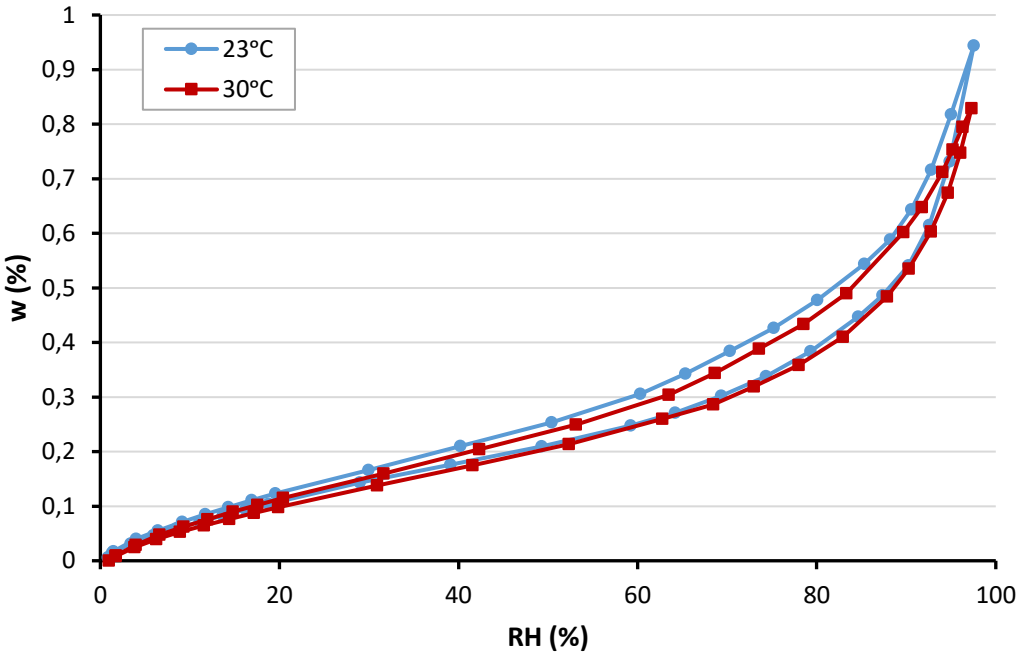

Figure 5.5- Temperature influence in the sorption isotherms of F5

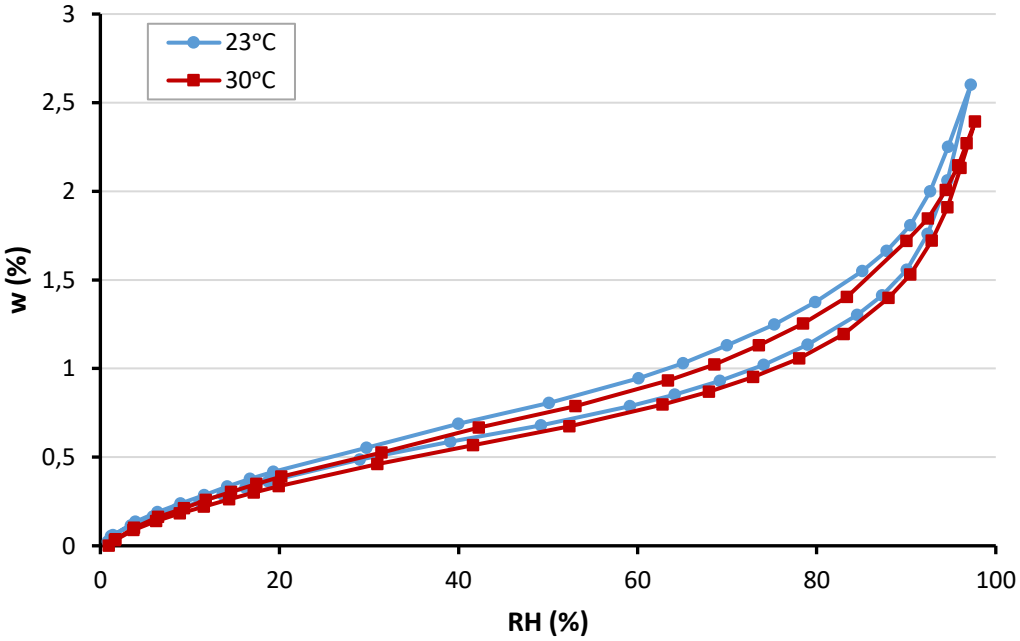

Figure 5.6- Temperature influence in the sorption isotherms of F6

5.2.2. Compressed earth blocks

In Figures 5.7, 5.8, 5.9 and 5.10 the sorption isotherms at 23ºC and 30ºC by DVS are presented for the STR, ALX, CRA and STA compressed blocks. As in Chapter 4.2.2. the STA reached the highest value of water content, 6.8% at 23ºC and 6.6% at 30ºC for 97.7% of RH. It was followed by CRA with a maximum of 4.6% and 4.3% at 23ºC and 30ºC, respectively. STR and ALX, again, exhibited the poorer performance

The results do not reveal much influence of the temperature on the amount of water, being in the figures almost imperceptible, except for the desorption where this difference is more evident.

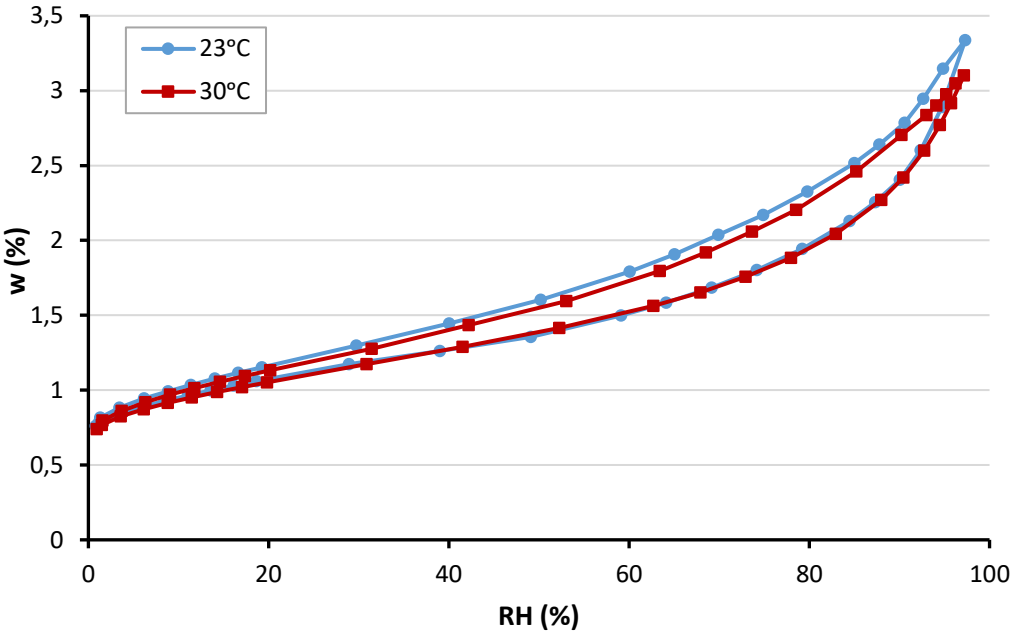

Figure 5.7- Temperature influence in the sorption isotherms of STR

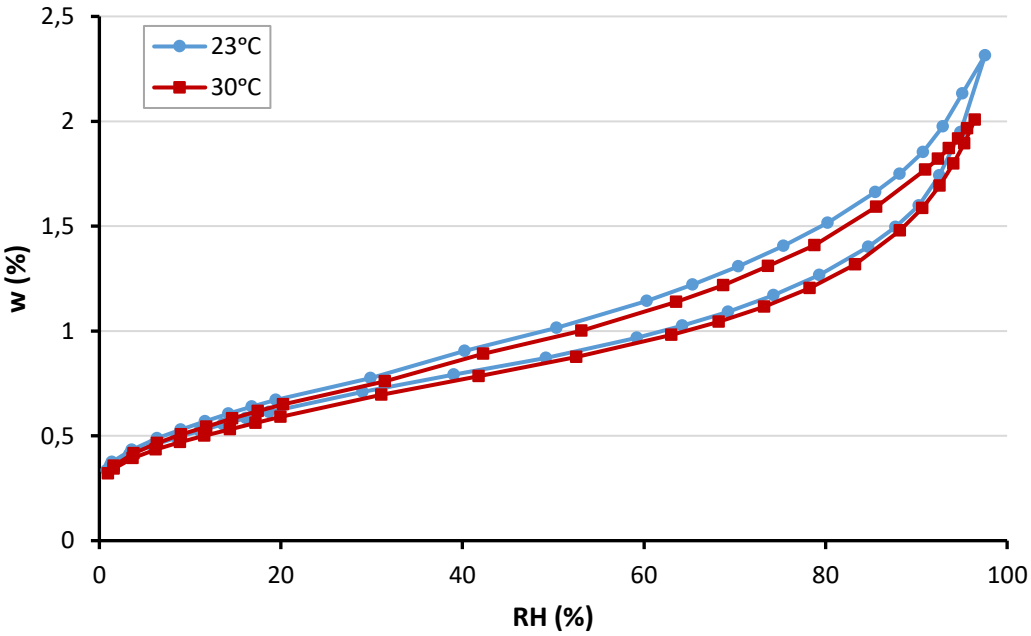

Figure 5.8- Temperature influence in the sorption isotherms of ALX

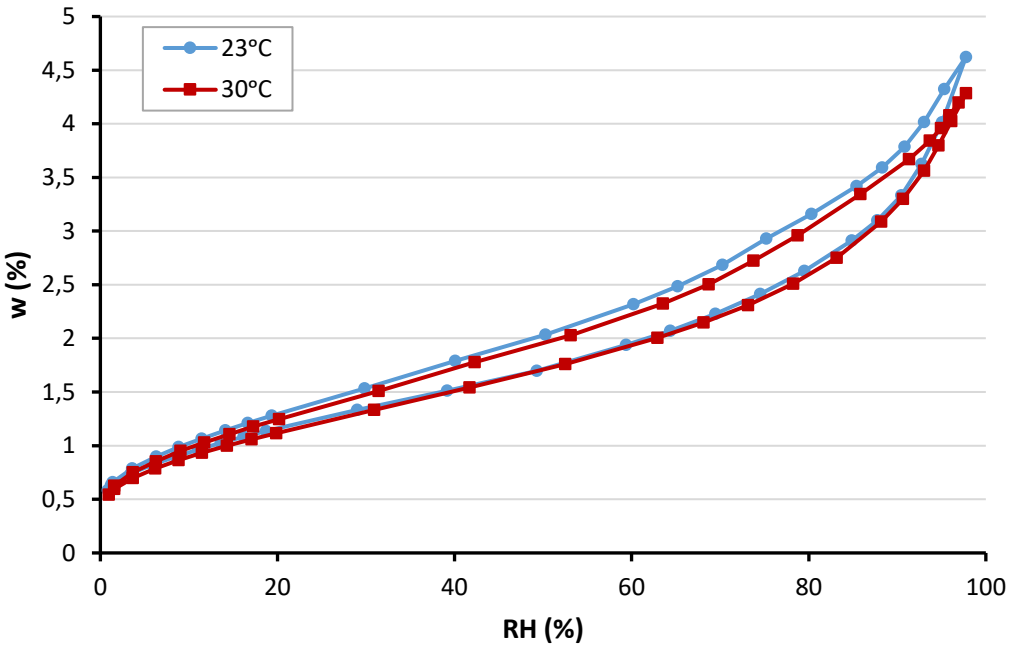

Figure 5.9- Temperature influence in the sorption isotherms of CRA

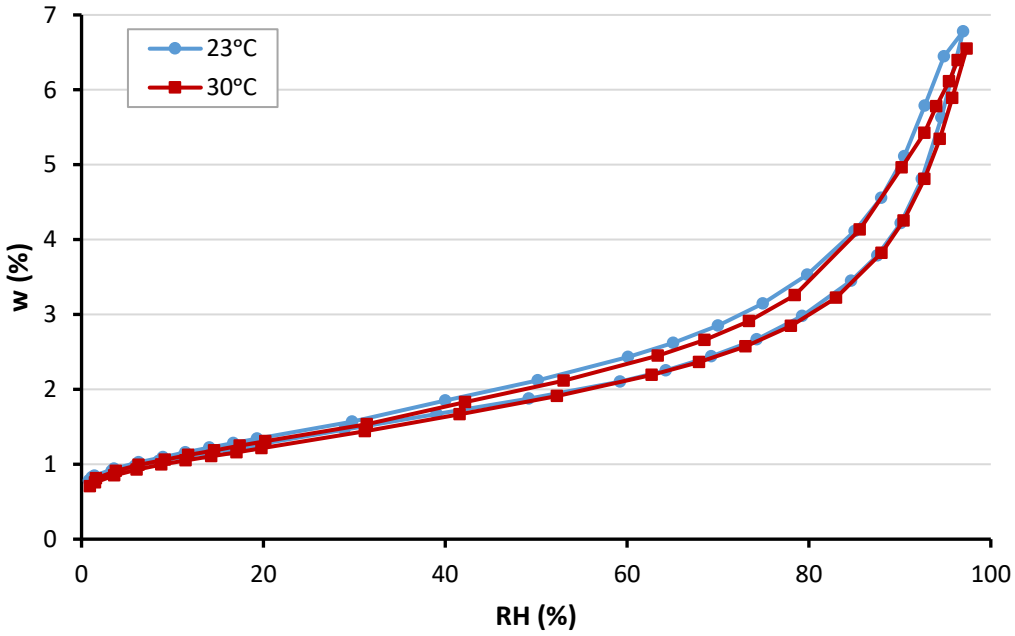

Figure 5.10- Temperature influence in the sorption isotherms of STA

5.2.3. 40ºC salt solutions isotherms

As already demonstrated in the chapter 4.2., by the salt solutions method the obtained isotherms are clearly less accurate than the DVS method, by all the imprecisions associated to the test himself. The similarity between the 23ºC isotherms was not perfect, even more if a comparison is made with the 40ºC isotherms - the values of all the samples are reported in Appendix II. By analysing Figure 5.11 for the F0 plaster, the obtained results are not coherent: higher water contents are reached with the 40ºC isotherm, which contradicts theory. On the other hand in Figure 5.12 for the STR, the 40ºC isotherm leads to lower values

of water content, much lower than expected this is even more visible when compared to the isotherms at 23°C and 30°C in Figure 5.7.

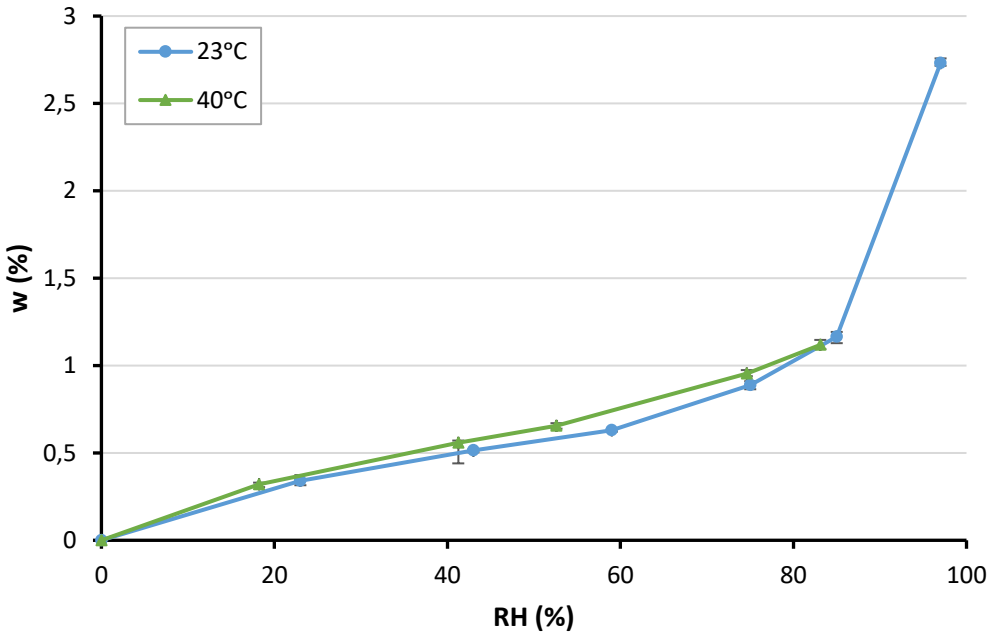

Figure 5.11- Temperature influence on the sorption isotherms of F0 plaster by the salt solutions method

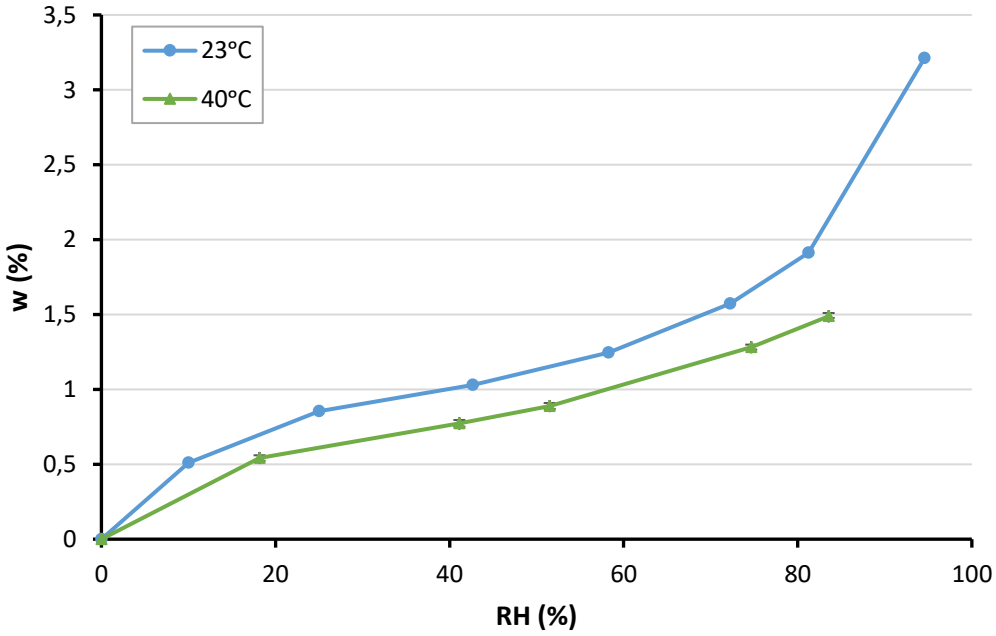

Figure 5.12- Temperature influence on the sorption isotherms of STR by the salt solutions method

At this stage is even more questionable the possibility to consider the results obtained from the salt solutions method; there are too much uncertainties associated to the method and the dry mass as explained before. The results will be discarded, in function of the precision and comparability of the DVS, and the 40ºC isotherms will be theoretically calculated in a further chapter.

5.3. Heat of sorption

As described in the chapter 2.4.2.2. the isosteric heat ΔH, also named by enthalpy of sorption or in this dissertation heat of sorption, is the energy associated to the adsorption of water vapour molecules to the pore walls. It can be calculated from the sorption isotherms, but at least the results from two different temperatures must be known. In literature this parameter is commonly calculated by the Clausis-Clapyron equation, or simply CC equation (Aït Oumeziane et al., 2016; Mihoubi & Bellagi, 2006; Poyet, 2009; Poyet & Charles, 2009).

In this dissertation the used equation is given by Rouquerol et al. (1999), that in turn is very similar to the Clausis-Clapyron equation - see equation 32:

$$\Delta H = R \cdot \frac{\ln\left(\frac{p_2}{p_1}\right)}{\frac{1}{T_2} - \frac{1}{T_1}} \tag{32}$$

where R is the molar gas constant (8.315 J/mol.K), T_2 (K) and T_1 (K) the higher and lowest temperature and P_2 (Pa) and P_1 (Pa) the pressures associated to T_2 and T_1, respectively.

To derive this equation, it is necessary to assume that the variations of ΔH between T_1 and T_2 are negligible, which is the case if the two temperatures remains sufficiently close to each other. In this manuscript, the temperatures T_1 = 23ºC and T_2 = 30ºC have been considered to estimate ΔH (J/mol) from the adsorption curves. The variation of ΔH in this range of temperature is about 0.3 kJ/mol, which is clearly negligible when compared to the absolute value of ΔH which is about 40kJ/mol.

To apply the equation 32, it is more convenient to plot w in function of P_v as in Figure 5.13. The method consists to find the respective pressures in the curve at 23ºC and 30ºC leading to the same water contents. If the pressures at 23ºC are taken as the reference ones, interpolation needs to be done in the curve at 30°C in order to determine the pressure corresponding to the fixed water content. An example of this calculation is shown below in Table 5.6, where the relative humidities corresponding to these interpolated vapour pressures are denoted by "new RH". The calculations are made with $p_{v,sat}$ = 2185.6 Pa at 23°C and $p_{v,sat}$ = 4247.0 Pa at 30ºC.

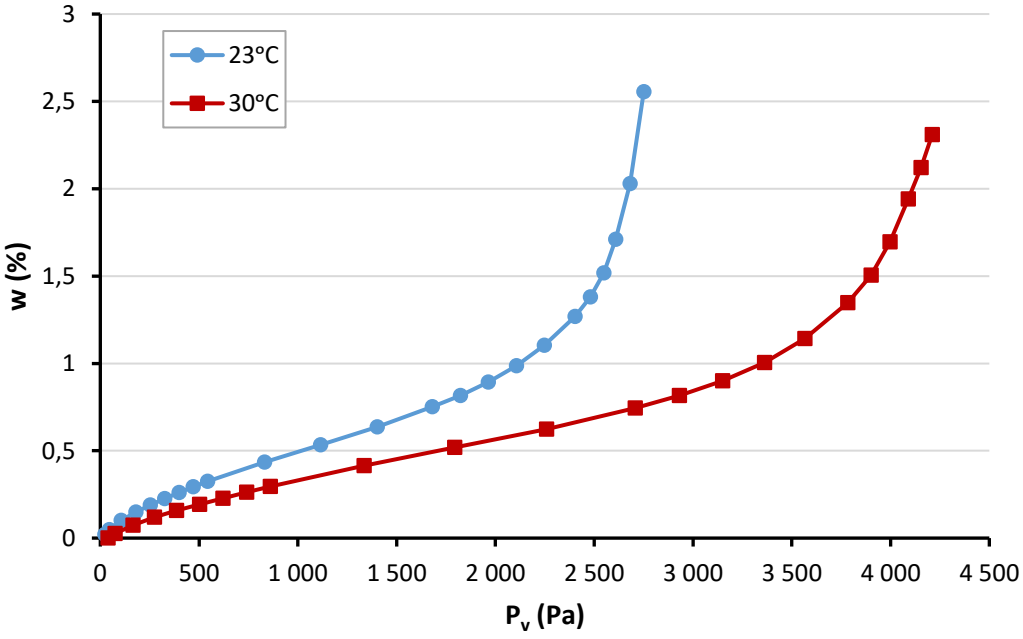

Figure 5.13- Sorption isotherms plotted vs the water vapour partial pressure for the F0 plaster

Table 5.6- Interpolation example for the F0 plaster

23°C			30°C		Interpolated 30°C	
RH	P_v	w	RH	w	New RH	P_v
0.82	23.09	0.00	0.93	0.00	0.93	39.50
1.62	45.61	0.03	1.77	0.03	1.80	76.46
3.75	105.58	0.08	3.88	0.07	4.21	178.75
6.37	179.35	0.13	6.45	0.12	7.01	297.84
8.95	251.99	0.17	9.08	0.16	9.83	417.63
…	…	…	…	…	…	…

Using this procedure, ΔH was calculated for all the samples. Even for this calculation, the dry mass plays a role. In consequence of what, in consistence with the previous analysis of the sorption curves, the dry mass from the DVS is considered for the earth plasters, while the dry mass at 105°C is considered for the compacted earth samples.
The obtained results are compared to the theoretical expression of the heat of sorption, which can be notably find in Soudani et al. (2016):

$$\Delta H = -\Delta H_{vap}(T) + R \cdot P_{v,sat} \cdot ln\left(\frac{RH}{100}\right) \tag{33}$$

where ΔH_{vap} (J/mol) is the heat of vaporisation of free water (that is for RH=100%), which depends on temperature: $\Delta H_{vap}(T = 23°C)$ = 44084.1 J/mol and $\Delta H_{vap}(T = 30°C) = 43785.0$ J/mol .

The results are presented in Figures 5.14, 5.15, for the F0 plaster and STA block, respectively. In both materials the estimated heat exhibits a similar trend with higher values at low water contents, believed to correspond to the monolayer covering, followed by a gradual decrease with the increase of the water content. The negative values means that the adsorption process releases heat. In general the estimatedd results are very consistent with the calculated ones, with a minority of incoherent points. The results for the other samples are presented in appendix IV.

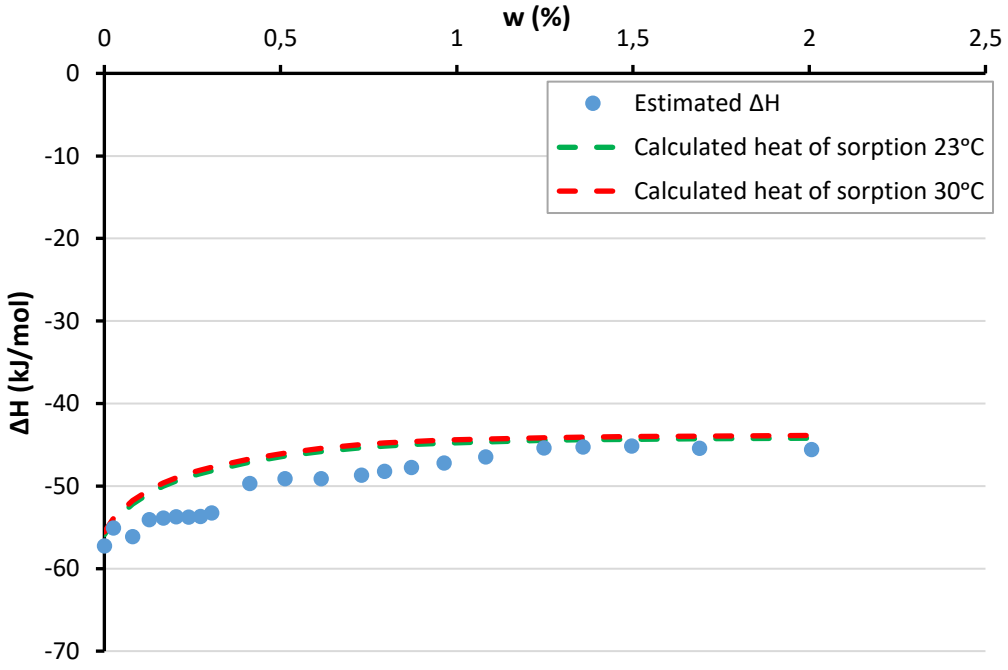

Figure 5.14- Heat of sorption of F0 plaster

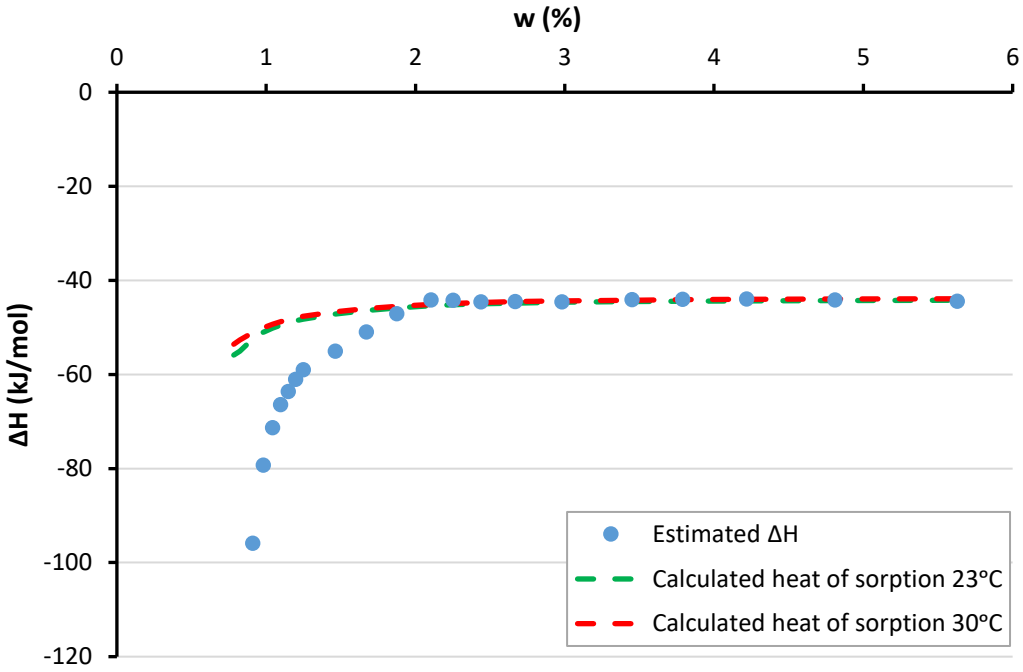

Figure 5.15- Heat of sorption of STA compressed block

This calculation was done by some authors: Poyet & Charles (2009) for cement-based materials, Aït Oumeziane et al. (2016) for hemp concrete and Mihoubi & Bellagi (2006) for bentonite. A similar trend is common between these results and the ones from this study. At lower water contents, a quite important difference is observed between estimated and calculated values of ΔH. This difference may have, at least, two origins. The first one may be the results uncertainty which strongly increase at low relative humidities. But it is also important to recall that, strictly speaking, the value of ΔH estimated for the Clapeyron equation is the opposite of the isosteric heat, while the equation 33 refers to the integral enthalpy of sorption. And, as it is mentioned in the previous chapters, at low water content, due to the strong interactions which exists between the adsorbed water and the pore surfaces, these two quantities are no more equal. A deeper analysis of the differences between integral and differential heats of sorption is, however, out of the scope of this dissertation.

5.4. Estimation of 0ºC and 40ºC isotherm

In the chapter 5.2.3. it was concluded that the sorption isotherm at 40ºC obtained by the salt solutions method was not sufficiently accurate in order to compare with the results from the DVS method. As it was one of the initial goals of this dissertation and in order to have a better evaluation of the influence of temperature on the sorption isotherms, a theoretical isotherm was calculated at 0ºC and 40ºC using the calculated heat of sorption results obtained in the last chapter. This estimation is possible to be done by using eq. 32 with p_2 vapour pressure for 40ºC curve with a reference temperature and in second time p_1 vapour pressure for the 0ºC curve with a reference temperature. For the estimation at 40ºC, with the known values of the calculated heat of sorption at 30ºC and considering p_2 the vapour pressure at 40ºC and p_1 the vapour pressure at 30ºC, all the range of the p_2 is reached. Applying the eq. 4 with $p_{v,sat}$ value of 7384.9 Pa at 40ºC, the estimated RH values is obtained for the DVS water contents. To estimate the curve at 0ºC the heat of sorption at 11,5ºC (average value between 23 and 0) was calculated, at this time with p_2 the vapour pressure at 23ºC and p_1 the vapour pressure at 0ºC, after the method to obtain the RH values was the same and considering $p_{v,sat}$ equal to 611.7 Pa.

The calculated isotherm at 0ºC and 40ºC was plotted with the other curves at 23ºC and 30ºC. To make diagrams easier to read, the water content is presented in function of the vapour pressure. Firstly, for the earth plasters in Figure 5.16, a good consistency is found between estimated and calculated values at 30°C.

This result gives some confidence on the accuracy of the predicted values at 0°C and 40°C. Once again the conclusion made in the chapter 5.2. is verified: the increase of temperature reduces the water content along the sorption cycle and this is supported with the results presented - see Figure 5.16.

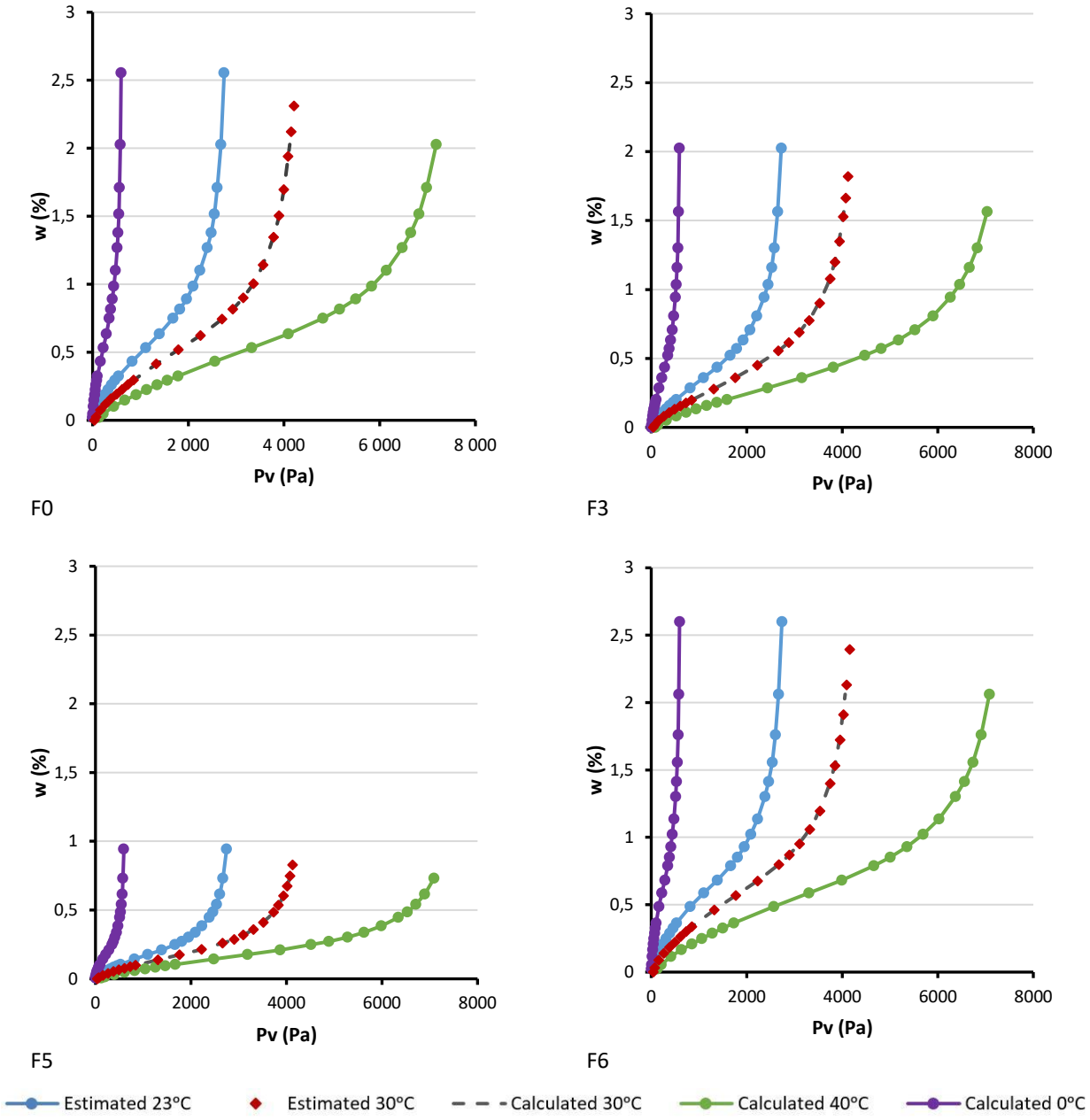

Figure 5.16- Temperature influence with the calculated isotherm at 0ºC and 40ºC of F0, F3, F5 and F6 plasters

The same calculations for the compressed earth samples are presented in the Figure 5.17. As for the earth plasters the calculation seems to be in accordance at 30°C with the experimental data.

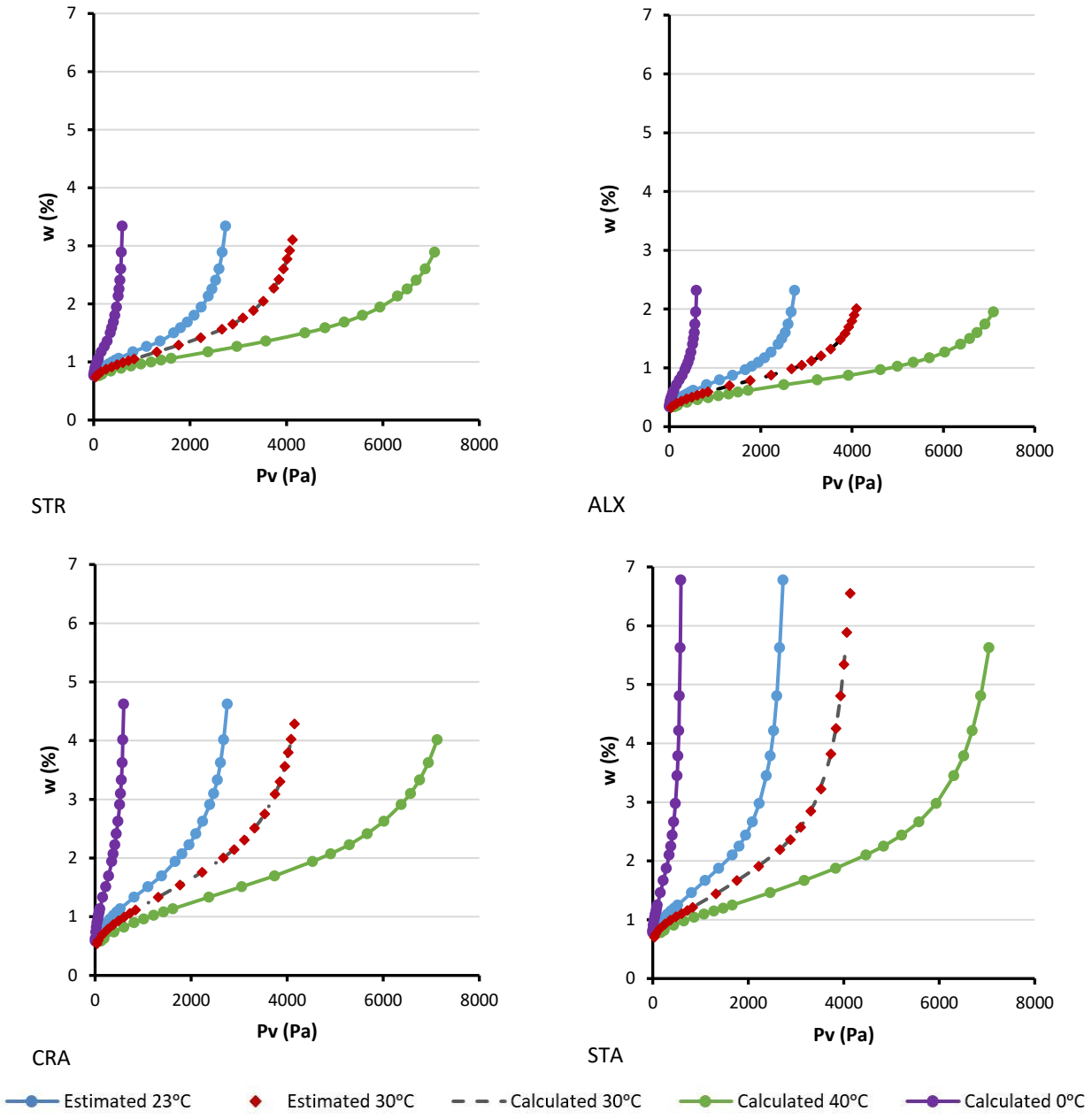

Figure 5.17- Temperature influence with the calculated isotherm at 0ºC and 40ºC of STR, ALX, CRA and STA compressed blocks

In order to analyse which samples were most influenced by the temperature, a simple calculation, as it is illustrated in Figure 5.18, is done. It consists, for the same RH of ±80%, at estimating the percentage difference between the water content and the results for all the earth plasters, presented in Table 5.7. By analysing this table it is visible that the F0 and F6 plasters are the ones with bigger influence by the temperature, slightly more for F0. The F3 and F5 plasters presented smaller influence of the temperature.

Also for the CEB the same method was used and the results are presented in Table 5.8. ALX and STR were the more influenced by temperature followed by STA and CRA. In a general view, the earth plasters are more sensitive to a temperature variation than the compressed earth blocks.

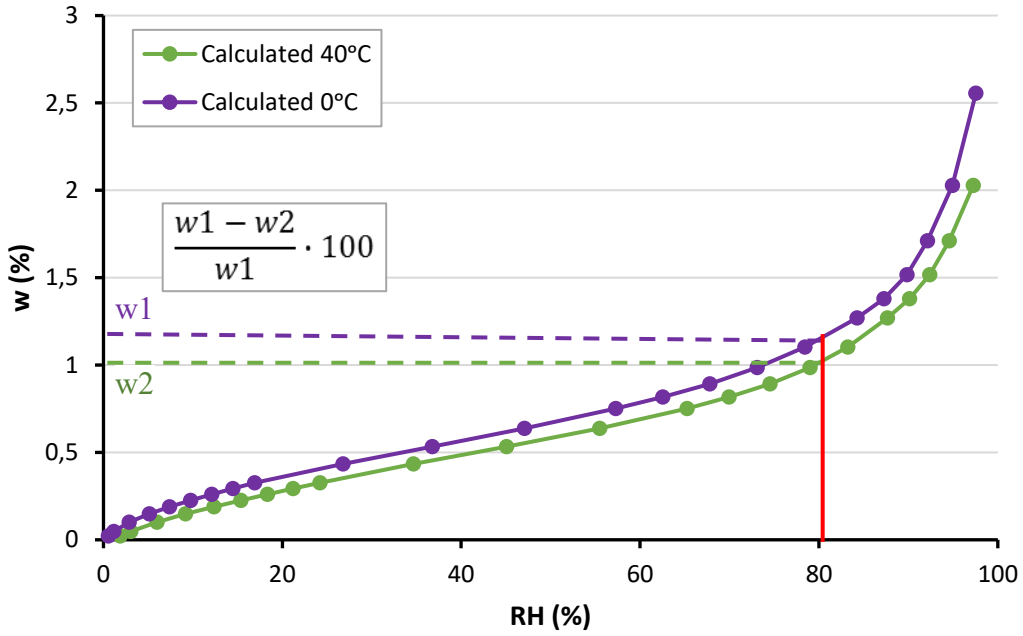

Figure 5.18- Influence of temperature on F0 plaster between 0ºC and 40ºC isotherms

Table 5.7- Influence of temperature between the 0ºC and 40ºC isotherms for the earth plasters

Plaster	Δ 40ºC-0ºC (%)
F0	11.7
F3	8.1
F5	9.1
F6	9.7

Table 5.8- Influence of temperature between the 0ºC and 40ºC isotherms of compressed earth samples

CEB	Δ 40ºC-0ºC (%)
STR	4.6
ALX	5.8
CRA	3.8
STA	3.4

This influence of temperature on the sorption isotherms has been already studied for other materials with approximately the same method to estimate isotherms at different temperatures. In the study by Aït Oumeziane et al. (2016) the desorption at 23ºC and 35ºC for hemp concrete were obtained, see Figure 5.19c. In the study by Poyet & Charles (2009) the desorption at 20ºC and 45ºC for cement-based materials were obtained and are presented in Figure 5.19b. Those can be compared with the results from this study in Figure 5.19a. It is clearly visible that the most sensible material to temperature is the hemp concrete with a difference of almost 8% on the w for the same RH between 23ºC and 35ºC, followed by the cement-based material which presented a difference of more or less 1% between the 20ºC and 45ºC curves. In general the materials studied in this dissertation are less influenced by the temperature, but it should be also taken into account that the other isotherms were determined by the salt solutions method and, as explained in Chapter 5.2.3., this method results are definitely not accurate.

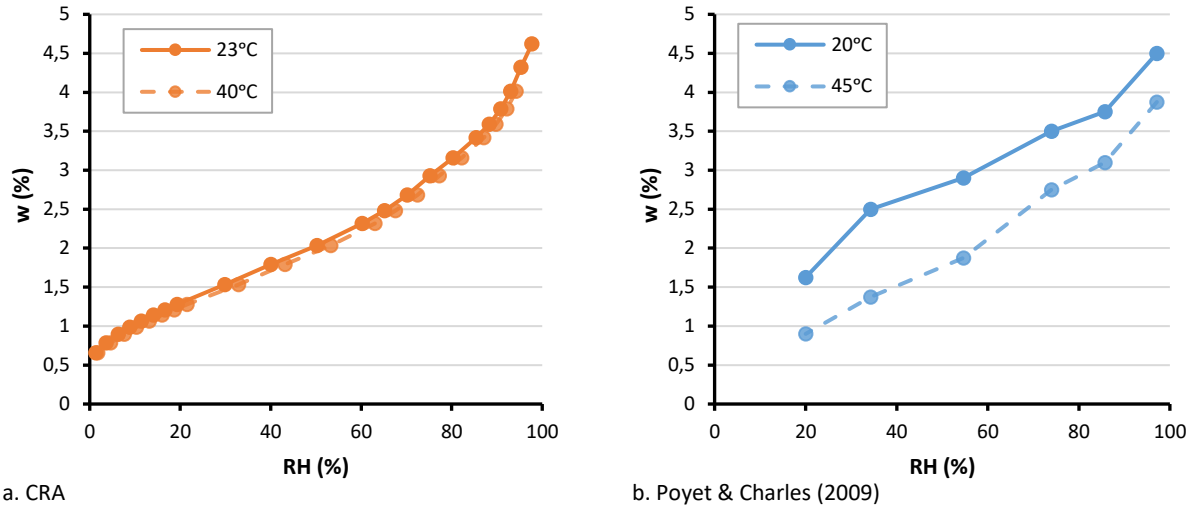

a. CRA

b. Poyet & Charles (2009)

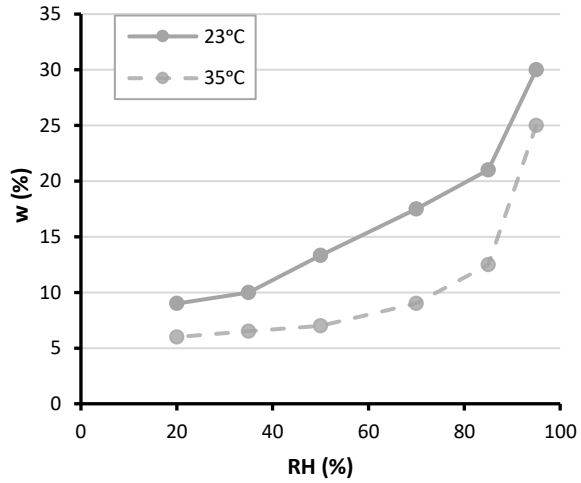

c. Aït Oumeziane et al. (2016)

Figure 5.19- Comparison of the influence of temperature between the desorption isotherms of CRA, Poyet & Charles (2009) and Aït Oumeziane et al. (2016)

5.5. Specific surface area

In this chapter it will be analysed if the calculated values for the specific surface area varies with temperature. As explained in the chapter 4.2.4. the DVS gave reliable results for the specific surface area at 23ºC; therefore at this time it was calculated at 30ºC. In table 5.9 the results for the earth plasters are presented. There is almost no difference between the two calculations, being even the same for the F5 plaster. Indeed this was expected since the specific surface area does not vary with temperature, although the DVS calculations could lead to some differences and it occurred for the compressed earth samples. By analysing table 5.10 some considerable variations are present mainly for CRA. This might have happened due to some inaccurate value used in the calculation.

Table 5.9- Comparison between the specific surface area of the earth plasters at 23ºC and 30ºC

Plaster	S_{BET} (m^2/g) 23ºC	S_{BET} (m^2/g) 30ºC
F0	14.2	14.3
F3	10.1	9.5
F5	4.8	4.8
F6	15.9	15.8

Table 5.10- Comparison between the specific surface area of the compressed earth samples at 23ºC and 30ºC

CEB	S_{BET} (m^2/g) 23ºC	S_{BET} (m^2/g) 30ºC
STR	16.4	17.2
ALX	12.4	12.2
CRA	24.5	31.5
STA	23.4	21.7

5.6. Discussion

In this chapter the results obtained before will be related in order to better understand and characterise the effect of temperature on the tested hygrothermal material properties. Starting by the water vapour resistance values, the effect of reproducing the test at a higher temperature of 40ºC leaded to a slight increase of the μ factor. The increase of the μ factor with temperature cannot be explained with the obtained results. A first hypothesis could be made that the temperature influences the vapour and liquid transfer process. A lower adsorbed water in the samples at 40°C should in theory increase the unsaturated porosity; therefore more pores could be available to transfer moisture. Yet this is in contradiction with the observed results. The vapour permeability test does, however, lack of accuracy; even if most of precaution has been made to avoid experimental variability, the difference could be due to this lack of precision in the test.

As expected and explained in the chapter 2.2. the sorption isotherms exhibited a "S" shape classified as the II B type isotherm, common in clayey materials. For all the studied samples it is clear that the temperature influenced the water content along the isotherm cycle, as higher temperatures leaded to lower water contents. Indeed, the rising temperatures promotes water molecule agitation and therefore desorption from the surface. However, this effect was not the same for all the samples: within the earth plasters the F0 and F6 were the most influenced by the temperature. This also corresponds with higher equilibrium moisture content, and surface area of these plasters.

For the compressed earth blocks there was no common trend between the ones with better performance and the ones more sensible to a temperature variation. STA stood out from the other CEB with the higher equilibrium moisture content followed by CRA; both also presented the higher surface area. In the opposite ALX reached lower water content levels and it was as well the CEB most influenced by temperature.

Comparing the earth plasters with the CEB, the plasters were much more influenced by the higher temperatures. This can be related to the presence of organic fibres in their composition as those are much more influenced by temperature as seen in the literature. In general it is observed that the CEB have a higher surface area, that increase molecular agitation and hampers desorption; yet they are still less influenced by temperature than the plasters, which leads to conclude that surface area alone does not determine the influence of temperature.

The estimated heat proved to be in accordance with the calculated values of heat of sorption, confirming to be a reliable tool for non-conventional earth based materials. It also revealed to be a proper method to estimate sorption curves at different temperatures (0ºC, 30ºC and 40ºC). However this estimation is clearly dependent on the precision of the heat values calculated from isotherms. As discussed earlier the DVS provides precise isotherms, which indeed helps to calculate accurate heat values. In fact, this was also concluded by various researchers who studied the heat of sorption and estimated isotherms through it. From the comparison it was found that the earth based materials are not so influenced by the temperature unlike cement based materials or hemp concrete.

6. Conclusion

6.1. Summary

The first stage of this study consisted on understanding the different assumptions and the reliability of the methods described in the experimental tests, in order to validate the steady state characteristics of the studied materials. The experimental determination of water vapour permeability is highly sensitive to the variation in test conditions. It was demonstrated the importance of choosing a quality desiccator for the dry cup test. Overall, a continuous monitoring of RH levels inside and outside the cup during the test is recommended to obtain the most accurate results.

The sorption isotherms performed with the salt solutions should be carefully prepared in order to obtain the expected RH levels, and confirm those levels regularly. However, this method showed to be much more imprecise than the DVS method. Even in the DVS specific care should be taken for the set up of the experiment. After this study it could be concluded on the importance of using the same specimen and taking care to obtain a stable dry air system in order to compare cycles at different temperatures. Also in the DVS, it was concluded that the dry mass should be obtained by the 0% RH stage before starting the adsorption-desorption cycles. However, the dry mass in this stage varies with temperature for the same specimen. In order to have accurate comparisons between curves at different temperature and also more realistic results, a dry mass correction is imperative. Because of the size of the DVS samples only composite materials with small fine particle size can be tested to assure representativeness. The relation between the sorption isotherms of the fine fraction and the bulk of the material is still to be investigated.

For the plasters, the analysis of the influence of temperature on the water vapour resistance showed a negligible effect with almost the same results at 23ºC and 40ºC. The F3 plaster, however, was more affected by the temperature with higher values at 40ºC. In general the obtained results are slightly lower than the ones presented by literature, but also as explained in the end of Chapter 5.1 this test has a big range of variation.

The sorption curves exhibited a decrease in the water content with the increase of temperature at constant RH, which confirms the statement that the water content increases with the increase of RH and decreases with rise in temperature. For the earth plasters the F6 was the one that reached higher water contents alongside with F0. This happened due to the presence of montmorillonite, a highly adsorbing clay mineral in the F6 composition. Furthermore, those two formulations were the most influenced by temperature: in the F3 and F5 almost no difference was exhibited, but even so F3 present a good hygroscopic behaviour while F5 presented the lowest potential.

For the compressed earth blocks the effect of temperature is even lower. Indeed the water content decrease but the variation was negligible for the formulations. These samples also exhibited higher amounts of adsorbed water, this can be related to their composition, compare to plasters there are no fibres but a higher clay content. This leads to a greater hygroscopic capacity compared to the earth plasters. Nevertheless in real buildings, it is common that the compressed earth materials (as rammed earth or blocks) are protected by a plaster and/or a paint system, which in turn can limit their hygrothermal behaviour. To profit from all the hygroscopic capacity the surface should remain uncoated.

Also the specific surface area and the heat involved in the sorption process were determined. The specific surface area gives an indication on the hygroscopic behaviour of the material and, indeed, in this study higher surface area corresponds to higher amounts of adsorbed water. The estimated heat revealed to be very accurate in accordance with the calculated results, which indicates that the DVS results as good enough to his determination. The estimated heat of sorption showed good agreement with values from the literature with maximum values occurring during the monolayer water covering stage followed by a exponential decrease. However the maximum heat obtained from the CEB results show a strong deviation with calculated results. This could either invalidated the assumption that the isosteric heat and the integral heat of sorption can be, for a sufficient water content, considered to be equal which at lower contents turns not be true. Or it may question the impact of the dry mass correction for these samples at lower water content.

The heat of sorption also proved to be an accurate tool to predict the effect of temperature on the sorption isotherms. The calculated and estimated 30ºC isotherm perfectly matched. The 0ºC and 40ºC isotherms followed a consistent trend compared to the measured curves. Finally, this allow a larger and proper analyse of the hygroscopic behaviour along different temperatures.

6.2. Future work

In order to continue the work developed in this dissertation, some future work should be done. This will confirm and increase the accuracy of the obtained results, and provide an inventory of these properties for this type of materials.

Enlarge experimental data:
All the tests performed should be repeated for a larger set of temperatures to increase the precision of predicted data and enlarge the experimental data validation.

Investigate representability of fine fractions:
Also a repetition of the sorption isotherms by the DVS method should be done with, at this time larger samples, to improve the representability of samples for macroporosity. A correlation can then be searched between the sorption isotherms of isolated fine fractions with the bulk of the material.

Determine a procedure to obtain dry mass:
A new procedure to determine the dry mass needs to be tested. An option could be to program a dry stage at, for example, 40ºC in the DVS, save the dry mass obtained and only afterwards start the sorption cycles at the desired temperatures. This will probably improve the accuracy of the dry mass correction defined in this dissertation and possibly the heat of sorption results. This study would have a larger impact on the methods to determine sorption curves for clay/bio-based composite materials.

Investigate relation between isosteric heat and the integral heat of sorption:
For the heat of sorption it is also imperative to study and analyse the difference between the isosteric heat and the integral heat of sorption at lower water contents. It should increase the understanding and accuracy of the results.

Numerical modelling of results:
Another improvement could be the utilisation of a programming software as for example Matlab to compute the results. It would allow better estimations of sorption curves at different temperatures. Finally studying the influence of these characteristics in a full scale building modelisation and also in other important material properties that were not study, like mechanical characteristics or the thermal conductivity will be important to predict the energy performance of a building.

Publications:

Part of the results obtained in this dissertation have been submitted to a scientific journal specially on the work done on the measurement of water vapour permeability.
Another publication will be submitted with the results on the isosteric heat of sorption

References

Abdul-Wahab, S., En, S., Elkamel, A., Ahmadi, L., & Yetilmezsoy, K. (2015). A review of standards and guidelines set by international bodies for the parameters of indoor air quality. *Atmospheric Pollution Research*, *6*(5), 751–767. http://doi.org/10.5094/APR.2015.084

Aït Oumeziane, Y., Moissette, S., Bart, M., & Lanos, C. (2016). Influence of temperature on sorption process in hemp concrete. *Construction and Building Materials*, *106*, 600–607. http://doi.org/10.1016/j.conbuildmat.2015.12.117

Al Horr, Y., Arif, M., Katafygiotou, M., Mazroei, A., Kaushik, A., & Elsarrag, E. (2016). Impact of indoor environmental quality on occupant well-being and comfort : A review of the literature. *International Journal of Sustainable Built Environment*, *5*(1), 1–11. http://doi.org/10.1016/j.ijsbe.2016.03.006

Allinson, D., & Hall, M. (2010). Hygrothermal analysis of a stabilised rammed earth test building in the UK. *Energy and Buildings*, *42*(6), 845–852. http://doi.org/10.1016/j.enbuild.2009.12.005

Ashour, T., Georg, H., & Wu, W. (2011). An experimental investigation on equilibrium moisture content of earth plaster with natural reinforcement fibres for straw bale buildings. *Applied Thermal Engineering*, *31*, pp.293-303. article.

Barbosa, R., Vicente, R., & Santos, R. (2015). Climate change and thermal comfort in Southern Europe housing : A case study from Lisbon. *Building and Environment*, *92*, 440–451. http://doi.org/10.1016/j.buildenv.2015.05.019

Bui, Q., Morel, J., Hans, S., & Walker, P. (2014). Effect of moisture content on the mechanical characteristics of rammed earth. *Construction and Building Materials*, *54*, 163–169. http://doi.org/10.1016/j.conbuildmat.2013.12.067

Cagnon, H., Aubert, J. E., Coutand, M., & Magniont, C. (2014). Hygrothermal properties of earth bricks. *Energy and Buildings*, *80*, 208–217. http://doi.org/10.1016/j.enbuild.2014.05.024

Chabriac P.A. Fabbri A., M. J. C. J. P. L. J. B.-G. (2014). A procedure to measure the in-situ hygrothermal behavior of earth walls,. *Material*, *7*, 3002–3020. article.

Champiré, F., Fabbri, A., Morel, J. C., Wong, H., & McGregor, F. (2016). Impact of relative humidity on the mechanical behavior of compacted earth as a building material. *Construction and Building Materials*, *110*, 70–78. http://doi.org/10.1016/j.conbuildmat.2016.01.027

Desogus, G., Benedetto, S. Di, & Ricciu, R. (2015). The use of adaptive thermal comfort models to evaluate the summer performance of a Mediterranean earth building. *Energy & Buildings*, *104*, 350–359. http://doi.org/10.1016/j.enbuild.2015.07.020

Douillard, J., & Salles, F. (2004). Phenomenology of water adsorption at clay surfaces. In *Clay Surfaces: Fundamentals and Applications* (pp. 119–151).

Dubois, S., McGregor, F., Evrard, A., Heath, A., & Lebeau, F. (2014a). An inverse modelling approach to estimate the hygric parameters of clay-based masonry during a Moisture Buffer Value test. *Building and Environment*, *81*(0), pp.192-203. article.

Dubois, S., McGregor, F., Evrard, A., Heath, A., & Lebeau, F. (2014b). An inverse modelling approach to estimate the hygric parameters of clay-based masonry during a Moisture Buffer Value test. *Building and Environment*, *81*, 192–203. http://doi.org/10.1016/j.buildenv.2014.06.018

F.McGregor. (2014). *Moisture buffering capacity of unfired clay masonry* (phdthesis). University of Bath.

Faria, P., dos Santos, T., & Aubert, J.-E. (2015). Experimental Characterization of an Earth Eco-Efficient Plastering Mortar. *Journal of Materials in Civil Engineering*, *28*(english). http://doi.org/10.1061/(ASCE)MT.1943-5533.0001363.

Feng, C., & Janssen, H. (2016). Hygric properties of porous building materials (II): Analysis of temperature influence. *Building and Environment*, *99*, 107–118. http://doi.org/10.1016/j.buildenv.2016.01.016

Fredlund, D. G., & Rahardjo, H. (1993). *Soil Mechanics for Unsaturated Soils*.

Hall, M., & Allinson, D. (2009). Analysis of the hygrothermal functional properties of stabilised rammed earth materials. *Applied Thermal Engineering*, *29*(4), 740–747. http://doi.org/10.1016/j.applthermaleng.2008.03.051

Hansen, E., & Hansen, M. H. (2002). Unfired clay bricks-moisture properties and compressive strength. In *Proceedings of the 6th Symposium on Building Physics in the Nordic Countries*. inproceedings.

Heathcote, K. (2011). El comportamiento térmico de los edificios de tierra, *63*, 117–126. http://doi.org/10.3989/ic.10.024

Henriques, F. M. A. (2007). Comportamento Higrotérmico De Edifícios. Faculdade de Ciências e Tecnologia - Universidade Nova de Lisboa, Monte de Caparica.

Hens, H. (2012). *Building Physics: Heat, Air and Moisture.* (2nd ed.).

Holcroft, N., & Shea, A. (2012). Moisture buffering and latent heat effects in natural fibre insulation materials, 221–228.

ISO-12571. (2000). Hygrothermal performance of building materials and products.Determination of hygroscopic sorption properties. standard, Geneva, Switzerland: International Organization for Standardization.

ISO-12572. (2001). Determination of water vapour transmission properties. standard, Geneva, Switzerland: International Organization for Standardization.

Kunzel, H. (1995). *Simultaneous Heat and Moisture Transport in Building Components* (Vol. 1995).

Labat, M., Magniont, C., Oudhof, N., & Aubert, J. (2016). From the experimental characterization of the hygrothermal properties of straw-clay mixtures to the numerical assessment of their buffering potential, *97*, 69–81. http://doi.org/10.1016/j.buildenv.2015.12.004

Laurent, J.-P. (1984). *Contribution a la caractérisation thermique des milieux poreux granulares*.

Likos, W., & Lu, N. (2002). Water vapor sorption behavior of smectite-kaolinite mixtures. *Clays and Clay Minerals*, *50*, 553–561.

Lima, J., & Faria, P. (2013). Eco-Efficient Earthen Plasters : The Influence of the Addition of Natural Fibers, 315–327. http://doi.org/10.1007/978-94-017-7515-1

Liuzzi, S., Hall, M. R., Stefanizzi, P., & Casey, S. P. (2012). Hygrothermal behaviour and relative humidity buffering of unfired and hydrated lime-stabilised clay composites in a Mediterranean climate. *Building and Environment*, *61*, 82–92.

Liuzzi, S., Hall, M. R., Stefanizzi, P., & Casey, S. P. (2013). Hygrothermal behaviour and relative humidity buffering of un fi red and hydrated lime-stabilised clay composites in a Mediterranean climate. *Building and Environment*, *61*, 82–92. http://doi.org/10.1016/j.buildenv.2012.12.006

Lustig-Rssler, U. (1992). *Untersuchungen zum feuchterverhalten von Lehm als Baustoff* (phdthesis). Inaugural dissertation, Gesamthochschule Universitat Kassel, Kassel.

McGregor, F. (2014). *Moisture buffering capacity of unfired clay masonry*.

McGregor, F., Heath, A., Fodde, E., & Shea, A. (2014). Conditions affecting the moisture buffering measurement performed on compressed earth blocks. *Building and Environment*, *75*, 11–18. http://doi.org/10.1016/j.buildenv.2014.01.009

McGregor, F., Heath, A., Shea, A., & Lawrence, M. (2014). The moisture buffering capacity of unfired clay masonry. *Building and Environment*, *82*, 599–607. http://doi.org/10.1016/j.buildenv.2014.09.027

Medjelekh, D., Ulmet, L., & Abdou, S. (2016). A field study of thermal and hygric inertia and its effects on indoor thermal comfort : Characterization of travertine stone envelope. *Building and Environment*, *106*, 57–77. http://doi.org/10.1016/j.buildenv.2016.06.010

Meunier, A. (2005). *Clays*.

Mihoubi, D., & Bellagi, A. (2006). Thermodynamic analysis of sorption isotherms of bentonite. *Journal of Chemical Thermodynamics*, *38*(9), 1105–1110. http://doi.org/10.1016/j.jct.2005.11.010

Minke, G. (2009). *Earth Construction Handbook*.

Morel, J. C., Mesbah, A., Oggero, M., & Walker, P. (2001). Building houses with local materials : means to drastically reduce the environmental impact of construction, *36*, 1119–1126.

Orosa, J. A., & Oliveira, A. C. (2012). A field study on building inertia and its effects on indoor thermal environment. *Renewable Energy*, *37*(1), 89–96. http://doi.org/10.1016/j.renene.2011.06.009

Poyet, S. (2009). Experimental investigation of the effect of temperature on the first desorption isotherm of concrete. *Cement and Concrete Research*, *39*(11), 1052–1059. http://doi.org/10.1016/j.cemconres.2009.06.019

Poyet, S., & Charles, S. (2009). Temperature dependence of the sorption isotherms of cement-based materials: Heat of sorption and Clausius-Clapeyron formula. *Cement and Concrete Research*, *39*(11), 1060–1067. http://doi.org/10.1016/j.cemconres.2009.07.018

Ramos, N. M. M., Delgado, J. M. P. Q., & De Freitas, V. P. (2010). Influence of finishing coatings on hygroscopic moisture buffering in building elements. *Construction and Building Materials*, *24*(12), 2590–2597. http://doi.org/10.1016/j.conbuildmat.2010.05.017

Roels, S., Carmeliet, J., Hens, H., Adan, O., Brocken, H., Cerny, R., … Pel, L. (2004). Interlaboratory comparison of hygric properties of porous building materials. *Journal of Thermal Envelope and Building Science*, *27*, pp.307-325. article.

Rouquerol, F., Rouquerol, J., & Sing, K. (1999). *Adsorption by powders & porous solids*. London: Academic Press.

Rouquerol, J., Avnir, D., Fairbridge, C., Everett, D., Haynes, J., Pernicone, N., … Unger, K. (1994). Recommendations for the characterization of porous solids, *66*(8), 1739–1758.

Rupp, R., Vásquez, N., & Lamberts, R. (2015). A review of human thermal comfort in the built environment. *Energy & Buildings*, *105*, 178–205. http://doi.org/10.1016/j.enbuild.2015.07.047

Serrano, S., Gracia, A. De, & Cabeza, L. F. (2016). Adaptation of rammed earth to modern construction systems : Comparative study of thermal behavior under summer conditions. *Applied Energy*, *175*, 180–188. http://doi.org/10.1016/j.apenergy.2016.05.010

Silva, H. E., & Henriques, F. M. A. (2014). Microclimatic analysis of historic buildings : A new methodology for temperate climates. *Building and Environment*, *82*, 381–387. http://doi.org/10.1016/j.buildenv.2014.09.005

Simões, T. (2015). Moisture buffering capacity of earth mortar plasters and hemp concrete Effect of temperature and thickness.

Sing, K. S. W. (1985). Reporting physisorption data for gas/solid systems with special reference to the determination of surface area and porosity (Recommendations 1984). *Pure and Applied Chemistry*, *Vol. 57*(Issue 4), 603–619. article.

Soudani, L., Fabbri, A., Morel, J.-C., Woloszyn, M., & Chabriac, P.-A. (2016). Assessment of the validity of some common assumptions in hygrothermal modelling of earth based materials. *Energy and Buildings, Accepted*, *116*, 498–511. http://doi.org/10.1016/j.enbuild.2016.01.025

Taylor, P., Fuller, R. J., & Luther, M. B. (2008). Energy use and thermal comfort in a rammed earth office building, *40*, 793–800. http://doi.org/10.1016/j.enbuild.2007.05.013

Tonelli, C., & Grimaudo, M. (2014). Timber buildings and thermal inertia : Open scientific problems for summer behavior in Mediterranean climate. *Energy & Buildings*, *83*, 89–95. http://doi.org/10.1016/j.enbuild.2013.12.063

Tuller, M., Dani, O., & Dudley, L. M. (1999). Adsorption and capillary condensation in porous media: Liquid retention and interfacial configurations in angular pores. *Water Resources Research*, *35*(7), 1949–1964. http://doi.org/10.1029/1999WR900098

Vololonirina, O., Coutand, M., & Perrin, B. (2014). Characterization of hygrothermal properties of wood-based products – Impact of moisture content and temperature. *Construction and Building Materials*, *63*, 223–233. http://doi.org/10.1016/j.conbuildmat.2014.04.014

Vololonirina, O., & Perrin, B. (2016). Inquiries into the measurement of vapour permeability of permeable materials. *Construction and Building Materials*, *102*, 338–348. http://doi.org/10.1016/j.conbuildmat.2015.10.126

Appendix

I. Diffusion test

A. Monitored relative humidity

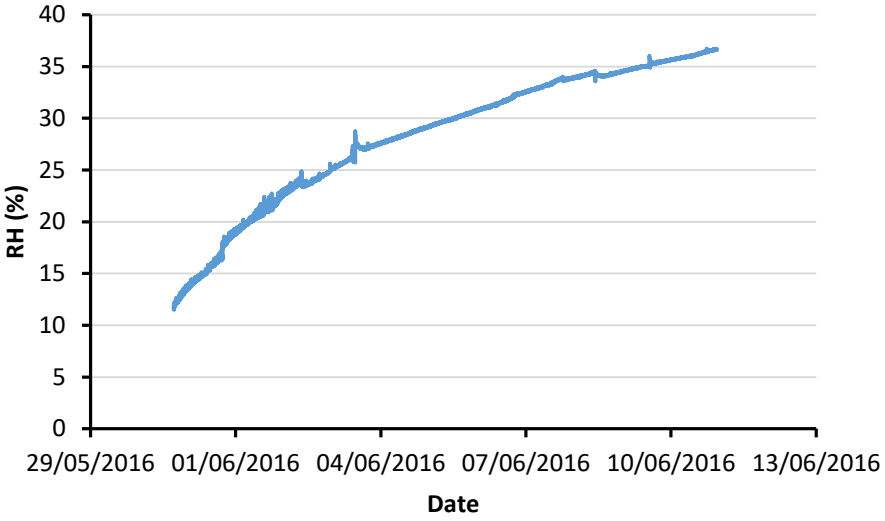

Figure A.1- RH evolution in the dry cup test with silica gel

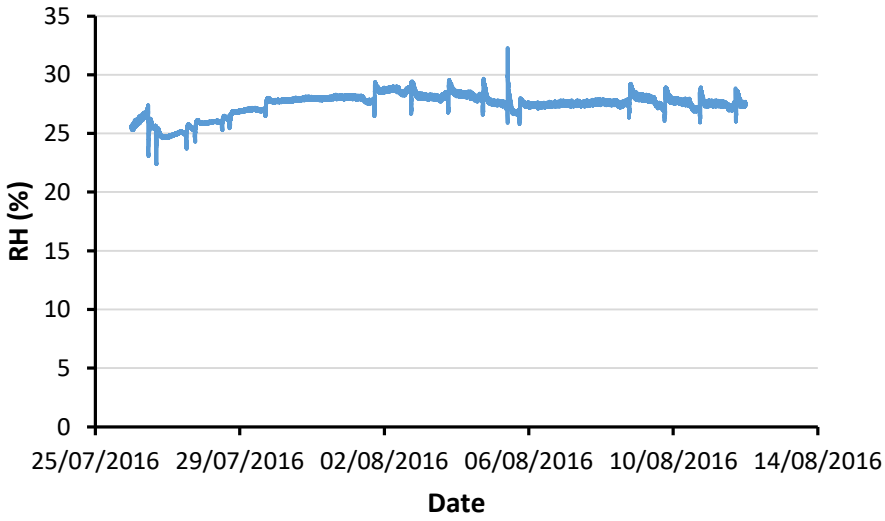

Figure A.2- RH evolution of the F0 1.3 plaster in the dry cup test with salt solutions (Potassium acetate)

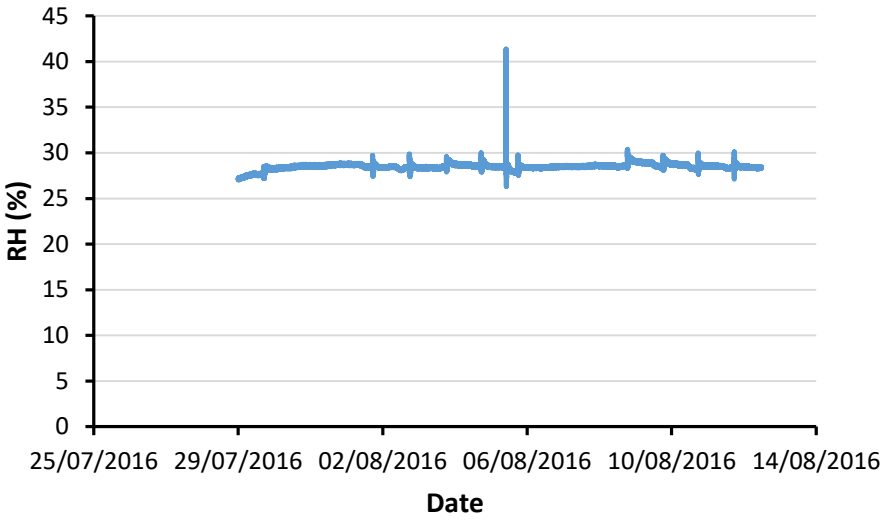

Figure A.3- RH evolution of the F3 1.3 plaster in the dry cup test with salt solutions (Potassium acetate)

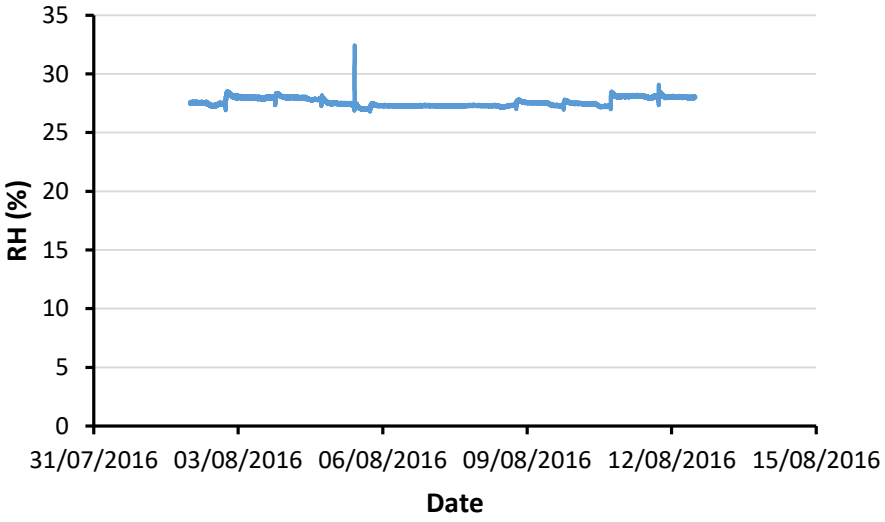

Figure A.4- RH evolution of the F5 1.2 plaster in the dry cup test with salt solutions (Potassium acetate)

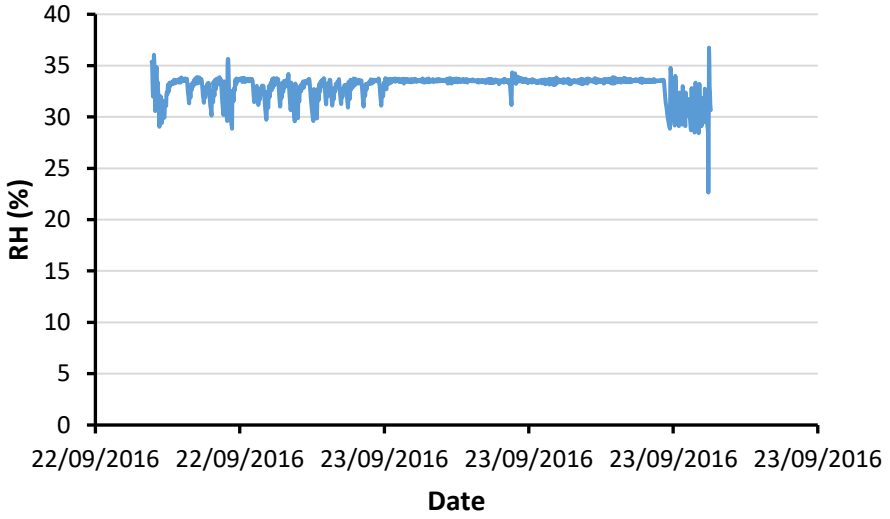

Figure A.5- RH evolution in the wet cup test t 40ºC

A.1. Variation of mass by time for the dry cup test with salt solutions

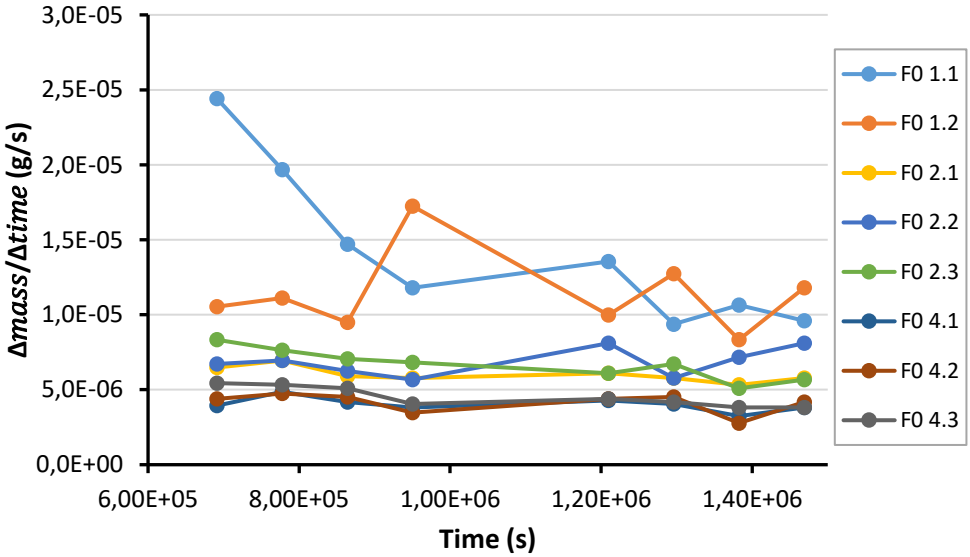

Figure A.6- Rate of mass variation of F0 plaster during the dry cup test with salt solutions (Potassium acetate)

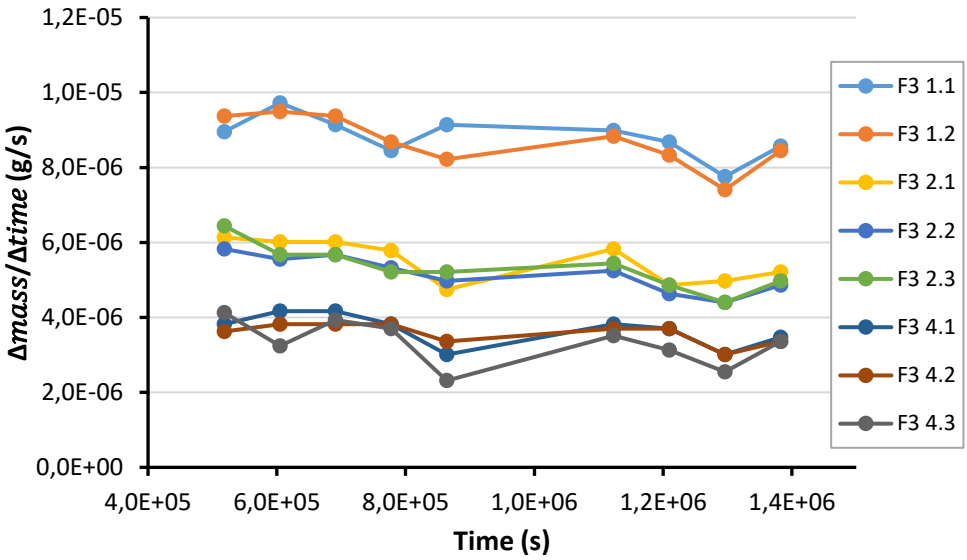

Figure A.7- Rate of mass variation of F3 plaster during the dry cup test with salt solutions (Potassium acetate)

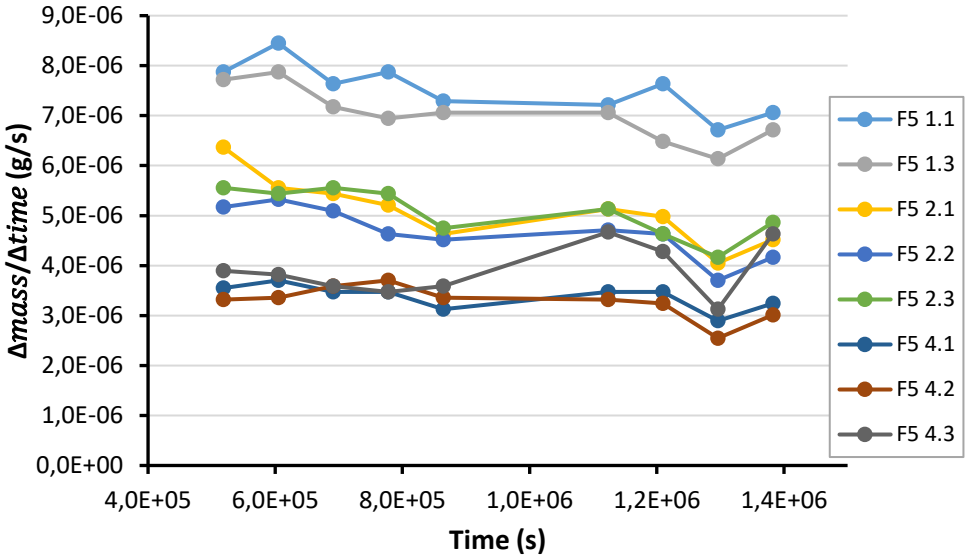

Figure A.8- Rate of mass variation of F5 plaster during the dry cup test with salt solutions (Potassium acetate)

A.2. β correction

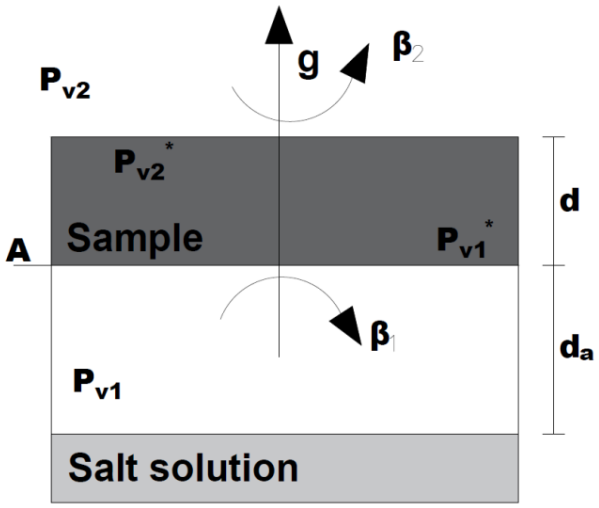

Figure A.9- Layout of the process during the test

- g is the density of water vapour flow rate;
- p is the partial vapour pressure;
- β is the surface transfer coefficient;
- A the exposed surface;
- d the thickness of the sample;

$$\frac{\Delta m}{\Delta t} = G = A \cdot \delta_p \cdot \frac{\Delta P_v^*}{d}$$

$$\frac{G}{A} = \beta_2 (P_{v2} - P_{v2}^*) = \beta_1 (P_{v1}^* - P_{v1})$$

$$\Delta P_v^* = \Delta P_v - \frac{G}{A \cdot \beta_2} - \frac{G}{A \cdot \beta_1}$$

$$\delta_p^\beta = \frac{G \cdot d}{A \cdot \Delta P_v - G\left(\frac{1}{\beta_2} + \frac{1}{\beta_1}\right)} = \frac{G \cdot d}{A \cdot \Delta P_v - \frac{G}{\beta}}$$

$$\delta_p^\beta = \frac{d}{\frac{d}{\delta_p^{agc}} + \frac{1}{\beta}}$$

A.3. Results

Dry cup 23°C (silica gel)

Plaster	G (kg/s)	g (kg/(s.m²))	W (kg/(s.m².Pa))	δ* (kg/(s.m.Pa))	Average	μ*	Average
F0 1.1	9,9E-09	8,71E-07	6,21E-10	6,21E-12	6,10E-12	31.94	32.48
F0 1.2	9,6E-09	8,52E-07	6,07E-10	6,07E-12		32.67	
F0 1.3	9,6E-09	8,48E-07	6,04E-10	6,04E-12		32.83	
F0 2.1	7,8E-09	6,91E-07	4,92E-10	9,85E-12	9,82E-12	20.13	20.18
F0 2.2	7,8E-09	6,90E-07	4,92E-10	9,83E-12		20.16	
F0 2.3	7,8E-09	6,87E-07	4,89E-10	9,79E-12		20.25	
F0 4.1	5,1E-09	4,54E-07	3,24E-10	1,29E-11	1,30E-11	15.32	15.23
F0 4.2	5,0E-09	4,46E-07	3,18E-10	1,27E-11		15.60	
F0 4.3	5,3E-09	4,71E-07	3,35E-10	1,34E-11		14,78	

Plaster	S_d (m)	W (kg/(s.m².Pa))	δ_p^{agc} (kg/(s.m.Pa))	Average	μ^{agc}	Average
F0 1.1	0,37	7,36E-10	7,36E-12	7,22E-12	26,94	27,48
F0 1.2	0,38	7,17E-10	7,17E-12		27,67	
F0 1.3	0,38	7,12E-10	7,12E-12		27,83	
F0 2.1	0,46	5,62E-10	1,12E-11	1,12E-11	17,63	17,68
F0 2.2	0,46	5,61E-10	1,12E-11		17,66	
F0 2.3	0,47	5,58E-10	1,12E-11		17,75	
F0 4.1	0,70	3,52E-10	1,41E-11	1,42E-11	14,07	13,98
F0 4.2	0,72	3,45E-10	1,38E-11		14,35	
F0 4.3	0,68	3,66E-10	1,47E-11		13,53	

Plaster	β	W (kg/(s.m^2.Pa))	δ^{β} (kg/(s.m.Pa))	Average	μ^{β}	Average
F0 1.1	1,264E-09	1,76E-09	1,76E-11	1,68E-11	11,26	11,79
F0 1.2		1,65E-09	1,66E-11		11,99	
F0 1.3		1,63E-09	1,63E-11		12,14	
F0 2.1		1,01E-09	2,03E-11	2,02E-11	9,79	9,84
F0 2.2		1,01E-09	2,02E-11		9,82	
F0 2.3		1,00E-09	2,00E-11		9,91	
F0 4.1		4,88E-10	1,95E-11	1,97E-11	10,15	10,06
F0 4.2		4,75E-10	1,90E-11		10,43	
F0 4.3		5,16E-10	2,06E-11		9,61	

Plaster	G (kg/s)	g (kg/(s.m^2))	W (kg/(s.m^2.Pa))	δ* (kg/(s.m.Pa))	Average	μ*	Average
F3 1.1	1,0E-08	9,14E-07	6,51E-10	6,51E-12	6,39E-12	30,47	31,03
F3 1.2	1,0E-08	9,00E-07	6,41E-10	6,41E-12		30,94	
F3 1.3	9,9E-09	8,78E-07	6,25E-10	6,25E-12		31,70	
F3 2.1	8,1E-09	7,12E-07	5,07E-10	1,01E-11	9,91E-12	19,54	20,02
F3 2.2	7,8E-09	6,85E-07	4,88E-10	9,76E-12		20,31	
F3 2.3	7,8E-09	6,89E-07	4,91E-10	9,81E-12		20,20	
F3 4.1	5,1E-09	4,50E-07	3,20E-10	1,28E-11	1,25E-11	15,47	15,86
F3 4.2	5,0E-09	4,42E-07	3,15E-10	1,26E-11		15,74	
F3 4.3	4,8E-09	4,25E-07	3,03E-10	1,21E-11		16,38	

Plaster	S_d (m)	W (kg/(s.m².Pa))	δ_p^{agc} (kg/(s.m.Pa))	Average	μ^{agc}	Average
F3 1.1	0,35	7,78E-10	7,78E-12	7,62E-12	25,47	26,03
F3 1.2	0,36	7,64E-10	7,61E-12		25,94	
F3 1.3	0,36	7,43E-10	7,43E-12		26,70	
F3 2.1	0,45	5,82E-10	1,16E-11	1,13E-11	17,04	17,52
F3 2.2	0,47	5,57E-10	1,11E-11		17,81	
F3 2.3	0,46	5,60E-10	1,12E-11		17,70	
F3 4.1	0,71	3,48E-10	1,39E-11	1,36E-11	14,22	14,61
F3 4.2	0,72	3,42E-10	1,37E-11		14,49	
F3 4.3	0,75	3,28E-10	1,31E-11		15,13	

Plaster	β	W (kg/(s.m².Pa))	δ^{β} (kg/(s.m.Pa))	Average	μ^{β}	Average
F3 1.1	1,453E-09	1,68E-09	1,68E-11	1,60E-11	11,82	12,39
F3 1.2		1,61E-09	1,61E-11		12,29	
F3 1.3		1,52E-09	1,52E-11		13,05	
F3 2.1		9,70E-10	1,94E-11	1,86E-11	10,22	10,69
F3 2.2		9,02E-10	1,80E-11		10,99	
F3 2.3		9,11E-10	1,82E-11		10,88	
F3 4.1		4,58E-10	1,83E-11	1,77E-11	10,81	11,20
F3 4.2		4,47E-10	1,79E-11		11,08	
F3 4.3		4,23E-10	1,69E-11		11,71	

Plaster	G (kg/s)	g (kg/(s.m²))	W (kg/(s.m².Pa))	δ^* (kg/(s.m.Pa))	Average	μ^*	Average
F5 1.1	8,2E-09	7,24E-07	5,15E-10	5,15E-12	5,12E-12	38,46	38,74
F5 1.2	8,1E-09	7,17E-07	5,11E-10	5,11E-12		38,80	
F5 1.3	8,1E-09	7,14E-07	5,09E-10	5,09E-12		38,97	
F5 2.1	6,4E-09	5,66E-07	4,03E-10	8,06E-12	8,32E-12	24,61	23,85
F5 2.2	6,7E-09	5,94E-07	4,23E-10	8,46E-12		23,44	
F5 2.3	6,7E-09	5,92E-07	4,22E-10	8,44E-12		23,50	
F5 4.1	4,3E-09	3,80E-07	2,71E-10	1,08E-11	1,15E-11	18,31	17,27
F5 4.2	4,6E-09	4,09E-07	2,91E-10	1,16E-11		17,03	
F5 4.3	4,8E-09	4,23E-07	3,01E-10	1,20E-11		16,46	

Plaster	S_d (m)	W (kg/(s.m².Pa))	δ_p^{agc} (kg/(s.m.Pa))	Average	μ^{agc}	Average
F5 1.1	0,38	5,92E-10	5,92E-12	5,88E-12	33,46	33,74
F5 1.2	0,39	5,87E-10	5,87E-12		33,80	
F5 1.3	0,39	5,84E-10	5,84E-12		33,97	
F5 2.1	0,49	4,48E-10	8,97E-12	9,29E-12	22,11	21,35
F5 2.2	0,47	4,73E-10	9,47E-12		20,94	
F5 2.3	0,47	4,72E-10	9,44E-12		21,00	
F5 4.1	0,73	2,91E-10	1,16E-11	1,24E-11	17,06	16,02
F5 4.2	0,68	3,14E-10	1,26E-11		15,78	
F5 4.3	0,66	3,26E-10	1,30E-11		15,21	

Plaster	β	W (kg/(s.m².Pa))	δ^{β} (kg/(s.m.Pa))	Average	μ^{β}	Average
F5 1.1	9.441E-09	1,59E-09	1,59E-11	1,56E-11	12,46	12,74
F5 1.2		1,55E-09	1,55E-11		12,80	
F5 1.3		1,53E-09	1,53E-11		12,97	
F5 2.1		8,54E-10	1,71E-11	1,83E-11	11,61	10,85
F5 2.2		9,49E-10	1,90E-11		10,44	
F5 2.3		9,44E-10	1,89E-11		10,50	
F5 4.1		4,20E-10	1,68E-11	1,85E-11	11,81	10,77
F5 4.2		4,71E-10	1,88E-11		10,53	
F5 4.3		4,98E-10	1,99E-11		9,96	

Dry cup 23ºC (salt solutions)

Plaster	G (kg/s)	g (kg/(s.m²))	W (kg/(s.m².Pa))	δ* (kg/(s.m.Pa))	Average	μ*	Average
F0 1.1	1,35E-08	1,20E-06	1,92E-09	1,92E-11	1,75E-11	10,33	11,40
F0 1.2	1,12E-08	9,91E-07	1,59E-09	1,59E-11		12,47	
F0 2.1	6,01E-09	5,31E-07	8,52E-10	1,70E-11	1,85E-11	11.63	10,75
F0 2.2	7,10E-09	6,28E-07	1,01E-09	2,02E-11		9.84	
F0 2.3	6,48E-09	5,73E-07	9,19E-10	1,84E-11		10.78	
F0 4.1	4,11E-09	3,63E-07	5,83E-10	2,33E-11	2,41E-11	8.51	8,29
F0 4.2	4,19E-09	3,70E-07	5,94E-10	2,38E-11		8.34	
F0 4.3	4,45E-09	3,93E-07	6,31E-10	2,52E-11		7.86	

Plaster	S_d (m)	W (kg/(s.m².Pa))	δ_p^{agc} (kg/(s.m.Pa))	Average	μ^{agc}	Average
F0 1.1	0,10	2,38E-09	2,38E-11	2,14E-11	8,33	9,40
F0 1.2	0,12	1,89E-09	1,89E-11		10,47	
F0 2.1	0,23	9,35E-10	1,86E-11	2,04E-11	10,63	9,75
F0 2.2	0,20	1,11E-09	2,24E-11		8,84	
F0 2.3	0,22	1,01E-09	2,03E-11		9,78	
F0 4.1	0,34	6,19E-10	2,48E-11	2,57E-11	8,01	7,74
F0 4.2	0,33	6,32E-10	2,53E-11		7,84	
F0 4.3	0,31	6,74E-10	2,70E-11		7,36	

Plaster	G (kg/s)	g (kg/(s.m²))	W (kg/(s.m².Pa))	δ* (kg/(s.m.Pa))	Average	μ*	Average
F3 1.1	8,8E-09	7,81E-07	1,29E-09	1,29E-11	1,29E-11	15,32	15,38
F3 1.2	8,8E-09	7,75E-07	1,28E-09	1,28E-11		15,45	
F3 2.1	5,5E-09	4,86E-07	8,06E-10	1,61E-11	1,55E-11	12,30	12,82
F3 2.2	5,1E-09	4,52E-07	7,48E-10	1,50E-11		13,25	
F3 2.3	5,2E-09	4,63E-07	7,67E-10	1,53E-11		12,92	
F3 4.1	3,7E-09	3,24E-07	5,37E-10	2,15E-11	2,06E-11	9,24	9,65
F3 4.2	3,6E-09	3,19E-07	5,29E-10	2,12E-11		9,37	
F3 4.3	3,3E-09	2,89E-07	4,79E-10	1,92E-11		10,34	

Plaster	S_d (m)	W (kg/(s.m^2.Pa))	δ_p^{agc} (kg/(s.m.Pa))	Average	μ_p^{agc}	Average
F3 1.1	0,15	1,49E-09	1,49E-11	1,48E-11	13,32	13,38
F3 1.2	0,15	1,47E-09	1,47E-11		13,45	
F3 2.1	0,25	8,77E-10	1,75E-11	1,68E-11	11,30	11,82
F3 2.2	0,26	8,10E-10	1,62E-11		12,25	
F3 2.3	0,26	8,32E-10	1,66E-11		11,92	
F3 4.1	0,37	5,67E-10	2,27E-11	2,17E-11	8,74	9,15
F3 4.2	0,37	5,59E-10	2,24E-11		8,87	
F3 4.3	0,41	5,04E-10	2,01E-11		9,84	

Plaster	G (kg/s)	g (kg/(s.m^2))	W (kg/(s.m^2.Pa))	δ^* (kg/(s.m.Pa))	Average	μ^*	Average
F5 1.1	7,4E-09	6,53E-07	1,04E-09	1,04E-11	1,01E-11	19,10	19,72
F5 1.3	6,9E-09	6,13E-07	9,75E-10	9,75E-12		20,34	
F5 2.1	5,0E-09	4,41E-07	7,01E-10	1,40E-11	1,37E-11	14,15	14,50
F5 2.2	4,6E-09	4,08E-07	6,49E-10	1,30E-11		15,28	
F5 2.3	5,0E-09	4,43E-07	7,05E-10	1,41E-11		14,07	
F5 4.1	3,4E-09	2,99E-07	4,75E-10	1,90E-11	2,02E-11	10,43	9,90
F5 4.2	3,3E-09	2,92E-07	4,64E-10	1,86E-11		10,69	
F5 4.3	4,1E-09	3,63E-07	5,77E-10	2,31E-11		8,59	

Plaster	S_d (m)	W (kg/(s.m^2.Pa))	δ_p^{agc} (kg/(s.m.Pa))	Average	μ_p^{agc}	Average
F5 1.1	0,19	1,16E-09	1,16E-11	1,12E-11	17,10	17,72
F5 1.3	0,20	1,08E-09	1,08E-11		18,34	
F5 2.1	0,28	7,54E-10	1,51E-11	1,47E-11	13,15	13,50
F5 2.2	0,31	6,94E-10	1,39E-11		14,28	
F5 2.3	0,28	7,59E-10	1,52E-11		13,07	
F5 4.1	0,42	4,99E-10	2,00E-11	2,13E-11	9,93	9,40
F5 4.2	0,43	4,87E-10	1,95E-11		10,19	
F5 4.3	0,34	6,13E-10	2,45E-11		8,09	

Wet cup 40°C

Plaster	G (kg/s)	g (kg/(s.m²))	W (kg/(s.m².Pa))	δ* (kg/(s.m.Pa))	Average	μ*	Average
F0 1.2	5,1E-08	4,5E-06	1,23E-09	1,23E-11	1,23E-11	16,83	16,87
F0 1.3	5,1E-08	4,5E-06	1,23E-09	1,23E-11		16,91	
F0 4.1	2,2E-08	1,9E-06	5,28E-10	2,11E-11	2,12E-11	9,82	9,77
F0 4.2	2,2E-08	2,0E-06	5,34E-10	2,14E-11		9,71	
F3 1.1	5,1E-08	4,5E-06	1,22E-09	1,22E-11	1,17E-11	16,98	17,74
F3 1.3	4,7E-08	4,1E-06	1,12E-09	1,12E-11		18,49	
F3 4.2	2,0E-08	1,8E-06	4,76E-10	1,90E-11	1,91E-11	10,90	10,85
F3 4.3	2,0E-08	1,8E-06	4,80E-10	1,92E-11		10,80	

Plaster	S_d (m)	W (kg/(s.m².Pa))	δ_p^{agc} (kg/(s.m.Pa))	Average	μ^{agc}	Average
F0 1.2	0,17	1,50E-09	1,5E-11	1,50E-11	12,66	12,70
F0 1.3	0,17	1,49E-09	1,5E-11		12,74	
F0 4.1	0,39	5,72E-10	2,3E-11	2,30E-11	8,31	8,26
F0 4.2	0,39	5,79E-10	2,3E-11		8,21	
F3 1.1	0,17	1,48E-09	1,5E-11	1,41E-11	12,81	13,50
F3 1.3	0,18	1,34E-09	1,3E-11		14,19	
F3 4.2	0,44	5,11E-10	2,0E-11	2,05E-11	9,29	9,25
F3 4.3	0,43	5,16E-10	2,1E-11		9,20	

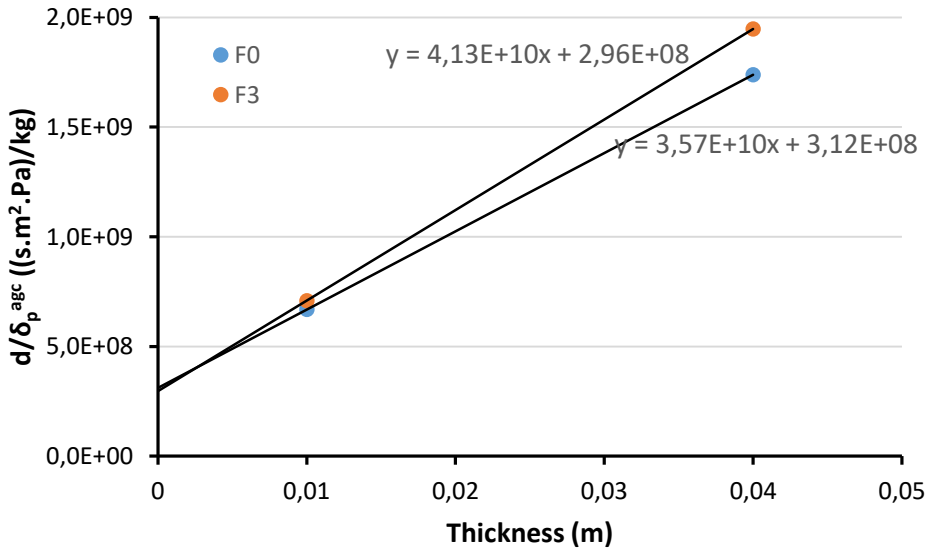

Figure A.10- Evolution of d/δ_p^{agc} as a function of the earth plasters thickness (wet cup 40°C)

II. Sorption isotherms by salt solutions

B. Earth plasters

Plaster	RH (%)	Dry mass (g)	Equilibrium mass (g)	w (%)	w Average (%)
F0 1	23%	44,26	44,41	0,33	0,32
F0 2		47,75	47,90	0,33	
F0 3		49,33	49,48	0,30	
F3 1		53,00	53,11	0,20	0,21
F3 2		54,87	54,99	0,21	
F3 3		49,23	49,34	0,21	
F5 1		54,25	54,31	0,12	0,12
F5 2		55,12	55,19	0,12	
F5 3		61,65	61,73	0,13	
F6 1		51,96	52,15	0,37	0,39
F6 2		43,85	44,02	0,39	
F6 3		51,46	51,67	0,41	

Plaster	RH (%)	Dry mass (g)	Equilibrium mass (g)	w (%)	w Average (%)
F0 1	43%	44,26	44,51	0,56	0,56
F0 2		47,75	48,02	0,57	
F0 3		49,33	49,60	0,54	
F3 1		53,00	53,19	0,35	0,37
F3 2		54,87	55,07	0,37	
F3 3		49,23	49,41	0,37	
F5 1		54,25	54,36	0,21	0,21
F5 2		55,12	55,24	0,21	
F5 3		61,65	61,78	0,22	
F6 1		51,96	52,31	0,68	0,70
F6 2		43,85	44,16	0,71	
F6 3		51,46	51,82	0,70	

Plaster	RH (%)	Dry mass (g)	Equilibrium mass (g)	w (%)	w Average (%)
F0 1	53%	44,26	44,55	0,66	0,66
F0 2		47,75	48,07	0,67	
F0 3		49,33	49,65	0,64	
F3 1		53,00	53,22	0,42	0,43
F3 2		54,87	55,11	0,43	
F3 3		49,23	49,45	0,45	
F5 1		54,25	54,39	0,26	0,26
F5 2		55,12	55,26	0,25	
F5 3		61,65	61,80	0,26	
F6 1		51,96	52,38	0,80	0,82
F6 2		43,85	44,21	0,82	
F6 3		51,46	51,89	0,84	

Plaster	RH (%)	Dry mass (g)	Equilibrium mass (g)	w (%)	w Average (%)
F0 1	75%	44,26	44,68	0,95	0,95
F0 2		47,75	48,21	0,97	
F0 3		49,33	49,79	0,94	
F3 1		53,00	53,35	0,66	0,66
F3 2		54,87	55,23	0,65	
F3 3		49,23	49,57	0,68	
F5 1		54,25	54,46	0,38	0,38
F5 2		55,12	55,33	0,38	
F5 3		61,65	61,89	0,39	
F6 1		51,96	52,57	1,18	1,19
F6 2		43,85	44,37	1,20	
F6 3		51,46	52,08	1,20	

Plaster	RH (%)	Dry mass (g)	Equilibrium mass (g)	w (%)	w Average (%)
F0 1	85%	44,26	44,75	1,11	1,12
F0 2		47,75	48,29	1,15	
F0 3		49,33	49,87	1,09	
F3 1		53,00	53,43	0,81	0,81
F3 2		54,87	55,31	0,79	
F3 3		49,23	49,64	0,82	
F5 1		54,25	54,52	0,49	0,49
F5 2		55,12	55,38	0,47	
F5 3		61,65	61,95	0,49	
F6 1		51,96	52,66	1,34	1,36
F6 2		43,85	44,45	1,38	
F6 3		51,46	52,17	1,37	

RH %	F0 (%)		F3 (%)		F5 (%)		F6 (%)	
	Sorption	Desorption	Sorption	Desorption	Sorption	Desorption	Sorption	Desorption
0	0,00	0,00	0,00	0,00	0,00	0,00	0,00	0,00
23	0,32	0,38	0,21	0,25	0,12	0,15	0,39	0,47
43	0,56	0,62	0,37	0,43	0,21	0,25	0,70	0,79
53	0,66	0,73	0,43	0,50	0,26	0,30	0,82	0,89
75	0,95	1,00	0,66	0,72	0,38	0,42	1,19	1,23
85	1,12	1,12	0,81	0,81	0,49	0,49	1,36	1,36

B.1 Compressed earth blocks (CEB)

CEB	RH (%)	Dry mass (g)	Equilibrium mass (g)	w (%)	w Average (%)
STR 1	23%	39,49	39,70	0,52	0,54
STR 2		40,62	40,84	0,54	
STR 3		41,06	41,29	0,56	
ALX 1		39,91	40,08	0,43	0,47
ALX 2		44,01	44,23	0,49	
ALX 3		39,00	39,19	0,50	
CRA 1		45,21	45,55	0,76	0,74
CRA 2		41,02	41,32	0,74	
CRA 3		38,70	39,98	0,73	
STA 1		36,22	36,59	1,01	0,99
STA 2		30,58	30,87	0,96	
STA 3		33,57	33,74	0,51	

CEB	RH (%)	Dry mass (g)	Equilibrium mass (g)	w (%)	w Average (%)
STR 1	43%	39,49	39,79	0,75	0,77
STR 2		40,62	40,93	0,77	
STR 3		41,06	41,39	0,80	
ALX 1		39,91	40,15	0,60	0,64
ALX 2		44,01	44,30	0,65	
ALX 3		39,00	39,26	0,66	
CRA 1		45,21	45,72	1,14	1,12
CRA 2		41,02	41,47	1,11	
CRA 3		38,70	39,13	1,11	
STA 1		36,22	36,76	1,50	1,46
STA 2		30,58	31,02	1,43	
STA 3		33,57	33,90	0,98	

CEB	RH (%)	Dry mass (g)	Equilibrium mass (g)	w (%)	w Average (%)
STR 1	53%	39,49	39,83	0,87	0,89
STR 2		40,62	40,98	0,89	
STR 3		41,06	41,43	0,91	
ALX 1		39,91	40,19	0,69	0,72
ALX 2		44,01	44,33	0,73	
ALX 3		39,00	39,29	0,74	
CRA 1		45,21	45,81	1,32	1,31
CRA 2		41,02	41,55	1,30	
CRA 3		38,70	39,20	1,30	
STA 1		36,22	36,86	1,76	1,71
STA 2		30,58	31,09	1,67	
STA 3		33,57	33,98	1,22	

CEB	RH (%)	Dry mass (g)	Equilibrium mass (g)	w (%)	w Average (%)
STR 1	75%	39,49	39,99	1,27	1,28
STR 2		40,62	41,14	1,28	
STR 3		41,06	41,59	1,30	
ALX 1		39,91	40,28	0,94	0,98
ALX 2		44,01	44,45	1,00	
ALX 3		39,00	39,39	0,99	
CRA 1		45,21	46,09	1,95	1,92
CRA 2		41,02	41,80	1,91	
CRA 3		38,70	39,44	1,90	
STA 1		36,22	37,14	2,54	2,50
STA 2		30,58	31,33	2,45	
STA 3		33,57	34,24	1,99	

CEB	RH (%)	Dry mass (g)	Equilibrium mass (g)	w (%)	w Average (%)
STR 1	85%	39,49	40,07	1,48	1,49
STR 2		40,62	41,22	1,48	
STR 3		41,06	41,68	1,51	
ALX 1		39,91	40,34	1,09	1,12
ALX 2		44,01	44,51	1,14	
ALX 3		39,00	39,44	1,14	
CRA 1		45,21	46,22	2,24	2,22
CRA 2		41,02	41,93	2,23	
CRA 3		38,70	39,55	2,20	
STA 1		36,22	37,30	2,97	2,91
STA 2		30,58	31,45	2,86	
STA 3		33,57	34,38	2,40	

RH %	STR (%)		ALX (%)		CRA (%)		STA (%)	
	Sorption	Desorption	Sorption	Desorption	Sorption	Desorption	Sorption	Desorption
0	0,00	0,00	0,00	0,00	0,00	0,00	0,00	0,00
23	0,54	0,59	0,47	0,51	0,74	0,73	0,99	1,04
43	0,77	0,88	0,64	0,73	1,12	1,30	1,46	1,58
53	0,89	1,02	0,72	0,83	1,31	1,50	1,71	1,83
75	1,28	1,35	0,98	1,03	1,92	2,04	2,50	2,59
85	1,49	1,49	1,12	1,12	2,22	2,22	2,91	2,91

III. Specific surface area

F0 Calculations

RH (%)	RH	w (%)	w	n = w/M_w (mol/g)	RH / [(1-RH)*n] (g/mol)
0,84	0,008	0,001	9,0E-06	5,02E-07	16832,44
1,62	0,016	0,027	2,7E-04	1,50E-05	1095,86
3,78	0,038	0,081	8,1E-04	4,50E-05	872,70
6,35	0,063	0,128	1,3E-03	7,11E-05	953,14
8,98	0,089	0,168	1,7E-03	9,33E-05	1057,42
11,56	0,115	0,205	2,0E-03	1,14E-04	1149,87
14,17	0,141	0,240	2,4E-03	1,33E-04	1238,14
16,68	0,166	0,274	2,7E-03	1,52E-04	1318,98
19,62	0,192	0,305	3,1E-03	1,69E-04	1407,78
29,50	0,295	0,414	4,1E-03	2,30E-04	1822,05

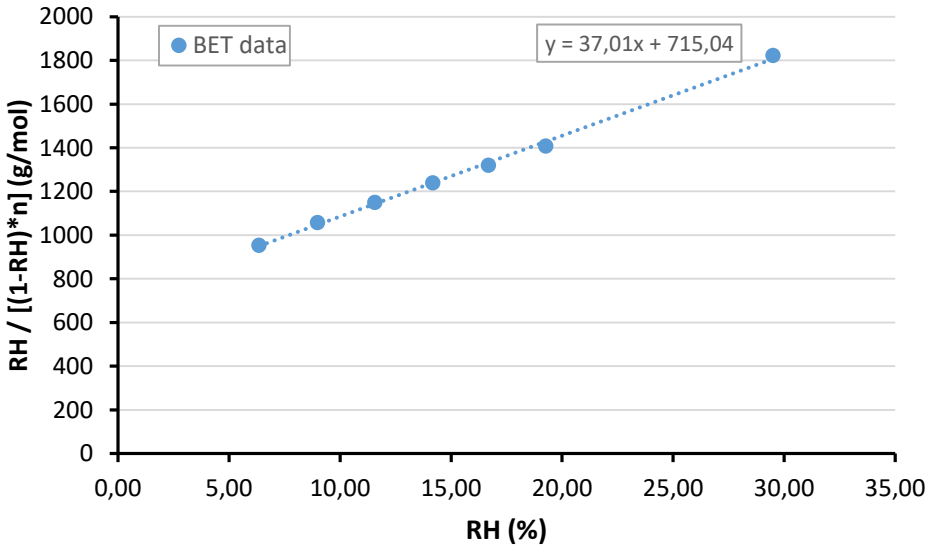

Figure A.11- BET plot for determine the specific surface area of F0

N_m	L (mol^{-1})	M_a (m^2)	S_{BET} (m^2/g)
2,26E-04	6,02E+23	1,05E-19	14,32

IV. Heat of sorption

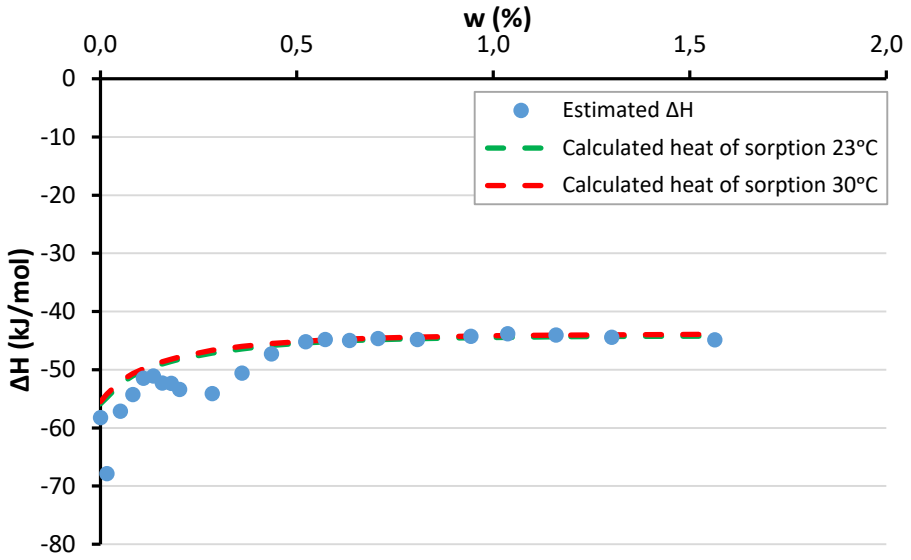

Figure A.12- Heat of sorption of F3 plaster

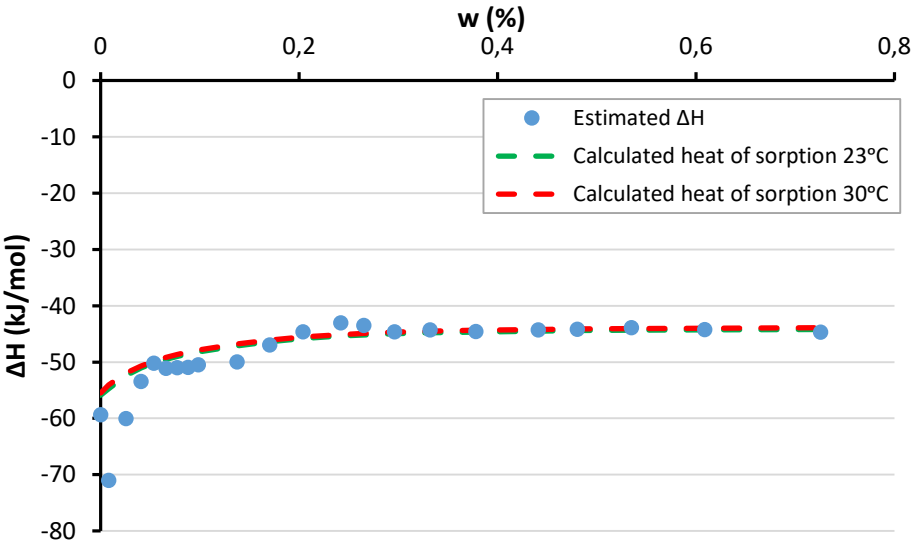

Figure A.13- Heat of sorption of F5 plaster

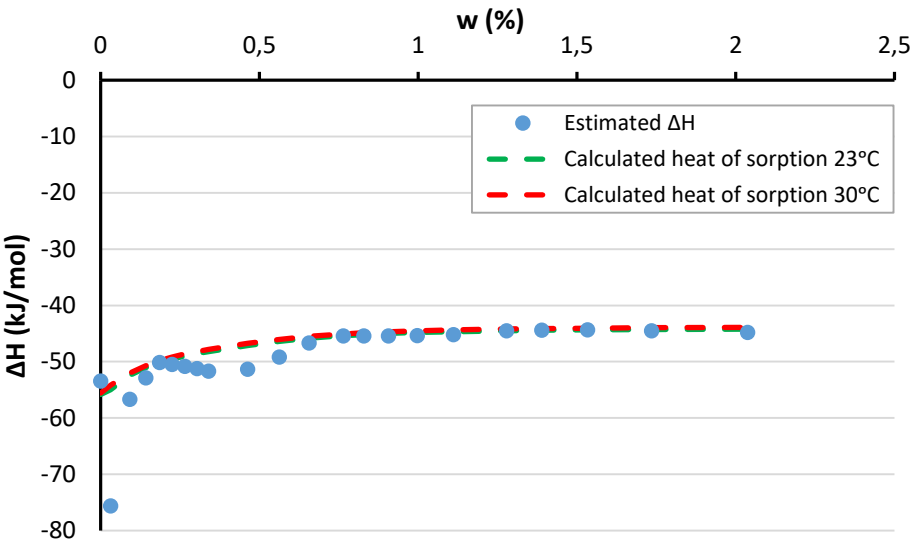

Figure A.14- Heat of sorption of F6 plaster

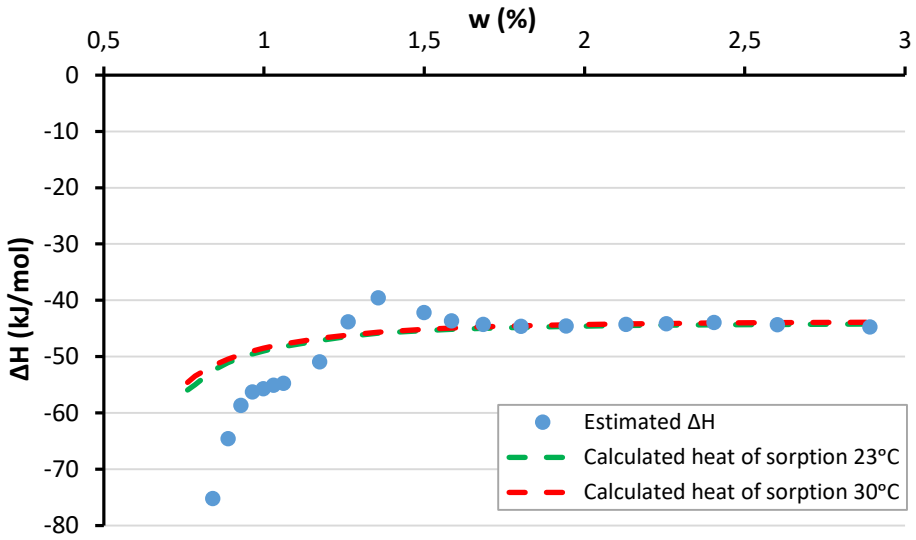

Figure A.15- Heat of sorption of STR block

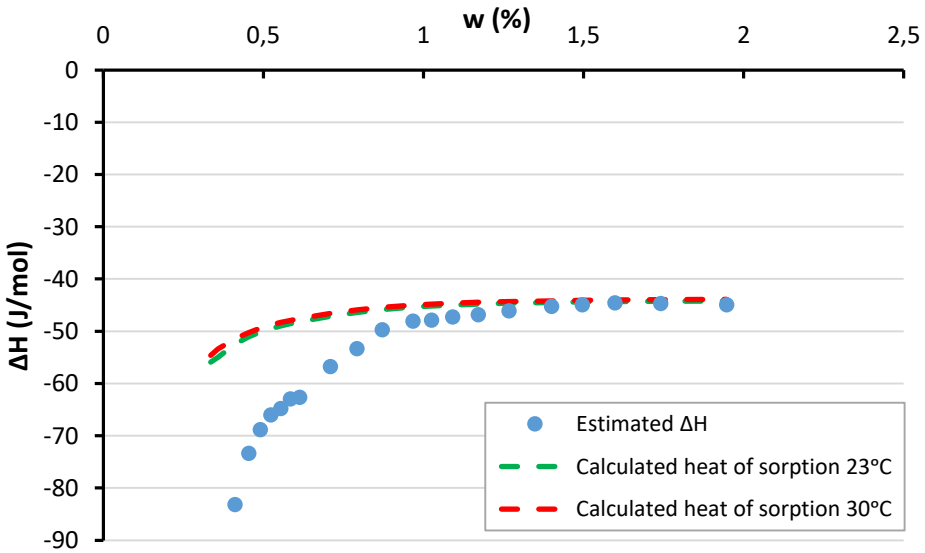

Figure A.16- Heat of sorption of ALX block

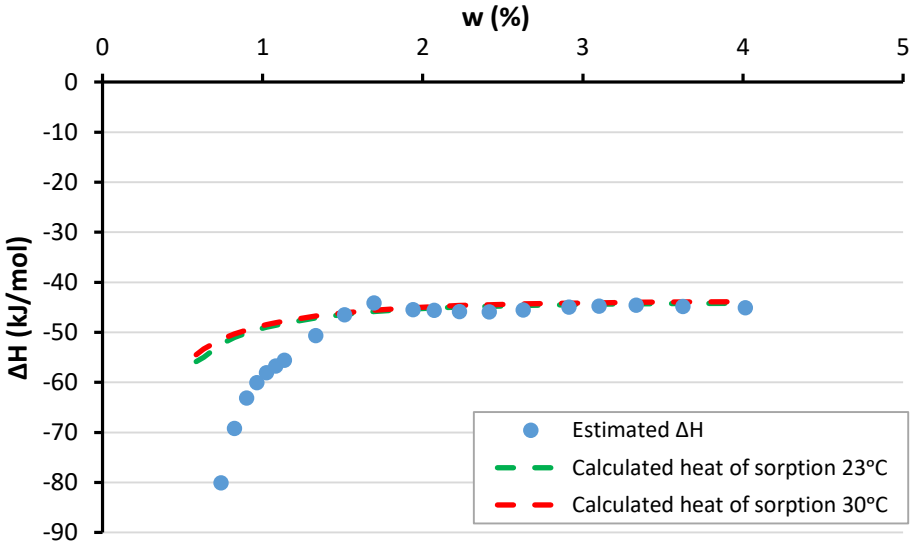

Figure A.17- Heat of sorption of CRA block